2008

Design guidelines for FRP honeycomb sandwich bridge decks

Bin Zou
West Virginia University

DESIGN GUIDELINES FOR FRP HONEYCOMB SANDWICH BRIDGE DECKS

By

Bin Zou

Dissertation submitted to the
College of Engineering and Mineral Resources
at West Virginia University
in partial fulfillment of the requirements
for the degree of

Doctor of Philosophy
in
Civil Engineering

Julio F. Davalos, Ph.D., Chair
Karl E. Barth, Ph.D., Co-Chair
An Chen, Ph.D.
Kenneth H. Means, Ph.D.
Jacky C. Prucz, Ph.D.
Indrajit Ray, Ph.D.

Department of Civil and Environmental Engineering
Morgantown, West Virginia
2008

Keywords: Fiber-reinforced polymer (FRP), bridge decks, shear connection, load distribution, composite action, effective width

DESIGN GUIDELINES FOR FRP HONEYCOMB SANDIWICH BRIDGE DECKS

Bin Zou

Advisor: Dr. Julio F. Davalos

Abstract:

Fiber-Reinforced Polymer (FRP) Bridge decks offer great advantages in highway bridge rehabilitation and new construction, due to reduced weight and maintenance costs, and enhanced durability and service-life. In practice, however, lack of bridge engineering design standards and guidelines have prevented wider acceptance and application of FRP bridge decks by transportation officials. This dissertation focuses on the study of an engineered FRP deck-steel stringer bridge system through experimental testing and both Finite Element analyses and analytical methods.

A prototype mechanical shear connection was developed and designed to be used with any type of FRP panels that can accommodate any panel heights. This non-grouted sleeve-type connector can secure the deck onto a welded stud and can sustain shear forces at FRP panel-steel stringer interface. Static and fatigue tests were conducted on push-out connection specimens, and later on a scaled bridge model. The strength, stiffness, and fatigue performance characteristics of the connection were fully investigated. Constructability issues were also evaluated, such as ease of installation and economic manufacturing of the connector. Design formulations were established based on the test results.

Following the connection study, a 1:3 scaled bridge model of a honeycomb FRP deck on steel stringers was evaluated. The deck was attached to three supporting steel stringers using the proposed sleeve-type mechanical connections. The model was designed as partially composite to satisfy AASHTO limits and requirements. Several issues were evaluated that included: (1) deck attachment procedures; (2) transverse load distribution factors; (3) local deck deflections; and (4) system fatigue behavior. After the bridge model was tested in the linear range, a 1.2-m wide T-section, of an FRP deck section attached to the middle stringer, was cutout from the bridge model and tested in bending for service and failure loads. The evaluations included: (1) Degree of composite action, (2) Effective deck-width, and (3) service-limit and ultimate-limit states under flexure loads. The behavior of the FRP deck under partial composite action was defined fully by these tests.

Finite element models of the scaled bridge model and T-beam section were formulated using ABAQUS. Besides the experimental tests and FE analyses, analytical solutions were developed to verify the test results. An explicit series solution for stiffened orthotropic plates was used to evaluate the bridge response and obtain load distribution factors of FRP deck-on-steel-stringer bridges. Also a harmonic analysis that was developed for FRP thin-walled sections was formulated to define effective-width for FRP decks as an explicit solution. The outcome of this study was to propose design guidelines and recommendations for FRP honeycomb bridge decks for applications in bridge engineering practice.

ACKNOWLEDGEMENTS

I would like to express my gratitude to my advisor and committee chair, Dr. Julio F. Davalos, for his continuing assistance, support, guidance, understanding and encouragement throughout my graduate studies. I am also thankful to my committee co-chair, Dr. Karl E. Barth, for the guidance and support he has offered, both on this project and in other aspects.

I would like to thank Dr. An Chen, Dr. Kenneth H. Means, Dr. Jacky C. Prucz, and Dr. Indrajit Ray for their participation in my advisory committee. The laboratory assistance of William J. Comstock is greatly appreciated. I would also like to thank Dr. Jerry D. Plunkett and KSCI for providing the experimental test samples; Their support is greatly appreciated. I also must thank my parents and family for their everlasting support and blessings in my life.

TABLE OF CONTENTS

LIST OF FIGURES

LIST OF TABLES

CHAPTER 1

INTRODUCTION

1.1. Overview of FRP Deck Applications in Bridge Engineering

In recent years, the increasing demands on highway bridges have provided great opportunities for development and implementation of Fiber-Reinforced Polymer (FRP) panels, both for rehabilitation projects and new constructions. FRP Bridge decks offer great advantages in bridge construction, because of their reduced weight and maintenance costs, and enhanced durability and service-life. In particular, for concrete deck replacement projects, an FRP deck can be installed in a matter of hours or a few days over supporting stringers, reducing the deck weight to about 1/5th; thus increasing the load carrying capacity of the structure, while minimizing user inconvenience. Also, an FRP deck usually has a service-life that can be two to three times greater than for traditional concrete decks due to its excellent corrosion resistance. This characteristic can greatly improve the service quality and relieve future maintenance work.

Basically, there are two types of FRP decks in the market: (1) tubular sections (trapezoidal shape or rectangular shape) produced through a forming-die by pultrusion (similar to extrusion) and bonded side-by-side to form cellular panels (Figure 1.1), and (2)

sandwich construction consisting of two stiff facesheets separated by a core (Figure 1.2). Sandwich panels with either honeycomb or foam cores have been shown in aerospace and automotive applications to be the most effective structural configurations to achieve high stiffness and strength for minimal material weight. Thus, it is not surprising that a recent review article (Bakis *et al.*, 2002) showed that Honeycomb FRP (HFRP) shown in Figure 1.2 is the lightest, stiffest, and least expensive of all commercial FRP decks. In addition, the flexibility of its manufacturing process permits custom production of panels of any depth, while a pultruded section has a fixed geometry dictated by the forming steel die used.

A typical honeycomb sandwich panel is made of two facesheets, separated by a corrugated honeycomb core. The facesheet of the sandwich panels can be designed with various cross laminates and lay-ups corresponding to the strength requirements, while the height of the core can be readily adjusted to meet design and construction requirements. The honeycomb sandwich panel offers great flexibility in designing for varied deflection, strength, and configuration requirements.

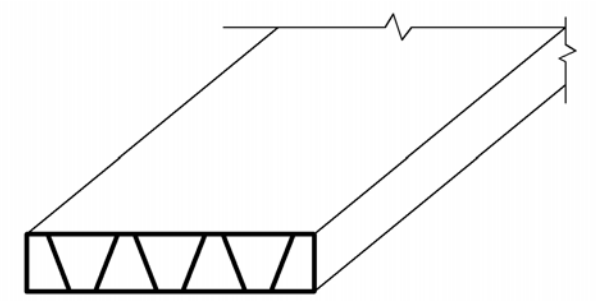

Figure 1.1 Typical Cellular FRP Panel

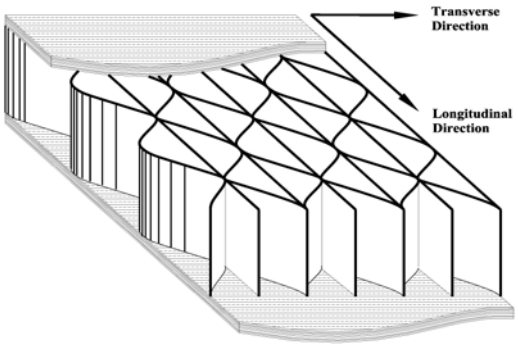

Figure 1.2 KSCI Honeycomb FRP Panel

1.2. Problem Statement and Research Significance

Because of favorable benefits of FRP decks, several bridges with FRP decks have been designed and constructed with positive results. In practice, however, the lacks of uniform performance targets and design guidelines have prevented wider acceptance and application of FRP bridge decks by transportation officials. Current FRP deck applications in bridge engineering are being implemented on case-by-case basis, following specialized or proprietary design guidelines. Different connection systems, such as mechanical connections and adhesive connections, are utilized with certain deck configurations. Different deck-stringer systems with full composite, partial composite, or non-composite behaviors are being designed for. Thus, the design of FRP bridge decks needs to be incorporated into established national codes of bridge engineering design practices. These issues are briefly reviewed in the following section.

First of all, the development of an efficient deck-to-stringer connection is needed for FRP bridge decks for both performance and constructability. Such connection should be easy to manufacture, install and inspect while providing adequate performance, such as transfer of shear force between decks and stringers. An effective shear connection should develop certain degree of composite action for FRP decks. It should also be able to accommodate various FRP deck configurations with different heights. The connection should also have fatigue resistance to meet AASHTO code requirements for highway bridges.

Secondly, there should be uniform design criteria for FRP bridge decks to achieve defined structural performance in highway bridge applications. While for conventional concrete deck over steel stringer bridges, full composite action is usually preferred and achieved due to the efficiency of the materials used, in the AASHTO code slab-on-girder bridges can be designed for a range of non-composite to full-composite action. No partial composite action is allowed. However, FRP decks are usually designed as partial composite action in practice. Several limiting practical factors lead to this application: (1) The hollow core configuration of FRP panels and lack of continuous connection at panel-stringer interface do not allow to develop contact and attachment between decks and connections; (2) the high modulus ratio between steel-girder and FRP-panel (about 30 compare to 8-10 for conventional concrete deck over steel girder) makes the contribution of FRP deck to the overall bridge stiffness much less significant; (3) the practical connection spacing of about 0.6 m (2ft) to 1.2 m (4ft) for FRP decks, compared to conventional concrete deck connection spacing of 0.15 m (6in) to 0.25 m (10in), is too large o develop full composite action. All these factors in turn lead to less shear force to

be transferred between deck-girder and achieve less degree of composite action. On the other hand, it may actually be desirable to accommodate some degree of deck-stringer relative displacement for differential thermal expansions between FRP and steel.

Therefore, a number of design issues related to partial composite action in FRP deck systems need to be investigated, including: (1) transverse load distribution factors; (2) degree of composite action; (3) effective deck-width; and (4) service-limit and ultimate-limit capacities such as fatigue resistance and ultimate failure mode. Other design issues that are distinct for FRP decks include: (1) local deck deflections; and (2) deck-connection installation procedures.

Lastly, design codes for FRP decks need to be developed, by accounting for the distinct behavior of FRP decks. However, the format of design guidelines for FRP decks should be consistent with current design codes (such as AASHTO LRFD Specification). Such design guidelines would enable design engineers and transportation officials to design and evaluate FRP bridge decks by a consistent approach, which in turn can stimulate wider acceptance and application of FRP bridge decks.

The issues discussed above are considered to be main hurdles in FRP deck applications and will be investigated and addressed in this study.

1.3. Objectives and Scope

The focus of this study is: (1) to propose an effective deck-stringer shear connection to mechanically attach any type of FRP bridge decks; (2) to investigate the structural behavior of FRP honeycomb deck, especially transverse load distribution factors, local deck deflections, degree of composite action, effective deck-width, service-limit and ultimate-limit loads, and fatigue resistance of FRP decks and connections; (3) to propose design guidelines for FRP honeycomb bridge decks. This study is conducted by experimental testing and verifications by both FE analysis and analytical method.

First, a prototype shear connection designed to be used with any type of FRP panels with various heights is proposed. It is a non-grouted type and provides shear transfer capability between FRP panels and steel stringers. Static and fatigue test are conducted on push-out connection specimens, and later on a scaled bridge model. The strength, stiffness, and fatigue performance characteristics of the connection are fully investigated, and design formulations are established based on the test results. Constructability issues are also evaluated, like ease of installation and economics of manufacturing.

Then a one-to-three scaled bridge model with honeycomb FRP decks is tested. The deck is connected to three steel supporting stringers by the proposed shear connection. The model is designed as partially composite and meets the AASHTO limits and requirements. Several issues are evaluated which include: (1) deck attachment procedures, (2) transverse load distribution factors, (3) local deck deflections, and (4) system fatigue

behavior. After completing the test with this bridge model, a 1.2 m wide T-section is cut out from the deck center portion of bridge model and tested to evaluate: (1) Degree of composite action, (2) Effective deck-width, and (3) service-limit and ultimate-limit states under flexure loads. The behavior of FRP decks with partial composite action is fully defined by these tests and evaluations.

Finite element models of the scaled bridge model and T-beam section are formulated by using ABAQUS. Besides the experimental tests and FE analysis, analytical solutions are obtained to verify the test results. An explicit series solution for stiffened orthotropic plates is proposed, and load distribution factors for FRP bridge decks are obtained based on this series solution. Also, a harmonic analysis that was originally developed for FRP thin-walled sections is formulated to evaluate effective-width for FRP decks. At the end of this study, design guidelines and recommendations for FRP honeycomb bridge decks are proposed.

1.4. Organization

This study contains a total of seven chapters. Chapter 1 presents the problem statement, objectives and scope, and organization of the study. In Chapter 2, a prototype shear connection for FRP decks is proposed and evaluated. This prototype shear connection is based on proven conventional shear stud-type connectors. The concept consists of a partially threaded stud welded on a steel-girder, and two circular steel sleeves inserted at bottom and top of a fitting hole pre-drilled through the FRP deck. This prototype shear

connection is tested at component level by conducting both static and fatigue tests on totally 18 push-out specimens, and strength, stiffness, and fatigue characteristics are evaluated.

In Chapter 3, load tests on a reduced scale FRP deck bridge are carried out. The test bridge model is a 1:3 scale of a reference bridge designed according to AASHTO limits and requirements. The model consists of 3 steel stringers with 5.4 m span and 1.2 m spacing on centers. An FRP deck 5.4 m x 2.74 m x 0.13 m was attached to the stringers using the prototype stud-sleeve connector, for two spacing conditions of 0.6 m and 1.2 m. The deck consisted of 3 individual FRP honeycomb panels from KSCI, each 1.83 m wide along the stringers and 2.74 m long across the stringers, assembled by tongue-and-groove connections along the two 2.74 m transverse joints. The longitudinal direction of the honeycomb core (Figure 1.2) was oriented along the 2.74 m width of the model, perpendicular to the traffic direction of the bridge. The objectives of testing of the scaled bridge model were to evaluate: (1) deck attachment procedures; (2) transverse load distribution factors; (3) local deck deflections; and (4) system fatigue behavior. After the bridge model test, a 1.2 m wide T-section was cut out from the deck center section of the bridge model and loaded under three point bending, to evaluate the following concepts: (1) Degree of composite action, (2) effective deck-width, and (3) service-limit and ultimate-limit behaviors.

In Chapter 4, finite element models of the scaled bridge model and T-section are formulated. The honeycomb sandwich deck is modeled with shell elements by using

equivalent properties (Davalos *et al.*, 2001). The shear connections are modeled by linear elastic spring elements to implement the actual shear stiffness of the connection, and the interface relative displacement of deck and stringer is accurately captured.

In Chapter 5, an approximate series solution for a simply-supported orthotropic plate stiffened by equally spaced stringers is presented, which is used as an efficient computational method to evaluate bridge response. This close form solution is calibrated by FE parametric study of 66 bridge models, and the data obtained for load distribution factors is used in a multiple regression analysis to propose regression functions that can be easily used in design practice. The results are then compared to current AASHTO Standard and LRFD specifications,

In Chapter 6, a shear lag model is presented for structurally orthotropic FRP decks compositely attached to supporting stringers. A harmonic analysis that was successfully developed for FRP thin-walled sections is formulated and used to predict the effective-width for FRP decks. Finite element study is conducted for selected 44 FRP deck-and-stringer bridges under AASHTO LRFD service loads. The effective-width for interior stringer is obtained to validate the shear lag model, which provides consistent and reasonably accurate results and is relatively simple for application in design practice. Finally in Chapter 7, design guidelines for FRP honeycomb sandwich decks are proposed.

CHAPTER 2

A NEW SHEAR CONNECTION FOR FRP BRIDGE DECKS

2.1. Introduction

In highway bridge engineering, bridges with concrete decks and steel supporting girders, usually referred as slab-on-girder bridges, are the most common types. In recent years, roughly about 1/3 of this kind of bridges is in need of repair or replacement. In response to this situation, FRP bridge decks are considered a useful option both for rehabilitation projects and new constructions. FRP Bridge decks offer great advantages for rapid replacement and new construction due to their favorable performance for minimum unit weight. In addition, the enhanced durability of FRP material provides prolonged service-life and keeps future maintenance costs to minimum. The high initial cost of FRP decks can be offset by the benefit gained.

Despite its favorable features, several issues hinder the widely application of FRP bridge decks. One of the most pressing problems is to develop an effective connection for FRP decks. For conventional concrete bridge decks, mechanical shear connectors such as stud

connector or channel connector have been widely used with success. Their structural behaviors are well defined by various studies and researches. The concrete deck would achieve full composite action with standard designed shear connection and its design guidelines have been adopted in AASHTO design specification for a long time. In contrast, because of the distinctive properties of FRP material and relatively short period of application time, shear connections for FRP decks has not been studied very thoroughly. There are various types of connections in FRP decks application, such as certain types of mechanical connections and adhesive connections. Both of these connections have their favorable features as well as shortcomings such as labor intensive, difficulty of inspection, lacking of ability of transferring shear force, or lacking fatigue resistance.

Thus, an effective connection that addresses all these issues is very much in need. In this chapter, a prototype shear connection will be proposed. Its structural behaviors and performances will be thoroughly investigated by static and fatigue tests on both components and reduced bridge models. Design formulation will be proposed based on the test results. This prototype connection will be used in an FRP deck-connection system studied later.

2.2. Background and Problem Statement

The development of existing shear connections for FRP decks is briefly reviewed. Their shortcomings are reviewed. Performance target for a new prototype shear connection for

FRP decks are identified.

2.2.1 Existing Shear Connections for FRP Decks

In current FRP panel industry; there are mainly two types of connections, mechanical and adhesive connection. For mechanical connection, the FRP deck and steel stringer are connected mechanically by shear stud, steel clamp, or mechanical bolt. Instead, adhesive connection is formed by applying adhesive glue at deck-stringer interface to establish bonding effect. Both types of connections have been reported in existing projects with certain success.

Mainly three types of mechanical connections are currently in use. They are bolted, clamped, and shear stud connections. Among them, shear stud type connections are conceptually related to those used in concrete deck. Moon *et al.* (2002) developed a shear stud type connection for trapezoidal sandwich panel, MMC Gen4 FRP deck. It was designed to transfer shear force between deck and stringers in order to develop composite action. The connection consisted of shear studs and enclosures within the deck. After installation of connection, concrete grout was post-poured to form a connection zone. The shear studs were pre-welded on the steel stringers, usually with 2 or 3 studs combined as one group. Then an enclosure was cut out on the FRP deck to accommodate the studs. After the FRP deck was in place onto supporting stringers, the enclosure was filled with non-expansive concrete grout. Three conceptually similar design options with different grout scheme and shear studs layouts were evaluated. Static tests on push-out specimens showed that this shear connection could sustain a maximum load up to 347kN with

12.7mm displacement. Substantial inelastic deformation occurred before failure, which was mainly from shear studs. FRP deck facesheet thickness had positive impact on shear connection strength. Also the stress concentration and the local crushing of concrete could be greatly alleviated by using larger volume of grout. The fatigue load was identified as 56kN where the specimens were loaded up to 10.5 million cycles. This load cycle was defined as equivalent 75 years bridge design life span. The specimens did not show any obvious damage throughout the loading and the stiffness remained almost constant. The shear connection was proved to have adequate fatigue resistance.

Following this shear connection study, Keelor *et al*. (2004) conducted a field test on a short span bridges with FRP decks located in Pennsylvania. The bridge had pultruded FRP decks using the same conceptual shear connections developed by Moon (2002). The bridge was designed as fully composite. The bridge was 12.6m long with five steel girders equally spaced at 1.8m. The spacing of the shear connection was 0.6m and each connection consisted of two headed shear studs side by side at the top flange of the girder. The field test showed that at service load, this FRP bridge was able to achieve full composite action. There was no slippage at the deck and stringer interface. The bridge exhibited an effective width that was close to 90% of the girder spacing for interior girders and approximately 75% of one-half of girder spacing for exterior girders.

Although the stud type connection is able to transfer the shear force and develop composite action in FRP decks, the problem is that it usually requires additional concrete grout which is labor intensive. Also, since the connection is expected to achieve full

composite action, high stress concentration at enclosed grout area could have negative impact on the integrity of FRP deck and connection.

Bolt and clamp connections are two other mechanical connections. For these two types of connections, the installation is required to be underneath the bridge deck which is difficult to perform. In addition, they are neither able to effectively transfer the shear force nor have adequate fatigue resistance.

Besides mechanical connections, adhesive bonded connection is another major connection type. Series of experiments studies on adhesive connections have been conducted by Keller *et al.* (2005). Two large scale T-beams were constructed with pultruded cellular FRP decks and steel girders. Stiffness, strength, and fatigue resistance of T-beams were investigated by static and fatigue tests. It was shown that: (1) The adhesive bond was able to achieve composite action in FRP decks. The stiffness and strength of FRP deck-steel stringer systems were considerably increased due to composite action; (2) No stiffness deterioration was observed under fatigue loading. However several issues for adhesive bonded connection still need to be investigated. First, the resistance of adhesive bond to environmental factors such as moisture and temperature change is critical. Also, the adhesive bond is difficult to be applied in field and the quality control will be a problem.

Therefore, a new type of shear connection is needed in order to address these shortcomings of present connections. The performance targets of a new type of shear

connection can be summed up as: (1) safely secure FRP decks on supporting stringers, preventing uplift and rotation; (2) be able to transfer shear force at deck and stringer interface, developing some degree of composite action in FRP decks; (3) have adequate fatigue resistance to AASHTO design live load; and (4) have relatively low cost and easy to install. In this chapter, a prototype shear connection will be proposed. Characteristics of strength, stiffness, and fatigue performance of the connection will be investigated at both component and system level. An empirical design formula will be proposed based on the test data.

2.2.2 Shear Connections for Concrete Composite Deck

In highway bridge engineering, bridges with composite action are usually preferred because of its more effective material utilization and better structural performance. For traditional bridges with concrete decks, the composite action is achieved by the use of shear connections, which are welded at steel stringers and encased by concrete deck. An effective shear transfer mechanism is established by bonding and interaction between concrete decks and shear connections.

The degree of composite action in deck-stringer system is mainly determined by the strength and stiffness of shear connections. For example, at a cross section of the bridge where bending moment is applied, the compression force C in deck element and the tension force T in stringer element form a resisting moment resultant to resist the applied moment. Force equilibrium and displacement compatibility are two conditions need to be satisfied at the deck and stringer interface. In order to satisfy the force equilibrium, the

shear connection shall have adequate strength which is at least equal to C or T to avoid shear failure at interface. On the other hand, in order to satisfy the displacement compatibility, the shear connection shall have adequate stiffness to accommodate interface slippage. Figure 2.1a, b, c show sections with no interaction, partial interaction and full interaction. Two extreme cases are: (1) the shear connection has infinite stiffness. There will be no slippage at deck-stringer interface. This condition corresponds to full composite action; (2) the shear connection stiffness approaches to zero. The deck and stringer are allowed to move freely at interface. This condition corresponds to non-composite action (Figure 2.2a, b). Partial composite action is between these two extreme cases.

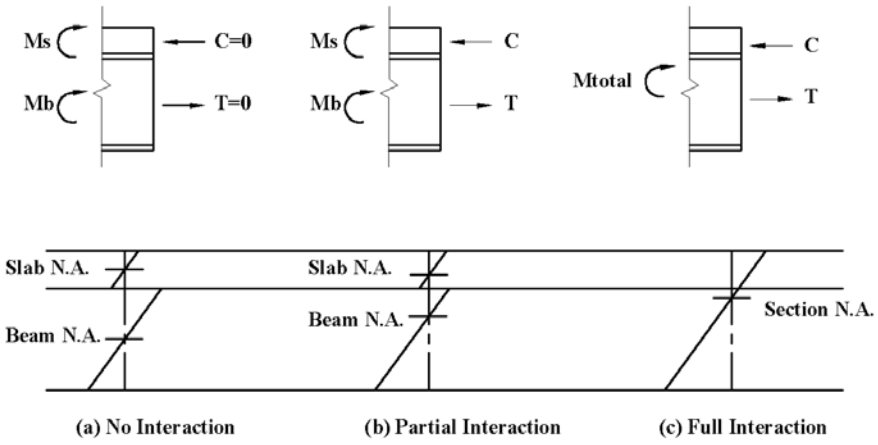

Figure 2.1 Force Equilibrium and Strain Compatibility of Deck-Stringer

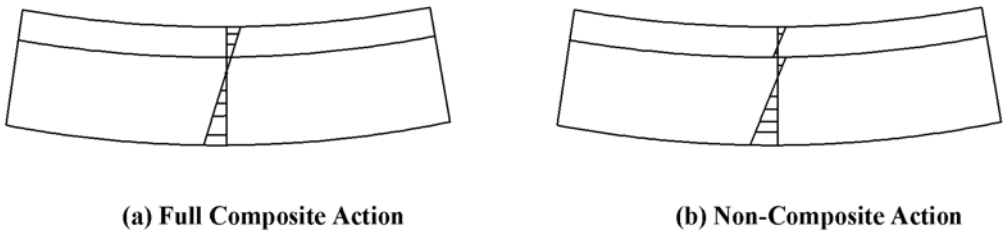

(a) Full Composite Action (b) Non-Composite Action

Figure 2.2 Full Composite Action vs. Non-composite Action Beams

Newmark *et al.* (1951) investigated the impact of shear connection on composite action of concrete decks. Generally, the interface slip of deck-stringer was described by formulation $\gamma = \frac{qs}{k}$, which was governed by horizontal shear q, spacing of connection s, and connection stiffness k. Thus, decks with higher connection stiffness and smaller connection spacings would have less interface slip, and in turn developed more complete composite action. Tests on concrete T-beam showed that if the shear connection was designed with adequate stiffness and strength, the minor slip at slab-stringer interface could be ignored. The T-beam would still be able to achieve full composite action. On the contrary, if the connections lacked strength or stiffness, only partial composite action could be achieved and interface slip must be properly considered.

Based on Newmark's study, the full composite bridge deck design concept has been since adopted in AASHTO design specification. The bridges are designed as full composite with the shear connections designed to meet strength and stiffness requirements. No partial composite case is allowed in AASHTO design specification.

2.2.3 Fatigue Resistance of Shear Connection

Slutter and Fisher (1966) conducted fatigue tests on 56 push-out specimens. They used both stud connector and channel connector as connections. The specimens were loaded with either monotonic loading or reversal loading. The control variables were stress range and minimum stress of shear connector. The tests results showed that stress range rather than absolute stresses value determined the fatigue resistance of shear connections. The fatigue resistance was represented by a linear function of logarithm. The corresponding curve was referred as S-N curve (S was stress range of shear connector, and N was fatigue load cycles). In S-N curve, stress range was negatively related to fatigue cycles, which means higher stress range on connection would have less fatigue life. The test also showed that specimens with reversal loading had significantly longer fatigue lives. Thus, the fatigue resistance estimation based on monotonic loading test was on the conservative side. In addition, push-out test gave conservative values compared to beam test method and was a lower bound test method.

Mainstone and Menzies (1967) conducted fatigue tests on both push-out specimens and T-beams. Three common types of shear connectors, stud connector, channel connector, and bar connector were studied. For the stud connector, it displayed two different failure modes that not only depended on the maximum load but also on the stress range. Failure mode I is the shear stud fracture due to partial tensile and partial shear, accompanied with local crushing and cracking of the concrete. This failure mode occurred at higher maximum fatigue load. Failure mode II is weld fracture due to shear stress and accompanied by little deformation of the shear stud or concrete. This failure mode

occurred at lower maximum fatigue load and higher fatigue stress range. They concluded that maximum shear force and stress range both contributed to the fatigue resistance of shear connection.

Oehlers (1990) proposed an alternative design method which was different from the current design methodology. In his proposed method, the static strength and fatigue resistance of shear connection were integrated and related. The test specimens were subjected to fatigue loading with predetermined load cycles. Then the specimen was statically loaded to failure. The test results showed that static strength decreased during fatigue loading, and the static strength and fatigue resistance were inter-related. The author suggested a new design method. The shear connection had initial strength P_1 and fatigue strength P_2. During the fatigue loading, the initial strength P_1 continuously decreased to fatigue strength P_2. The shear connection was failed at this point which was the shear connection fatigue design life.

2.2.4 Experimental Methods on Shear Connections

Push-out and beam tests were two major test methods for shear connection study. Beam test specimens were full or reduced-scale composite beams that were representative of actual girders. The specimens usually consisted of a steel beam, concrete slabs, and shear connectors. Beam tests were most suitable to study the shear connection behavior at system level, like fatigue resistance of a bridge. Push-out test specimens normally consisted of concrete slab section and single shear connector. Push-out specimens were more suitable to study the connection at component level, where the test variables need to

be carefully controlled. Both of these test methods were proved to be effective and accurate. Push-out test was more widely used because of its simplicity, cost effectiveness, and easiness of controlling the test variables. Comparing with beam test, push-out test usually gave conservative value and was a lower-bound test method.

2.2.5 Problem Statement

Based on the review, the development of an efficient deck-to-stringer connection is needed in FRP deck bridges, for both performance and constructability. The connection should be easy to manufacture, install and inspect while having adequate performance such as transferring shear force between decks and stringers. The goal of the new shear connection is to develop a certain degree of composite action in FRP decks. It also needs to be able to accommodate various FRP deck configurations with different heights. The connection should also have fatigue resistance to meet AASHTO code requirement for highway bridges.

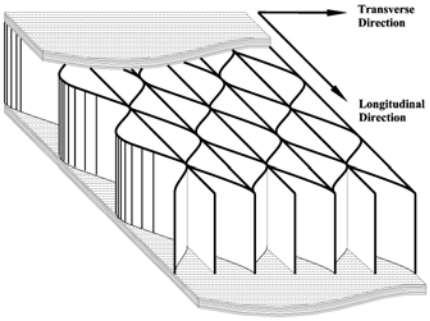

Figure 2.3 KSCI Honeycomb Sandwich Panel

2.3. Objectives and Scope

The objectives of this chapter are to: (1) propose a prototype shear connection, which is suitable to be used with any type of FRP panels; (2) investigate its strength, stiffness, and fatigue resistance; and (3) propose design formulas based on test results.

Both push-out and scaled bridge model test will be conducted to investigate the strength, stiffness, and fatigue resistance of the connections. The push-out specimen consists of a square FRP honeycomb sandwich section and a single shear connection. The test includes two phases. Phase I is a static test. 8 push-out specimens are loaded to failure. Phase II is a fatigue test. 10 push-out specimens are loaded under cyclic load at varied stress ranges until fatigue failure. Empirical design expressions for shear connection, such as $P-\Delta$ curve (load-displacement curve) and $S-N$ curve (stress range-fatigue life curve), are formulated. Then the shear connection is tested on a 1:3 scaled bridge model to investigate its fatigue resistance at system level. The shear connection is then used for further study on FRP bridge model and T-beam test.

2.4. Prototype Shear Connection and Test Procedure

A prototype shear connection is proposed in this section. This prototype shear connection can accommodate any type of FRP decks with varied height. Under test push-out specimen consists of one KSCI sandwich honeycomb panel and a single shear connection. Totally 18 specimens are tested under static and fatigue load, followed by a reduced scale

bridge model test. The strength, stiffness, and fatigue resistance of this shear connection are thoroughly investigated at both component and system levels.

2.4.1. Prototype Shear Connection

The proposed prototype shear connection is basically a mechanical type connection. The concept is initiated from the work done by Righman *et al.* (2004). It consists of two steel sleeves, designated as top and bottom sleeves (Figure 2.4a, b). The top sleeve is a 90mm long, 75mm diameter tubing welded with two washers; the top washer has a 130mm outside diameter and the bottom washer has a 32mm inside diameter. The bottom sleeve is a 90mm long and 75mm diameter tubing welded to a bottom washer of 130mm outside diameter. The height of the tubing can be varied in order to accommodate FRP panels with different thicknesses.

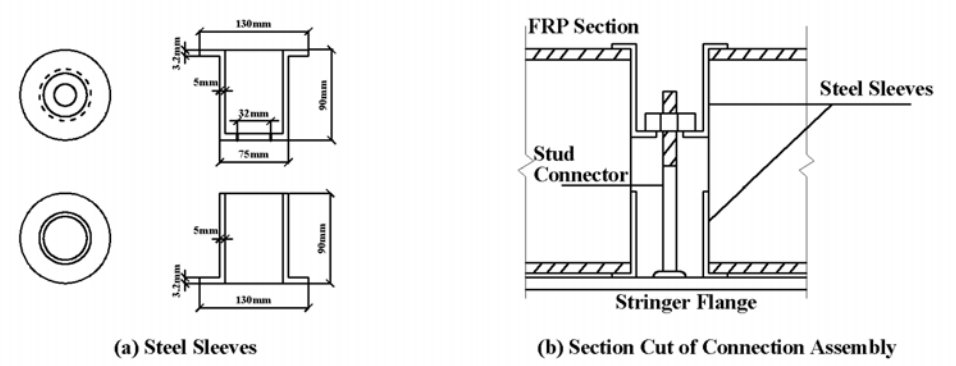

Figure 2.4 Prototype Shear Connections

Illustration of the installation of this shear connection is shown in Figure 2.5a. To install this shear connection on FRP decks, an 80mm diameter round hole (element No.5 in

Figure 2.5a) is pre-drilled in the deck (element No.4) at the location where the shear connection is to be placed. Then the two steel sleeves (element No.3 and No.6) are fitted into the predrilled hole. These steel-sleeve connector and FRP deck are clamped using a nut (element No.7 and No.8) through the partially-threaded shear stud (element No.2) and tighten against the inner washer of the upper sleeve. The shear stud is welded onto the top flange of the steel stringer (element No.1) before installation. Figure 2.5b show the installation procedure of the shear connection in the test. It could be done in short period of time.

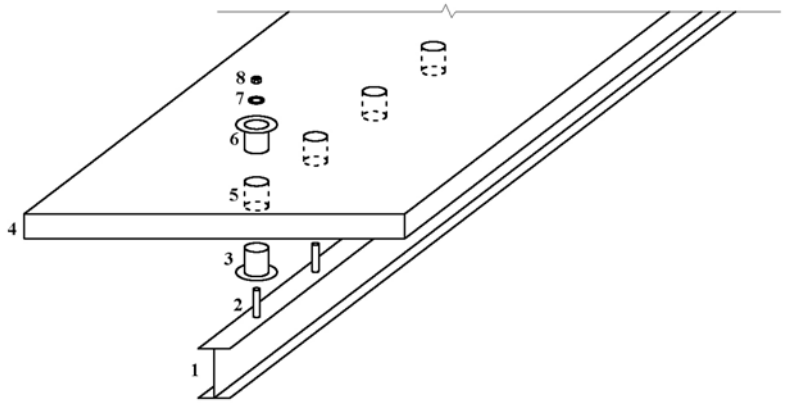

Figure 2.5a Installations of Shear Connection to FRP Decks

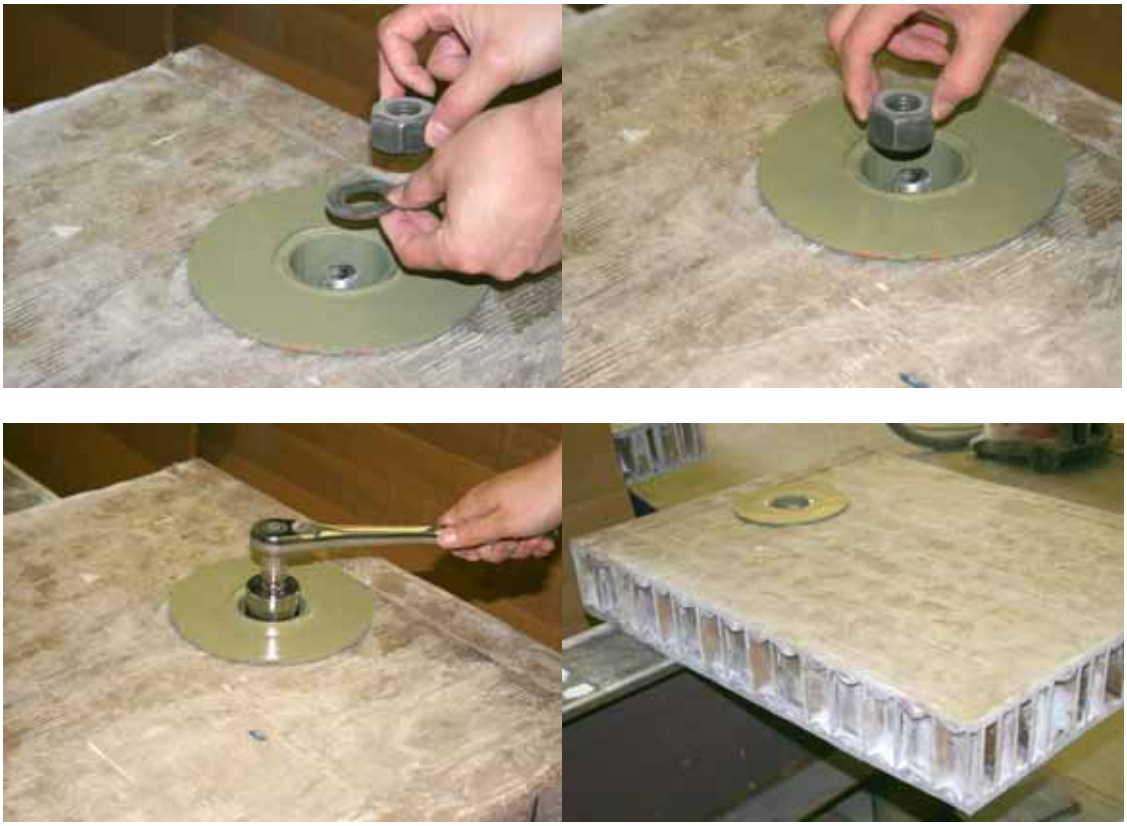

Figure 2.5b Installations of Shear Connection to FRP Decks

The function of the tubing is to provide a protective enclosure for the panel and to allow mechanical attachment to the welded shear stud. The top exterior washer serves to clamp the panel and stringers, while protecting the FRP panel by distributing the stresses over an adequate area. The smaller washer inside the tubing, with an additional pressure washer under the nut, is used to secure the sleeves with the shear stud. The interface shear force goes from the shear stud to the inside washer and tubing, and then to the FRP panel. Because the height of tubing can be easily adjusted, this shear connection can accommodate FRP decks with varied heights for either pultruded or sandwich FRP panels.

2.4.2. Push-out Specimen and Test Setup

Push-out specimen was designed to investigate the strength and stiffness characteristics of connection. The specimen consisted of a square FRP honeycomb sandwich panel section with a single shear connection at the center of the panel (Figure 2.6). The square panel section was 0.9m*0.9m, and 0.2m deep. The honeycomb panels were provided by Kansas Structural Composites Inc. (KSCI). This sandwich geometry consisted of two facesheets and a sinusoidal core (Figure 2.2). The overall 0.2m depth of the panel had a 0.17m height honeycomb core and two 15mm thick facesheet.

The push-out specimen was loaded horizontally to simulate the interface shear transfer in composite bridge decks. The push-out specimen was attached to a floor beam connected to strong floor. At one end of the floor beam parallel to the loading direction, a 245kN actuator was installed to exert an axial force on the side of the specimen (Figure 2.7a, b). The positions of the actuator and panel were carefully adjusted to ensure they were at the same level to minimize eccentricity during the loading. In order to prevent the panel from rotating around the shear stud, an aluminum frame was installed around the FRP panel and connected to the actuator head. A side beam with rubber rollers was placed on each side of the push-out specimen to laterally support the specimen. The aluminum frame evenly distributed the horizontal force on the loading surface of the panel. Two LVDTs were placed at the end of the specimen opposite to the actuator loading head. The displacement of the specimen and the corresponding load were continuously recorded during the test.

Figure 2.6 Shear Connection Test Setup

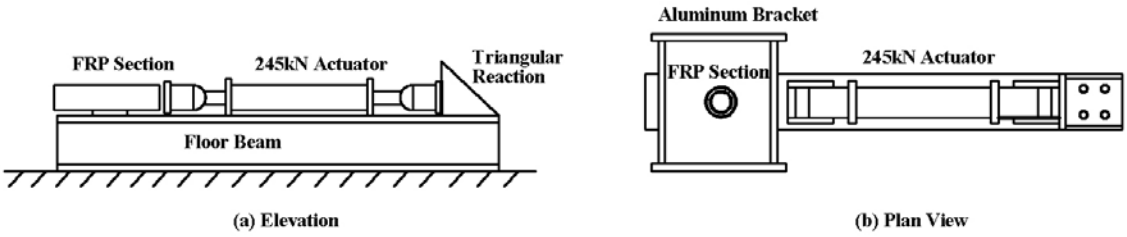

Figure 2.7 Shear Connection Test Setup

2.4.3. Test Procedure

The tests consist two phases, phase I and phase II. Phase I is static tests on a total of 8 specimens, which were numbered as S1 to S8. The push-out specimen was loaded continuously until failure. A preliminary test was first conducted on specimen S1 in order to evaluate the failure mode and the damage to the shear connection. The specimen S1 was loaded and unloaded at every 11kN load intervals by force control. The specimen is

disassembled at these intervals for inspection on shear connection and FRP panel. Then the specimen was reassembled and loaded to the next load interval. The following tests on the specimen S2 to S8 are conducted with displacement control at loading rate 3mm/min with displacement range as 0 to 38mm. From the test results of these 8 push-out specimens, a load displacement curve of the shear connection was established.

Fatigue test is then conducted on 10 push-out specimens as test Phase II. The test specimens are numbered as F1 to F10. The same push-out specimens and test setup are used for fatigue test. Stress ranges on the shear stud and corresponding fatigue life cycles are two primary control parameters. A pilot test on specimen F1 was conducted to obtain preliminary data and define the subsequent testing program. The load range is defined as 30% of the connection ultimate strength and is from 11kN to 47kN. The corresponding stress range is 93MPa. Here, the stress range is defined as load divided by the cross section area of stud.

Subsequently, tests on F2 to F10 are conducted on five different stress ranges, or load ranges, which correspond to 15%, 20%, 40%, 60%, and 70% of shear connection ultimate strength. The load ranges are, 11kN - 29kN, 11kN - 35kN, 11kN - 59kN, 11kN - 83kN, and 11kN - 95kN. The corresponding stress ranges are 46MPa, 62MPa, 124MPa, 186MPa, and 217MPa (Table 2.1). All the specimens are subjected to unidirectional cyclic loading with a loading frequency of 4Hz, which is close to the fundamental frequency for normal highway bridges, 2Hz-5Hz.

Based on test results, an S-N curve is established as a function of stress ranges versus corresponding life cycles, which is the fatigue resistance of the connection.

Table 2.1 Fatigue Test Results

Test	Fatigue Load (kN)		Stress Range (MPa)	Load Ratio	Rate (Hz)	Life Cycles (million)
	Min	Max				
F1	11	47	93	30%	4	2.58
F2	11	29	46	15%	4	13.84
F3	11	35	62	20%	4	8.36
F4	11	35	62	20%	4	10.25
F5	11	59	124	40%	4	1.01
F6	11	59	124	40%	4	1.55
F7	11	83	186	60%	4	0.39
F8	11	83	186	60%	4	0.69
F9	11	95	217	70%	4	0.13
F10	11	95	217	70%	4	0.25

2.4.4. Fatigue Test on a Scaled Bridge Model

Following the test on push-out specimens, the shear connection was tested on a scaled bridge model (Figure 2.8a, b). An FRP deck was attached to three steel stringers to form a scaled bridge model. The FRP deck was 5.5m long by 2.74m wide. The FRP deck has the same honeycomb sandwich geometry as push-out specimens which was also produced by KSCI. The three stringers were steel wide-flange sections, W16x36. Each stringer had 9 shear studs welded on the top flange at 0.6m center-to-center spacing. Correspondingly, the shear connections were installed at these locations. There were 27 shear connections in total for this model. A concentrate load was applied at the mid-span

of the middle stringer. The model was then subjected to 10.5 million cyclic loading, which was equivalent to 75 years bridge service life-span (Moon *et al.*, 2002). The fatigue load was predetermined as a comparable level to the corresponding fatigue load of a reference full scale bridge, which was designed to withstand AASHTO LRFD fatigue truck load. Based on this relationship, the stress range on the shear connection of the scaled bridge model was determined as 3.3MPa. The loading was stopped at every 2 million load cycles and the stiffness of the model was measured.

Figure 2.8a Scaled Bridge Model

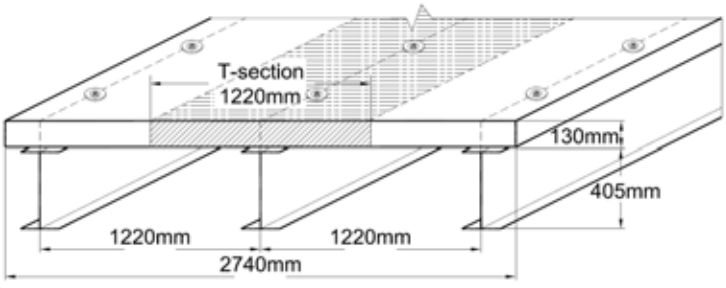

Figure 2.8b Scaled Bridge Model

2.5. Test Results and Design Formulation

Test results are evaluated in this section. Based on the test results, design formulations are proposed for both strength and fatigue resistance of shear connections.

2.5.1. Static Strength and Load Displacement Formulation ($P-\Delta$ Curve)

The preliminary test and inspection on specimen S1 revealed the deformation and failure mechanism of connection. The details of the preliminary test are briefly described below.

The shear stud started to deform at about 11kN with a displacement of about 10mm from the initial position. The shear stud deformation continued to increase as the load increased. When the load reached about 122kN, the deformation of the stud was about 38mm. The top steel sleeve displayed warping at both outside and inside washers (Figure 2.9). The purpose of the outside washer was mainly to constrain the FRP section. The purpose of the inside washer was to secure the panel and sustain the initial contact with the shear stud and transfer the shear force to the FRP section. Both outside and inside washers continuously deform throughout the loading. No delamination or crushing was observed on the top facesheet of the FRP section.

The bottom sleeve first made contact with the shear stud at about 22kN, and deformation was observed at the contact position between the bottom sleeve and the shear stud (Figure 2.10). Similar to the top sleeve, the outside washer of the bottom sleeve continuously

deform as the load increased. The deformation was more significant than the top sleeve. At the 22kN load stage, there was a steep slope change on the load-displacement response (Figure 2.16). The stiffness of connection increased significantly afterwards. This was mainly due to the bottom sleeve making contact with the shear stud and significantly increasing the stiffness of the shear connection.

For the FRP top facesheet, there was virtually no damage throughout the loading. While large deformation was observed at bottom facesheet where it makes contact with the stud and sleeve (Figures 2.11 and 2.12). However, the large deformation only occurs after yield of connection. The stud will finally be shear off at end of loading. The failure mode of this shear connection was defined as fracture of the root of the shear stud and delamination of the bottom facesheet.

Figure 2.9 Deformation to Outside and Inside Washer of Top Steel Sleeve

Figure 2.10 Deformation to Bottom Sleeve

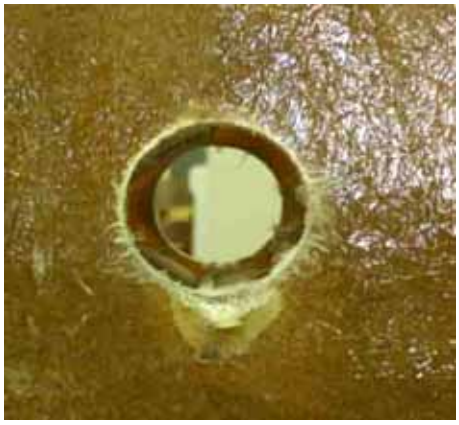

Figure 2.11 Bottom Facesheet at Yield

Figure 2.12 Bottom Facesheet at Failure

After the preliminary test, the following tests on specimens S2 through S8 were conducted. The yield strength and ultimate load of these specimens are listed in Table 2.2. From the load displacement relation (Figure 2.13), the connection displays two stages behavior with a separation point at 22kN.The shear connection has relatively low stiffness at early load stage for a range of about 22kN. Beyond this load, the stiffness of the connection increases significantly, with nearly linear elastic behavior until reaching yield strength. After yield strength and before failure, the connection continues to deform

at almost constant load plateau. The shear connection displays good ductility performance, which is provided mainly by yielding of the stud and delamination of the bottom facesheet.

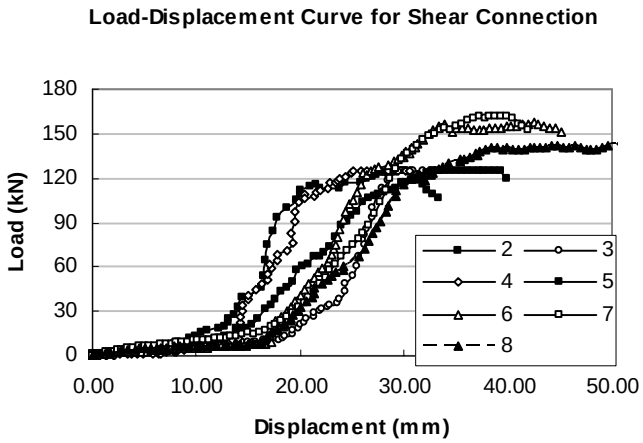

Figure 2.13 Loads and Displacements Data (Specimens S2-S8)

Table 2.2 Static Strength of Shear Connections

Specimen	Yield Strength (kN)	Ultimate Strength (kN)
S2	112	123
S3	113	126
S4	109	123
S5	103	124
S6	122	153
S7	125	161
S8	115	141

The yield strength of the shear connection varied from 103kN to 125kN, while the ultimate load varied from 123kN to 161kN. The variations are about 22% and 32%, respectively. The lower yield and ultimate strength in $P-\Delta$ curve are taken as lower bound values, 102kN and 120kN respectively. The discrepancies of strength values in the tests are largely due to: (1) manufacture and material non-uniformity of facesheet; and (2) manufacture imperfection of steel sleeves.

The recorded load displacement curve is idealized as a segmentally-linear model (Figure 2.14). The first inflection point is (22kN, 15mm). The stiffness of shear connection is increased about 5.4 times afterwards, from 1.46kN/mm to 7.87kN/mm. This stiffness change is mainly due to the bottom sleeve comes into contact with shear stud and FRP section. The shear connection exhibits elastic behavior until reaching yield strength, which is the second inflection point (102kN, 25mm). A nearly constant plastic deformation follows, until ultimate strength. The shear connection displays ductile behavior accompanied by larger deformation until the stud is sheared off. The stiffness of this shear connection is expressed as

$$\begin{cases} k = 1.46kN/mm, & \Delta = 0-15mm \\ k = 7.87kN/mm, & \Delta = 15-25mm \\ k = 7.87kN/mm, & \Delta > 25mm \end{cases} \tag{2-1}$$

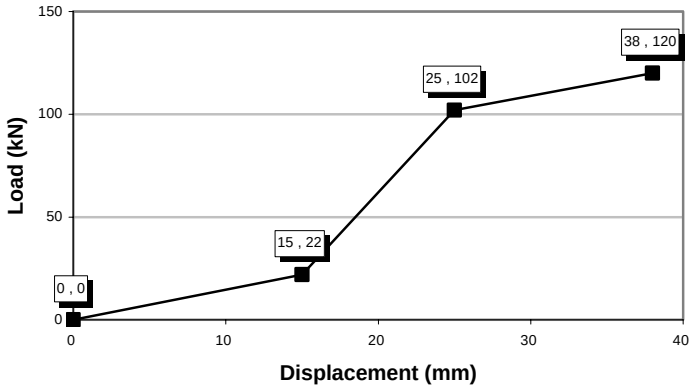

Figure 2.14 Segmental Linear Load Displacement Curve

2.5.2. Fatigue Strength and S-N Curve

The fatigue failure mode is identified as shear stud fatigue fracture accompanied by bottom facesheet delamination. The fatigue test results are shown in Table 2.1. By inspection of preliminary test specimen, the fatigue crack was initiated at the perimeter of the stud shank and weld area. As the load cycles increasing, the crack extended into steel base plate causing a concave depression. While the remaining uncrack stud area unable to sustain the fatigue loading, the shear stud is fractured and causes the connection failure (Figure 2.15). The bottom facesheet displays delamination at contact point with shear stud root (Figure 2.16).

Figure 2.15 Fracture of Shear Stud

Figure 2.16 Delamination of Bottom Facesheet

From relationship of fatigue load cycle and stress ranges (Table 2.1), a logarithm function is obtained by curve fitting (Figure 2.17), which is

$$\log N = 7.6 - 0.076S \qquad (2\text{-}2)$$

N - Number of load cycles

S - Stress range of shear connection (MPa).

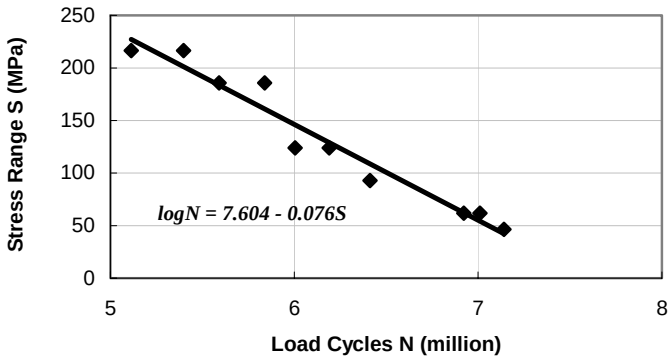

Figure 2.17 $S - N$ Curve of Shear Connection

From the regression function, when the fatigue stress range $S \leq 53MPa$, the shear connection life-cycle is longer than 10.5million, which corresponds to 75 years bridge service life span (Moon, 2002). Thus, this limit of $S \leq 53MPa$ is designated as the shear stress range threshold for 75 years fatigue life, for which the shear connection detail is defined as category A per AASHTO code.

2.5.3. Fatigue Resistance of Connection in Bridge Model

During the fatigue loading, the test was stopped at every 2 million cycle intervals. Then the model was loaded to investigate any stiffness degradation. As can be seen in Figure 2.18, the stiffness of this bridge model remained nearly constant throughout the loading history. No obvious stiffness degradation occurred. The shear connection and FRP deck showed that they are able to meet the fatigue resistance requirements by the AASHTO code.

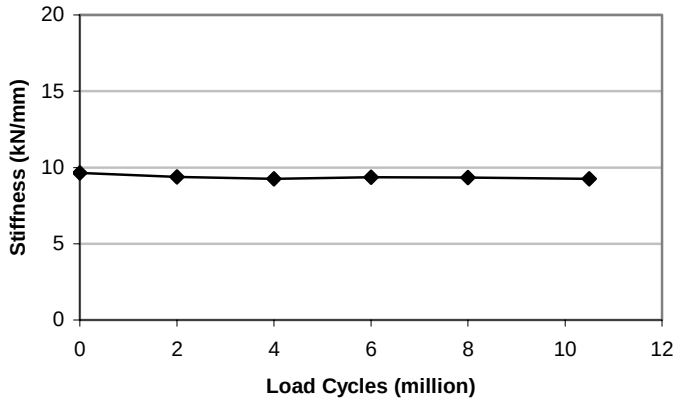

Figure 2.18 Bridge Stiffness Variations during Fatigue Test

2.6. Conclusion

A new type of shear connection is designed and proposed for FRP bridge decks with either sandwich or pultruded configurations. The shear connection is able to secure the FRP deck with the stringers and to transfer the interface shear force between the deck and stringers. Push-out specimens were tested to study both static and fatigue resistance of connection. The load displacement curve was established as a segmentally linear model. The connection shows good ductility after yield. The S-N curve was established for this shear connection by fatigue test. The shear connection was able to sustain cyclic fatigue loading equivalent to 75 years bridge service life-span. The shear connection was then further tested in a scaled FRP bridge deck model to evaluate its performance in a bridge system, showing nearly no stiffness degradation.

Several conclusions can be made: (1) the proposed shear stud type deck-to-girder connection provides adequate connectivity for FRP sandwich panels. The shear connection can effectively transfer shear force between deck and girder. Therefore, by using this connection in FRP bridges decks, composite action can be developed; (2) the sleeve connection design can prevent damage to FRP decks. In addition, it allows certain amount of differential displacements at interface and this property will develop partial composite action in FRP decks; (3) this shear connection is capable of sustaining cyclic fatigue loading of about 75 years bridge service-life span under AASHTO live load; (4) the installation process is also straightforward and easy.

The study on prototype shear connection shows that this connection is structurally efficient and can be used in practice. Further study on degree of composite action, effective flange width, and load distribution for FRP decks with this type of connection are being conducted on scaled bridge model and T-beam model in the following chapters.

CHAPTER 3

EXPERIMENTAL STUDY ON REDUCED SCALE FRP BRIDGE MODEL

3.1. Introduction

As shown in Chapter 2, the prototype shear connection proved to have the ability to secure the FRP decks as well as transferring shear force. A scaled FRP deck bridge model is then designed and tested in this Chapter. This bridge model is designed with FRP sandwich honeycomb deck connected to steel stringers by the prototype shear connection with partial composite action. The main objectives of the test are to evaluate the performance of FRP deck-connection system in the bridge. The partial composite FRP deck system with prototype shear connection will be accurately captured by the test. The test results will be later verified by FE analysis and analytical solution.

The test program consists of three phases. Phase I is a scaled FRP deck bridge model test with the objectives to investigate: (1) field deck attachment procedure; (2) transverse load distribution factors; and (3) local deck deflections and strains. Phase II test is a bridge model fatigue test with the objectives to evaluate FRP deck-connection system fatigue behavior. Phase III test is a T-section of 1.2 m wide, which is cut from the bridge model,

tested to failure. Phase III test focuses on: (1) effective deck-width; (2) degree of composite action and spacing of connectors; and (3) service-limit and ultimate-limit states under flexure loads.

3.2. Background and Problem Statement

In AASHTO slab-on-girder composite bridge analysis, the bridge is simplified to be an equivalent T-section, which is referred as beam line analysis. This procedure reduces the 3D bridge analysis into 1D composite beam analysis and could be easily solved by elementary beam theory. Commonly, two major parameters that need to be determined in this design procedure are the loading on the T-beam, which is defined by load distribution factor, and the resistance capacity of T-beam, which is defined by effective flange width.

The loading on T-beam usually includes dead load and live load. Dead load could be easily obtained as it is the unit weights of material multiply the section area. On the other hand, live load distribution is more complicated. Since for bridge deck-stringer system, which usually has high span to width ratio, the live load is distributed along the bridge width direction and depends on several factors, such as girder spacing, bridge section stiffness, and span length. In AASHTO code, the live load on an equivalent T-section is determined using by a load distribution factor multiplying the live load effect on the entire bridge cross section.

At meantime, the resistance capacity of the equivalent T-section is mainly determined by the effective flange width of the section. The effective flange width determines how much

deck portion participates in the T-section resistance. In AASHTO code, only full composite action is allowed and effective width is defined accordingly. However, for bridges with partial composite action such as FRP decks bridges, effective flange width is also affected by degree of composite action the bridge can achieve. Therefore, effective flange width for partial composite action bridges needs to be investigated.

Background materials and literature reviews on these topics will be briefly reviewed in the following sections. Also, current application of FRP deck bridges will be briefly reviewed as well.

3.2.1 Load Distribution Factor

The live load effect, induced by AASHTO truck load/tandem load and lane load, are distributed along the bridge cross section. The live load distribution is governed by several factors, such as girder spacing, girder stiffness, and span length. As a simplified design procedure, live load distribution factor is defined in AASHTO code to determine the corresponding load effect on an equivalent T-section. In both AASHTO Standard and LRFD code, the live load distribution factor is defined as the proportion ratio of live load on the most critical girder section to the total live load on the bridge. For example, the flexural moment on the girder section is $M = LDF * M_{total}$ (LDF is load factor, and M_{total} is the total moment induced by live load).

AASHTO has incorporated load distribution factor in bridge design for a long period of time, most notably since the first edition of the AASHO Standard Specifications in 1931.

AASHTO standard specification (1996) maintained its expression format with minor modification and defined distribution factor as $g = S / D$, which girder spacing divided by a constant. The constant D was defined for different bridge types. This load distribution factor was applied for one wheel line of truck load, which was half of the total truck load. The distributed live load effect was obtained by multiplying the governing live load effect induced by one line of wheel load with the distribution factor. The equation was valid for specified superstructure type, lane configuration, and girder spacing. The main problem for this distribution factor expression was that only limited number of parameters was included, which did not include all major variables that affect load distribution factor. Also the parameter ranges were very limited at the time developing this distribution factor expression. The distribution factor results are inconsistent and inaccurate in nowadays use for the bridges outside of these parameter limits.

In AASHTO LRFD specification (2004), distribution factors formulations were defined as a set of empirical function. They are obtained by parametric studies on large amount of bridges database. Because of its empirical nature, these load distribution factors would only be able to serve for bridges fall within its applicable limitations. For bridges that fall outside its limitation, the load distribution factor formulation usually gives poor results. Distribution factors were obtained for moment and shear effect separately. Girder spacing, span length and cross section properties were selected as major parameters in load distribution factor formulations. In AASHTO LRFD specification, the distribution factors were used for bridges with constant deck width and the number of beams was no less

than four. Also the beams were parallel and had approximately the same stiffness. For bridges outside of these ranges, overly conservative results were often obtained. The unit of this load distribution factor was one lane of live load, which was twice as much as in AASHTO Standard code (1996). The distributed load was obtained by multiplying the load effect of one lane of live load with the distribution factor.

Early Canadian Highway Bridge design code, CAN/CSA-S6-88, used the similar S/D expression as in AASHTO Standard specification to define the distribution factors. Different D values were defined for moment and shear distribution respectively. The Ontario highway bridge code, OHBDC 1983, used the similar distribution factors equations $g = S/D_d$. The D_d was determined based on the limit state and load effect and was a function of bridge types, class of highway, number of design lanes, girder location, span length and width of design lane.

Current CAN/CSA-S6-00 specification used an amplification factor to account for the transverse load distribution. The amplification factor for ultimate and service limit state was $F_m = \dfrac{SN}{F(1+\dfrac{\mu C_f}{100})}$. It was conceptually related to Ontario Highway Bridge Design Code (1991), which was based on the research by Bakht and Moses (1988) and Bakht and Jaeger (1990). F and C_f were determined from tables and were functions of the type of bridge, class of highway, girder location (interior vs. exterior), and span length, while μ was determined by design lane width.

In order to calibrate the accuracy of current codes on load distribution factors, many researches have been conducted FE analysis, analytical study and load test. Hays et al. (1986) investigated a set of bridges with varied span length from 9.1m to 36.6m. The analytical results of distribution factors were compared with the values from AASHTO Standard specifications and the Ontario Highway Bridge Design Code. Results showed that the AASHTO Standard specifications were unconservative for interior girders with span lengths less than 18.3m. While the Ontario Highway Bridge Design Code was somewhat conservative, the Ontario code was also very accurate in capturing the non-linear relationship between distribution factor and span length.

Mabsout *et al.* (1999) studied the accuracy of distribution factors on AASHTO Standard and LRFD Specification. Typical one- and two-span, two, three-, and four-lane straight composite steel bridges were selected with major parameters varied. The FE results were compared with AASHTO Standard and AASHTO LRFD codes. It was found that the AASHTO Standard specifications were less conservative than the AASHTO LRFD code for bridges with span lengths up to 18.3m and girder spacing up to 1.83m. As span length and girder spacing increasing, the AASHTO Standard code gave out more conservative results. Their study showed that the AASHTO LRFD code had better accuracy and matches well with FE analysis on distribution factor.

Shahawy and Huang (2001) conducted FE analysis to evaluate the load distribution in AASHTO LRFD code. The accuracy of AASHTO LRFD load distribution factors equations was assessed and the discrepancies with FEA and field results were found.

Totally 645 bridges were modeled by finite element method. The prediction by AASHTO LRFD code was quite accurate for interior girder under one lane loaded case and for exterior girder under two or more lanes loaded. However, large difference was found for certain conditions. Especially when the girder spacing exceeded 2.44m and deck overhang exceeds 0.9m the error could be up to 30%. Based on numerical data from this analysis, correction factors were developed for the load distribution factors formulations in AASHTO LRFD Specifications to ensure a more accurate and economic design of highway bridges.

Kim and Nowak (1997) performed field testing on two simply supported, steel I-girder bridges. Test results showed that AASHTO LRFD code overestimated the distribution factors by 28% and 19%. Fu *et al.* (1996) conducted live load tests on four steel bridges. It showed that the AASHTO code underestimated 13% to 34% for the tangent bridges and overestimated 13% for the skewed bridge. Eom and Nowak (2001) conducted load tests on seventeen steel bridges with span length from 33m to 148m. It was found that the AASHTO Standard codes were overly conservative for short spans bridges with small girder spacing, while AASHTO LRFD codes gave out more accurate distribution factors at these situations.

Effect of different variables on load distribution factors for slab-on-girder bridges had also been studied. Tarhini and Frederick (1992) showed that while girder spacing significantly affects live load distribution characteristics, their relationship was not linear. Their study showed that span length also affected the load distribution factors to some

extent. Bishara *et al.* (1993) and Tabsh *et al.* (2001) conducted FE analysis on highway bridges to study the span length effect on load distribution factor. The similar conclusions were reached that the span length had only minor effect on the live load distribution factor. On the contrary, works from Zokaie (2000), Mabsout *et al*. (1999), and Finch and Puckett (1992) showed that the live load distribution factor significantly decreased when the span length of the bridge increased. As result of their research efforts, girder spacing, span length, and girder stiffness had been determined to be the major parameters affecting the load distribution characteristics of bridges.

Besides the simplified formulations in design codes, analytical solutions were available and used in researches to study the structural behavior of slab-on-girder bridges, which was usually simplified to stiffened plate system. Some of them were approximate solutions, like orthotropic plate model and energy method. Others were finite element method or other numerical methods like finite difference methods or boundary element methods. Exact analytical solutions like, micro-approach, macro-approach, or U-transformation method, was also available. All of these methods had their unique advantages while dealing with certain type of problem, either as computational efficiency, getting tractable solution or dealing with more variables. But none of them could be a perfect match for all the problems. These analytical methods were briefly presented in the following paragraphs.

In orthotropic plate theory, the stiffeners were assumed to be smeared into the plate and the structure was replaced by an equivalent structurally orthotropic plate. The governing

equation of this orthotropic plate could be solved as a fourth-order partial differential equation with simple boundary condition. The solution was tractable so that continuous field solutions were able to be obtained. The orthotropic plate theory demanded equal and close spacing of stiffeners to ensure approximate homogeneity of stiffness. Also the stiffeners were to have almost identical section stiffness. Another limitation of the orthotropic plate theory was that the ratio of stringer rigidity to the slab rigidity could not be too large. Otherwise the beam action would be predominant. These restrictions limited the application of orthotropic plate theory. As the beam spacing increasing, the error became large compared to more accurate method like finite element method. And the stress evaluation between stiffener and plate was impossible, which was important to evaluate shear lag phenomenon. The plate stress result was only good at where it is away from the stiffener.

Energy based approach was available to analyze ribbed and grid plate system (Kukreti *et al.*, 1987, 1993). The accuracy of the energy based method mainly depended on the form of selected deflection function. Several polynomial and trigonometric series deflection functions were selected, which satisfied the essential boundary condition. The strain energy of supporting stringer and plate were computed along with potential energy of applied load. The solution was then compared with finite element result to select a most accurate deflection function. The advantage of energy based approach was that it can easily obtain the shear interaction between beam and plate or the torsion action of the beam. If the assumed deflection function was accurate, this approach was very computationally efficient.

Micro approach was a discrete-continuous field approach for the analysis of a ribbed plate (Dean and Omid'varan, 1969). Two independent variables were defined for field coordinates. One was continuous field coordinate along the beam line and the other was discrete field coordinate for the beam which was under consideration. For two side simply supported plate, double Fourier series with infinite number of terms was designated to continuous variables and finite number of terms for discrete variables. Equilibrium condition could be obtained from plate-beam interaction at each beam line. Then the force and deformation compatibility relations could be expressed by use of the plate stiffness coefficients. The deformations were in terms of plate deflection at beam line and rotations and could be solved by satisfying the boundary condition. The Micro approach could model membrane and flexural actions as well as torsion between beam and plate. It could get exact solution for two-dimensional problem, like structural lattice, but it could not be used in three dimensional problems which were widely used in building floor-column system.

Macro approach was mainly developed for ribbed and grid plate systems (Gangarao *et al.*, 1975). Compared to Micro approach, Macro approach got displacement solutions first for major components, plate and beam, under the unknown interactive force between those components. Then the unknown interactive force between beams and plate was solved by ensuring displacement compatibility condition at beam lines. Exact closed-form solution could be obtained with less computational effort. The stress and displacement functions were able to be obtained at any point directly. The restriction of Macro approach was that

the interior beams had to be evenly spaced with identical elastic properties. Macro approach was applied to solve series of plate problem with skewed and triangular shape plates (Gangarao *et al.*, 1986, 1988). Lopez and Gangarao (1995) extended the Macro approach to the stiffened orthotropic plate system under out-of-plane action. Based on the solution for stiffened orthotropic plate, Macro approach was applied to deck-and-stringer bridge system. An approximate series solution was proposed to compute the load distribution of this bridge system under symmetric and asymmetric load condition (Salim and Davalos, 1995). Experimental tests on two stress-laminated timber bridges were conducted. The series solution was validated by experimental and FE analysis results. This series solution then was applied on an FRP bridges system (Salim *et al.*, 1997).

Although there have been quite thoroughly studies on load distribution of concrete bridges, no systematic study has been conducted on load distribution of FRP deck bridges. The current design of FRP deck bridges can only based on engineering judgment and FE analysis.

3.2.2 Effective Flange Width

Due to in-plane shear flexibility of the deck section, the longitudinal normal stress in a bridge deck is non-uniform along its transverse cross section, which is known as shear lag phenomenon. The normal stress in the deck, along the longitudinal stringer or bridge-span direction, reaches maximum at the mid-line junction of the bridge stringer and deck; and the stress decays along the deck transverse section away from the junction line.

Exact solutions for stress distribution of the flange are complex. The flange stress distribution depends not only on dimension and cross section stiffness of the flange and stringer, but also on the loading conditions. Therefore, in design practice, effective flange width is used in design practice as an alternative to issue the shear lag phenomenon. Subsequently, the effective width is defined as a reduced width of deck, in relation to center-to-center spacing of stringers, over which the normal or longitudinal stresses are assumed to be uniformly distributed as in beam theory for a relatively compact T-beam section (Figure 3.1). The stress integral over the effective width should equal to stress integral over actual flange width. This effective width is uniform along the span length for simplicity. It is generally expressed as $b_e = \frac{\int_{-b/2}^{b/2} \sigma_x dx}{\sigma_{\max}}$, b_e is the effective flange width, b is the actual flange width, which is center-to-center of girder spacing in bridges, σ_x is the normal stress on the flange, and $\sigma_{\max}$ is the maximum normal stress at the junction point of flange and web.

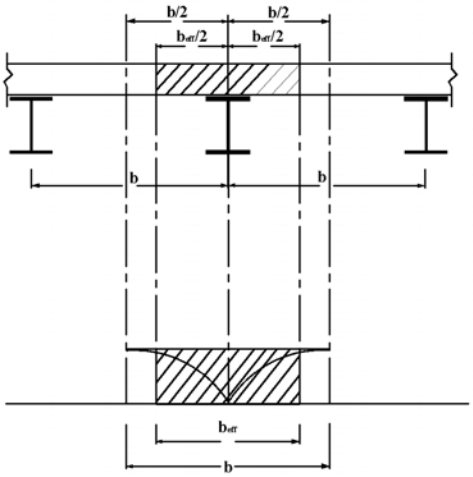

Figure 3.1 Effective Flange Width Definition

The effective width concept was adopted in both AASHTO Standard and AASHTO LRFD specifications. In AASHTO standard specification (1996), effective flange width was defined primarily for concrete decks in composite steel bridges to account for shear lag phenomenon. It distinguished the interior and exterior girders. For interior girders, the effective flange width took the least of following: (1) One-fourth of the span length of the girder; (2) The distance center to center of girders; (3) Twelve times the least thickness of slab. For exterior girders, the effective flange width took the least of following: (1) One-twelfth of the span length of the girder; (2) One-half the distance center to center of girders; (3) Six times the least thickness of slab.

In AASHTO LRFD bridge design specification (2004), for interior girders, the effective flange width took as the least of following: (1) One-quarter of the effective span length; (2) 12 times the average thickness of the slab, plus the greater of web thickness or one-half the width of the top flange of the girder; (3) The average spacing of adjacent girders. For exterior girders, it took as one-half the effective width of the adjacent interior girders, plus the least of: (1) One-eight of the effective span length; (2) 6 times the average thickness of the slab, plus the greater of half the web thickness or one-quarter the width of the top flange of the girder; (3) The width of the overhang. The main difference between AASHTO LRFD code and AASHTO standard code was that AASHTO LRFD adds girder dimension into consideration.

Canadian highway bridge design codes (1988) defined the effective flange width in

similar form as the AASHTO Standard code. After adopting the Ontario highway bridge design code, the current Canadian highway bridge design codes (2000) used the formulations primarily developed by Cheung and Chan (1978). In the formulations, the effective flange width consisted of the sum of a central flange part and overhang flange parts. The central flange part corresponded to the flange on a steel beam, and the side part was determined as follows:

$$\frac{B_e}{B} = 1 - [1 - \frac{L}{15B}]^3 \qquad \text{for} \qquad \frac{L}{B} \le 15$$

$$\frac{B_e}{B} = 1 \qquad \text{for} \qquad \frac{L}{B} > 15$$

Where L was the span length for simply supported spans, or length of positive or negative region under dead load moments, B_e was the effective width (overhang or one-side), and B was the left-hand, right-hand overhang. Unlike AASHTO codes, which used lists of description, it used two formulae that considered span length and girder spacing at the same time to account their combined effect on effective width.

In these design codes, AASHTO standard and LRFD codes both used lists of description to define effective flange width. The new Canadian highway bridge code used two equations. Both AASHTO and Canadian codes considered span length and girder spacing as most important parameters that affected effective width. Additionally, AASHTO LRFD codes also included slab thickness and girder dimension as other parameters. From the literatures, at ultimate limit state, the slab would be in plastic stress range after yielding of structures. Therefore, effective flange width was larger in ultimate limit state than in service limit state. However, for conservative and simplicity consideration, both

AASHTO and Canadian codes applied same effective flange width definition for service limit state and ultimate limit state.

Researches on accuracy of effective flange width formulation in specifications had largely been focused on one or more variables. These researches were conducted by mainly using FE analysis and load test. Moffat and Dowling (1975) studied the shear lag phenomenon in steel box girder bridges by FE analysis. The box girder bridges were loaded with both uniform load and point load. The girder spacing to span length ratio b/L of flange was the most significant parameter affecting the effective flange width. As for the orthotropic properties of steel flange, when the ratio of longitudinal extensional rigidity to the shear rigidity increased, the effective flange width would decrease. The loading type and load position were two other factors that affect the effective flange width. While the point load moved away from mid-span section, the effective flange width decreased. For uniform load, the effective flange width was practically constant over the span length.

Moffat and Dowling (1978) later studied the effective flange width provision in British bridge code. It was concluded that the nondimensional parameter, the flange width to span length ratio b/L, was of the most dominant parameters in determining the effective width. It was also concluded that for most practical bridges, girder size and deck thickness had little effect on the effective flange width. Since majority of the governing loads in bridge design could be approximate to uniformly distributed loads, it was justified that only the effective width for uniform load was included in the code, which

meant the effective width was taken uniform value along the span.

Cheung and Chan (1978) used finite strip method to study a wide range of steel bridges and box girder bridges. It was also concluded that the variables that girder spacing and bridge span length were major variables on determining effective flange width, while slab thickness and girder section had little effect on it. The effective flange width was found to be independent of the number of traffic lanes. The analysis results showed that the effective flange width obtained from multiple girder bridge models under uniformly distributed load was the upper bound value, while the effective flange width obtained from single T-beam under point load was lower bound value.

Davalos and Salim (1993) studied effective flange width for 125 stress laminated timber bridges by FE analysis. Empirical equation for effective flange width was proposed for stress laminated timber bridges. The regression function included the predominant variables on the effective flange width of stress laminated timber bridges. Stringer spacing b, bridge span length L, ratio of stringer depth to deck thickness $\frac{D}{t}$, ratio of longitudinal stringer elastic modulus to deck elastic modulus $\frac{E_s}{E_d}$ were included in the empirical functions as major variables.

Tenchev *et al.* (1996) conducted FE parametric study on the shear lag phenomenon in orthotropic T-beams. Empirical equations for effective flange width were proposed based

on this parametric study, which included major parameters $\frac{E}{G}$, $\frac{b}{L}$, and $\frac{T_f}{T_w}$. E is extensional modulus of the slab. G was shear modulus of the slab. b was actual flange width. L was beam span length. T_f was flange thickness and T_w was beam web thickness. In case of small $\frac{T_f}{T_w}$ and high $\frac{E}{G}$ ratio (i.e. fiber reinforced laminated composite plate with stiffeners), this empirical equations displayed better accuracy compare to the available analytical solution. The empirical equations also provided good result when applied to beams with longitudinal stiffeners, thin steel plate with stiffeners and fiber reinforced laminated composite plate with stiffeners.

Ahn *et al.* (2004) used a simply supported reference bridge to compare the effective width value from several design codes, AASHTO, BS5400, Canadian code, Japanese code, and Eurocode 4. The flange width to span length ratio b/L was used as a controlled variable. Among these codes, BS5400 gave out the largest effective flange width when L/b was between 2 to 7. For $7 \le L/b \le 15$, Eurocode 4 gave out the largest effective flange width. The full flange width was obtained after L/b reached 8 for Eurocode 4, 15 for Canadian code, and 20 for the Japanese code. Because of the slab thickness limitation, effective flange widths from AASHTO varied considerably compare to others.

Amadio *et al*. (2004) evaluated the effective flange width in Eurocode 4 at ultimate strength state. Tests were conducted on four composite T-beams until failure. It was found that the effective flange width approached the whole slab width when the T-beam was

close to failure. While same effective flange width was defined for service limit state and ultimate limit state in Eurocode 4, it was concluded that it was overly conservative for ultimate limit state. A modification formula was proposed. Different effective flange width definitions were used at service limit state and ultimate limit state in order to have a more economy design.

Among all those researches on effective flange width, major factors that affected the effective flange width were determined as span length and girder spacing, while extensional modulus, shear modulus, slab thicknesses, load condition, continuity condition, and limit state, were also affect the effective flange width to some extent.

Although theoretical methods were usually overly complicated to be directly used in design practice, analytical solutions were developed in order to have better understanding in shear lag phenomenon. Adekola (1968) developed an analytical method that counts for both plane stress effect and bending stress effect in shear lag phenomenon. Effective breadth was subsequently divided into shear effective breadth and bending effective breadth. Both dead load and live load were considered in analysis. It was found that when L/b greater than five, effective width was almost constant throughout the span length.

Adekola (1974) proposed a more rational basis in defining effective flange width. The effective flange width was defined from girder deflection perspective rather than flange stress perspective, which was widely accepted by most of the researchers. In his definition, effective flange width was defined as that the T-section has same deflection as

the T-section with actual flange width. By adopting this new effective width definition, study on shear lag phenomenon with partial interaction in steel and concrete composite structures was conducted. The results showed that effective flange width increases with degree of interaction.

Song (1990) conducted harmonic shear lag analysis using plane stress for the flanges of simple or continuous beams with different girder cross sections. Simplified empirical formulas and diagrams for determining the shear lag effects in simple beams under various loading conditions were presented.

3.2.3 Degree of Composite Action

Park (Park *et al., 2006)* developed the expression for degree of composite action as $\frac{N_p - N_0}{N_{100} - N_0} = DCA$ (DCA is degree of composite action; N_0 is neutral axis position of non composite action; N_{100} is neutral axis position of full composite action; N_p is neutral axis position of partial composite action). Usually, N_0 and N_{100} could be easily obtained by analytical method. While N_p is normally obtained by experimental method.

3.2.4 Current Development and Application of FRP Deck Bridges

There have been many projects of FRP bridge decks with either sandwich and pultruded panel configurations. Some of them used mechanical connection while others used adhesive connection to the stringers. The studies on FRP bridge decks were mostly based on field- or lab-scale testing results. Keelor *et al.* (2004) conducted a field study on a

short-span bridge located in Pennsylvania. This bridge had a pultruded FRP deck over five steel girders equally spaced at 1.75m; the span-length was 12.6m, and the deck thickness was 195mm. The FRP deck was assumed to achieve full composite-action through grouted stud connections welded to the stringers. Their results showed that under service load condition, this full composite action design resulted in effective-widths corresponding to about 90% for interior and 75% for exterior, respectively, of stringer-spacing and half stringer-spacing.

Keller and Gurtler (2005) conducted lab tests on two large scale T-sections to study composite action and effective-width. Each test model was 7.5m long with a pultruded FRP deck section of 1.5m wide adhesively bonded to the top flange of a steel supporting beam. The normal strain distribution across the width of the FRP section was recorded at both upper and lower FRP facesheet components. The results showed that under service limit state, the normal stress was almost uniform across the panel section. While under failure limit state, the normal stress decreased towards the panel edges, indicating a more pronounced effect of shear lag under ultimate load.

Later, two reduced scale T-sections were tested to service limit state and ultimate limit state (Keller and Gurtler, 2005). One of the T-section was fatigue loaded to 10 million cycles. The FRP pultruded flanges, which were adhesively bonded to the steel stringers, were able to achieve full composite action. At ultimate limit state, the failure mode was deck compression failure with the yielding of steel stringer. The structural behaviors of this full composite model were well established at service limit state and ultimate limit

state. The deflection and ultimate strength could both increase by 30% and 56% by considering composite action. There were strain differential between top and bottom facesheet due to low in-plane shear stiffness of the core. The strain distribution of top and bottom facesheet showed that the top facesheet fully participated as a top cord, while bottom facesheet showed more shear lag phenomenon. The effective flange width was smaller than the effective flange width of a comparable concrete deck. Also the T-section could sustain 10 million cycles of fatigue loading, which was comparable to the Eurocode 1 fatigue load on a reference bridge.

Further more, fatigue tests on two T-beams with 7.5m span length and adhesively bonded FRP flange and steel stringers were conducted (Keller and Tirelli, 2005). The pultruded FRP flange was full compositely connected to the steel stringers and the FRP flange participated as the top cord of this T-section. The fatigue limit was to be 25% of static failure load at 10 million load cycles, which was far above the actual fatigue load in FRP bridges. The adhesive bond connection was proved to be able to sustain the fatigue loading induced by fatigue truck load.

3.2.5 Problem Statement

For conventional concrete deck steel stringer bridges, full composite action is usually preferred due to its better performance and efficiency in material utilization. In AASHTO code, slab-on-deck bridges are designed with non-composite or full-composite action. No partial composite action is allowed in concrete deck bridge design. However, FRP decks are usually designed with partial composite action in practice. Several limiting practical

factors lead to this application: (1) The hollow core configuration of FRP panels and lack of continuous connection at panel-stringer interface are difficult to develop adequate contact and bonding between decks and connections; (2) the high modulus ratio between steel-girder and FRP-panel (about 30 compare to 8-10 for conventional concrete deck to steel girder) makes the contribution of FRP deck in overall bridge stiffness less significant; (3) the practical connection spacing of about 0.6m to 1.2m for FRP decks, compare to conventional concrete deck connection spacing of 0.15m to 0.25m, is not enough to develop full composite action. All these factors in turn will lead to less shear force to be transferred between decks-girder and achieve less degree of composite action. On the other hand, it may actually be desirable to accommodate some degree of deck-stringer relative displacement for differential thermal expansions between FRP and steel.

Therefore, certain behaviors to reflect the partial composite action in FRP decks system need to be investigated. Several issues like: (1) transverse load distribution factors; (2) degree of composite action; (3) effective deck-width; and (4) service-limit and ultimate-limit capacity such as fatigue resistance and ultimate failure mode; need to be thoroughly studied. Issues that bring up by distinctive properties of FRP deck like: (1) local deck deflections; and (2) deck-connection installation procedure also need to be evaluated.

3.3. Objectives and Scope

Based on the prototype shear connection in Chapter 2, the FRP deck-connection system is identified as partial composite structure. Therefore, its structural behavior needs to be investigated. In this Chapter, experiments on a scaled bridge model, and a T-section

model will be carried out. The tests will be followed by FE analysis and analytical solution verification in Chapter 4 and 5.

The test consists of three phases. Phase I is a static test on a scaled bridge model. The scaled bridge model consists of FRP honeycomb deck and is connected to three supporting stringers. The bridge model is designed as comparable to a reference bridge, and conforms to current AASHTO code. The model is point loaded to simulate AASHTO truck load. The objectives are to investigate live load distribution factor and local deflection of FRP decks.

In Phase II test, the bridge model undergoes cyclic loading up to 10.5 million cycles, which equals to 75 years bridge service life span defined by AASHTO LRFD code. The fatigue resistance of the FRP bridge decks and shear connections are evaluated.

In Phase III test, a T-section is cut out from the bridge model. It is loaded under flexural loading until failure. The objectives of this T-beam test are to investigate the effective flange width, degree of composite action, and the failure mode and ultimate strength of the T-beam.

3.4. Scaled FRP Bridge Model

This scaled bridge model is a 1:3 scale of a reference bridge, which is designed according to AASHTO limits and requirements. The model consists of an FRP deck honeycomb deck and steel supporting girders. The FRP deck is connected to steel stringers by the

prototype shear connections. The static and fatigue tests are carried out as three phases. Their objectives are to study FRP decks behavior and performance, such as load distribution, effective deck width, panel local deflection, degree of composite action, and fatigue resistance. The results will be later verified and validated by FE analysis and analytical solutions.

3.4.1. Bridge Model Description

The bridge model consists of 3 steel stringers (W16x36, Gr50) with span=5.5m and spaced 1.22m on centers (Figure 3.2). A 5.5 m x 2.74 m x 0.13 m FRP deck was attached to the stringers using the prototype stud-sleeve connector, for two spacing conditions of 0.6 m and 1.2 m. The deck consists of 3 individual FRP honeycomb panels from KSCI, each is 1.8 m wide and 2.74 m long, assembled by tongue-and-groove connections along the two 2.74 m transverse joints. The longitudinal direction of the honeycomb core (Figure 3.2) is oriented along the 2.74 m width of the model, perpendicular to the traffic direction of the bridge. Later a 1.2 m wide T-section will be cut out from the model (Figure 3.3) and tested to failure.

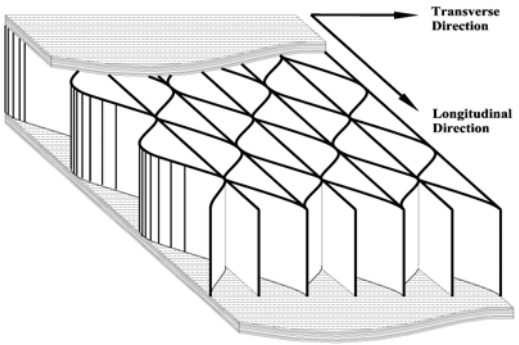

Figure 3.2 KSCI honeycomb FRP panel

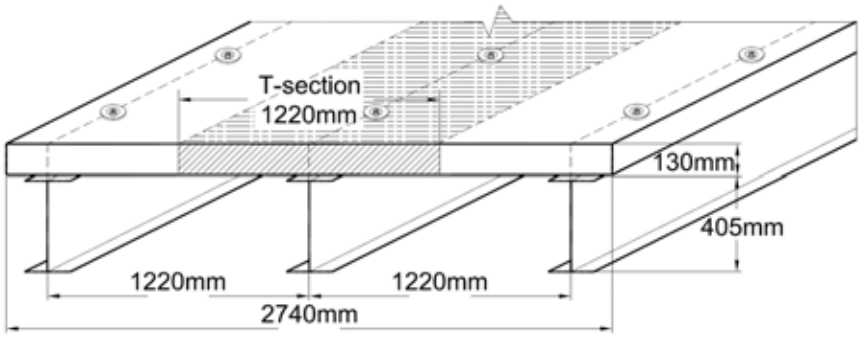

Figure 3.3 Scaled bridge model

The tongue and groove connections are filled with polymer resin and the joint area are covered by fiber glass sheet covered (Figure 3.4, Figure 3.5). During the assembly of the model, the steel stringers were first erected and braced at the supports and mid-span. The shear studs were already welded at 0.6 m spacing beforehand. Then, 80 mm circular holes were drilled at 0.6 m spacing on the FRP panels, and the panels were fitted through the studs on top of the steel stringers. The 3 panels were snug-fitted by transverse tongue-and-groove connections, which were joined by polymer resin and strips of fiber glass sheets bonded atop and along the joints. As shown in Figure 3.4, each of the tongue and groove honeycomb-core sections of about 0.15 m wide were filled with polymer concrete in order to strengthen the joint. The deck installation was relatively simple and straightforward (Figure 3.6).

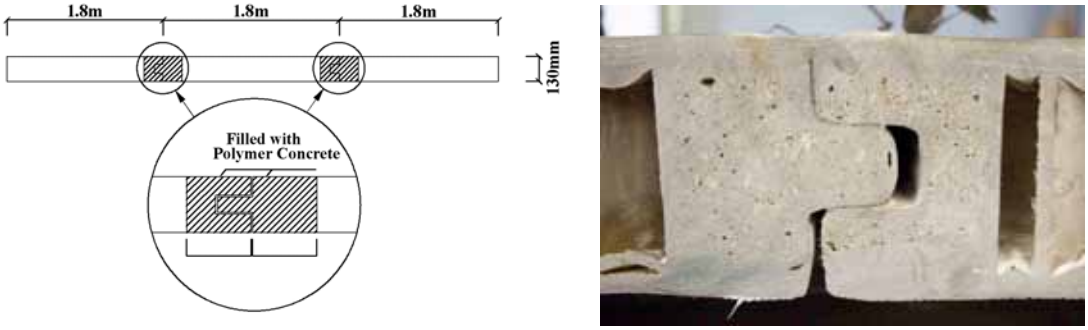

Figure 3.4 Tongue-and-groove connections

Figure 3.5 Tongue and Groove Connection with FRP Sheet Covered

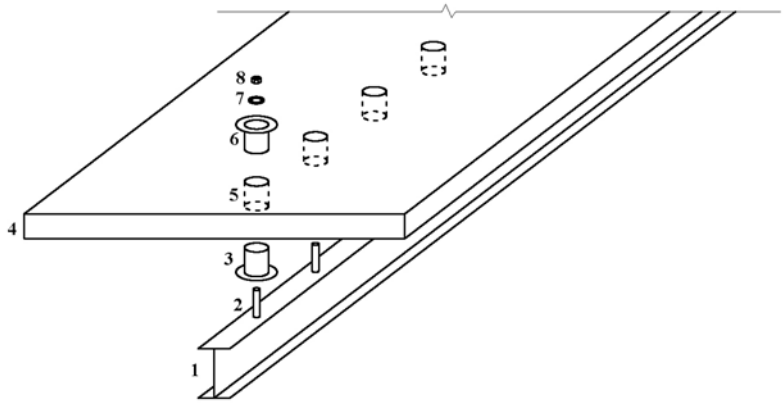

Figure 3.6 Installations of Shear Connection to FRP Decks

The model was tested at 0.6 m and 1.2 m connection intervals, using the mechanical stud-sleeve connector described above. The model is first tested at 0.6m connection intervals. Then, by taking off top sleeve of the connections at every 1.2m intervals, the rest of the connections are spaced at 1.2m interval and the test will continue.

For field-assembly, the author is investigating a more practical approach: delivering engineered panel sections with tongue-and-groove ends and pre-drilled holes with bottom sleeves already installed; then assembling the bridge deck in the field over the stringers by bonding and reinforcing the panel-to-panel connections; then welding the partially threaded shear studs through the cut-out holes using a stud-gun with a special tip (the appropriate size of pre-drilled holes on FRP decks is an issue for further consideration); finally placing the top sleeves and secure the deck by tightening the connections with a torque range. After completion of connection assembly, the bridge model is erected (Figure 3.7, 3.8, 3.9). Phase I and II test will be conducted on the bridge model.

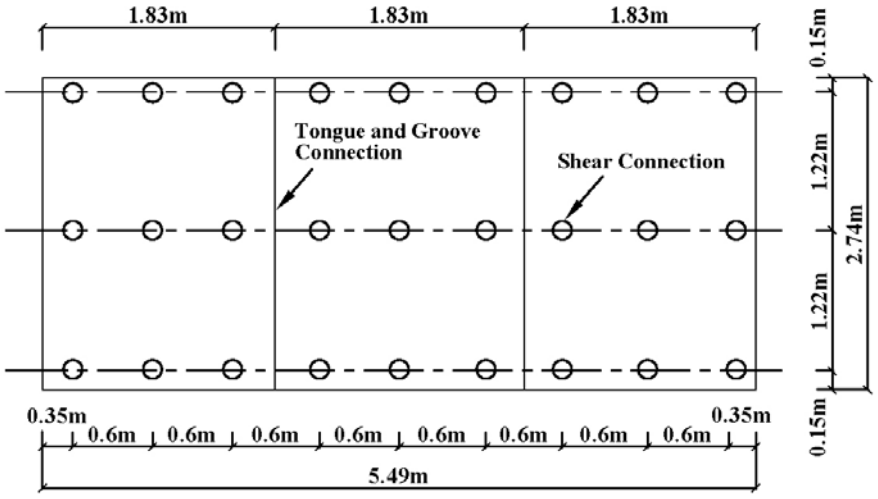

Figure 3.7 Plan View of Bridge Model

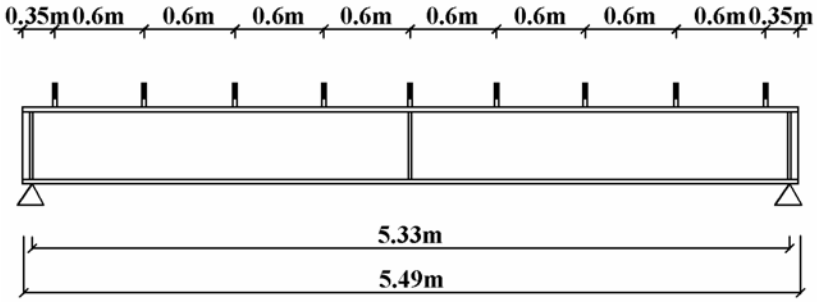

Figure 3.8 Elevation View of Bridge Model

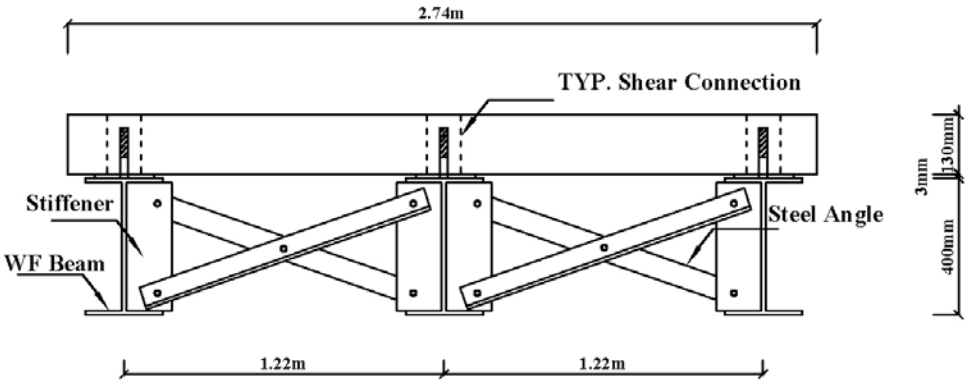

Figure 3.9 Cross Section of Bridge Model

3.4.2. T-section Model Description

After completion of Phase I and II test, a T-section is cut out from the scaled bridge model (Figure 3.3). The T-section is 1.22m flange width supported by a steel stringer. Three brackets were placed on each side of the flange to provide lateral support to the flange section. A 0.6 m by 0.25 m patch load was applied at the mid-span of the T-beam by a 490 kN actuator (Figure 3.10). Phase III test will be conducted on T-section Model.

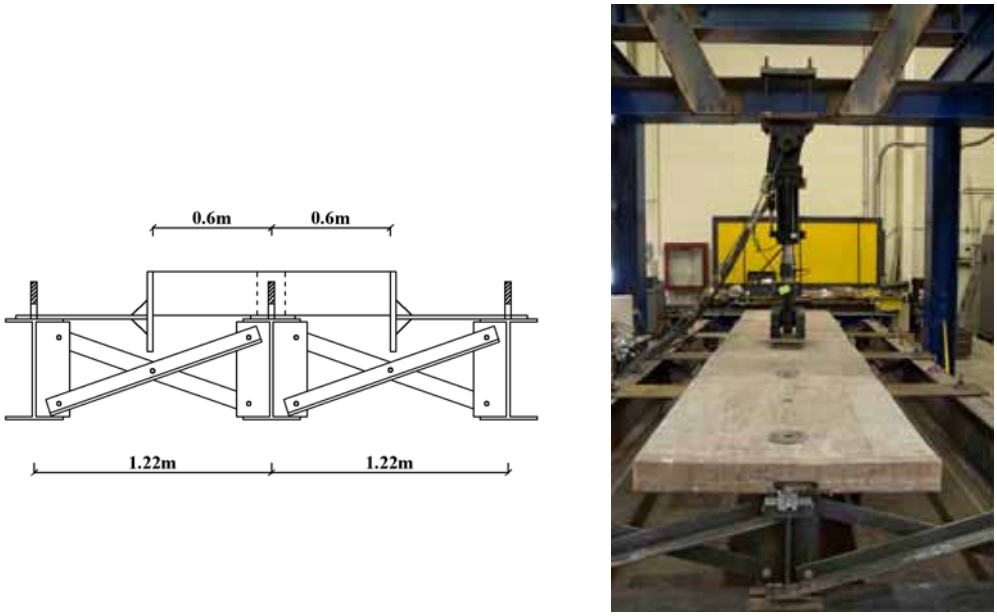

Figure 3.10 Cross Section of Test Model

3.5. Test Procedure

The test consists of three phases. Phase I is the static test on FRP deck bridge model. It is followed by Phase II test, fatigue test on the bridge model. In Phase III test, the cut-out T-section is tested to failure.

3.5.1. Phase I Test

In Phase I, the objectives of testing the scaled bridge model were to evaluate: (1) deck attachment procedures; (2) transverse load distribution factors; and (3) local deck deflections and strains. Load case 1 is a concentrate load at mid-span and over the middle stringer (Figure 3.11). The concentrate load was applied over an area of 0.6 m by 0.25 m, using a 245 kN actuator to simulate truck wheel load. The model was loaded to 50% service limit load by displacement control rate of 1mm/min.

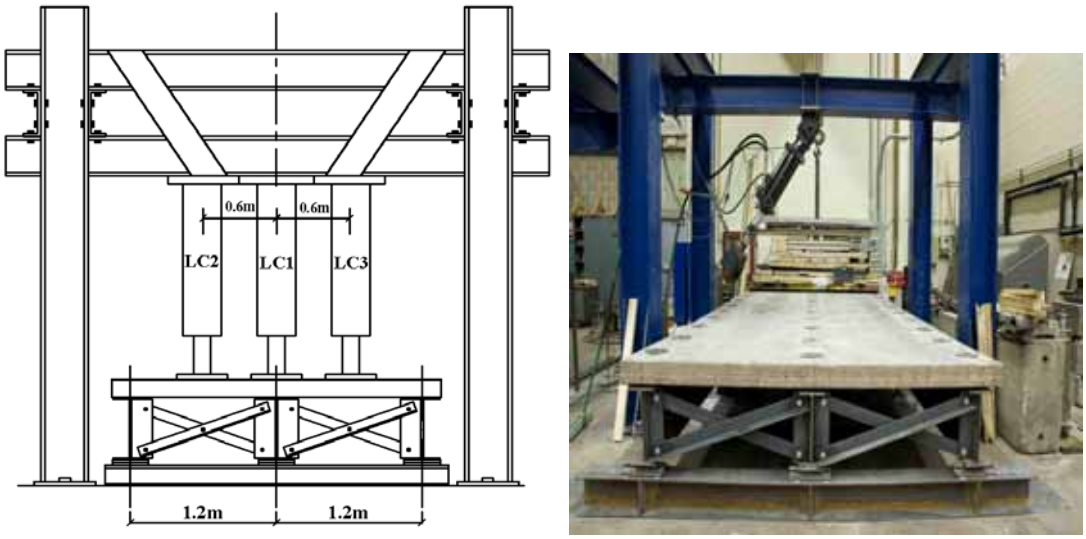

Figure 3.11 Bridge model test

The 50% service load was defined according to AASHTO LRFD specification (2004). For both steel flanges of the non-composite sections the stress limit is defined as

$$f_f \le 0.80 R_b R_h F_{yf} \tag{3-1}$$

Accordingly, the service stress limit was 275 MPa for the Gr50 steel stringers in this

model. Therefore, the model was loaded until it reaches 138 MPa flange stress and it corresponds to 50% service stress limit.

The load distribution factor was evaluated under this load condition. The model was instrumented accordingly. As defined by Eom and Nowak (2001), load distribution factor is expressed as

$$LDF = \frac{\varepsilon_i}{\sum_{i=1}^{3} \varepsilon_i} \tag{3-2}$$

where ε_i is the maximum strain at the bottom flange of the ith stringer. Therefore, maximum strains for each stringer were measured by strain gauges bonded at bottom flanges of the stringers. Strain gauges were placed on both sides of the flange to minimize possible measurement errors (Figure 3.12).

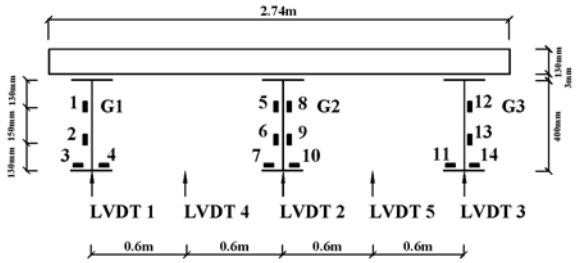

Figure 3.12 Instrumentation of bridge model

Load cases 2 and 3 were defined to study the deck local deflection (Figure 3.12). A 36kN concentrate load, corresponding to a rear wheel-load of an HS20 truck load, was applied at either between stringers 1 and 2 or stringer 2 and 3 (Figure 3.11). Load cases 2 and 3

were symmetrically positioned and final deck local deflection results were taken as the mean values of these two load cases.

Table 3.1 Load Case Designation

Load Case	Transverse Load Position	Connection Spacing (m)	Label
1	Aligned with stringer 2	0.6	LC1
1	Aligned with stringer 2	1.2	LC1
2	Aligned with mid-point of stringer 1,2	0.6	LC2
2	Aligned with mid-point of stringer 1,2	1.2	LC2
3	Aligned with mid-point of stringer 2,3	0.6	LC3
3	Aligned with mid-point of stringer 2,3	1.2	LC3

Measurement of local deflection is obtained by the transverse deflection profile which is plotted by 5 transducers (LVDT) across the mid-span section, with LVDT 1, 2, and 3 placed under the stringers 1, 2, and 3; and LVDT 4 and 5 placed under the FRP panels and centered between the two supporting stringers. Theoretically, the local deflection is the vertical displacement of panels induced by wheel loads. Thus, the local deflection (h) was defined as the relative displacement of the panel between the two supporting stringers by linear interpolation, as shown in Figure 3.13 (h_1 and h_2 are the deflections of the stringers, h_3 is the deflection under the concentrate load over the panel).

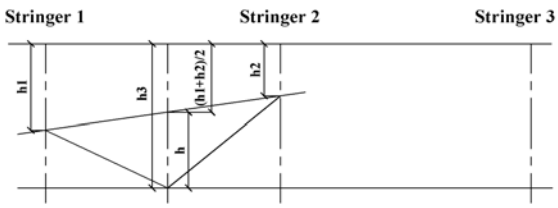

Figure 3.13 Local deflection definitions

3.5.2. Phase II Test

Phase II test is the fatigue test of the bridge model. The model was subjected to 3-Hz cyclic loading of up to 10.5 million cycles, which was equivalent to a service lifespan of 75 years (Davalos and Zou, 2008). The fatigue loading is limited below the threshold design stress limit which is obtained on the connector's S-N curve in Chapter 2.

The fatigue load on shear connection is designed as comparable to the corresponding fatigue load of a reference bridge, which is loaded by AASHTO LRFD fatigue truck configuration. Detailed design procedure is referred to appendix A. The stress range on shear connection of reduced scale bridge model is defined as 53MPa and the fatigue load range is from 0 to 112kN. During the fatigue loading, at every 2 million cycle interval, the loading is stopped and the model is unloaded to measure the bridge stiffness.

3.5.3. Phase III Test

In Phase III test, a T-beam section was loaded under three point bending with displacement control rate of 1mm/min until failure. Load-displacement relation, service load, and ultimate load are recorded. The objectives are to evaluate the following: (1) degree of composite action; (2) effective deck-width; and (3) service-limit and ultimate-limit states behavior under flexure loads.

As the effective flange width is defined $b_e = \frac{\int_{-b/2}^{b/2} \sigma_x dx}{\sigma_{\max}}$ (b_e is the effective flange width, b

is the actual flange width, which is center-to-center of girder spacing in bridges, σ_x is the normal stress on the flange, and $\sigma_{\max}$ is the maximum normal stress at the junction point of flange and web). The effective width is obtained by integration of the normal strains of FRP flange. In the test, strain values are measured at the discrete locations and $\int_0^b \sigma_x dx$ are obtained as the summation of trapezoidal area created by these strains (Figure 3.1). Totally 20 strain gauges were attached at top and bottom surfaces of deck, 10 at quarter-span and 10 at mid-span (Figure 3.14), to measure the longitudinal normal strain of the FRP flange.

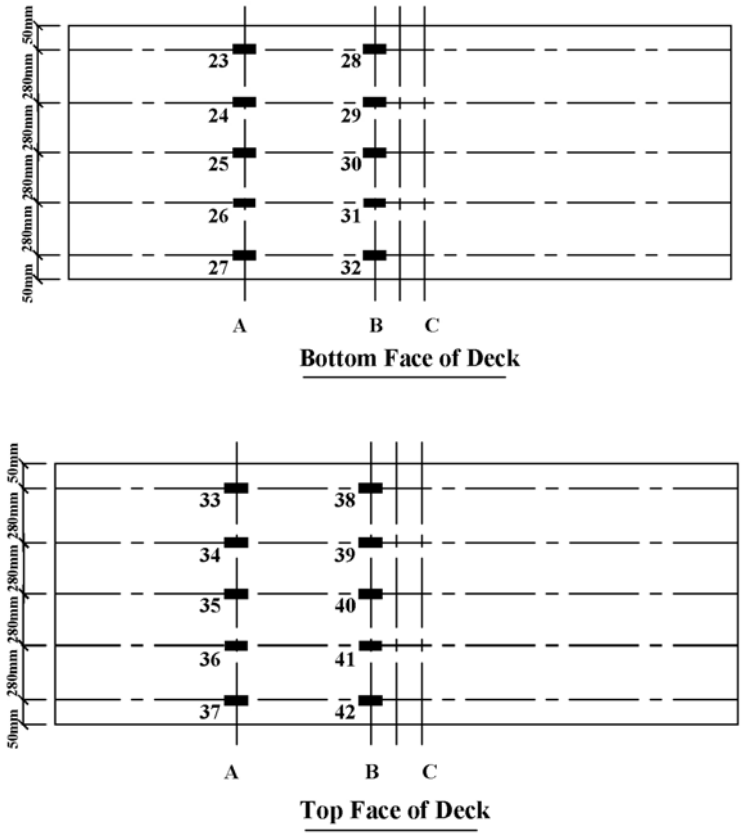

Figure 3.14 Instrumentation of T-beam FRP deck section

In addition, strain gauges were attached along the depth of stringer to measure the longitudinal normal strain of the stringer (Fig. 3.15). Neutral axis of T-section can be plotted accordingly as the strain distribution along section depth. Subsequently, degree of composite action is obtained by expression $\frac{N_p - N_0}{N_{100} - N_0} = DCA$ (Park *et al.*, 2006). For the tested T-section, N_0 and N_{100} are 202mm and 256mm, respectively.

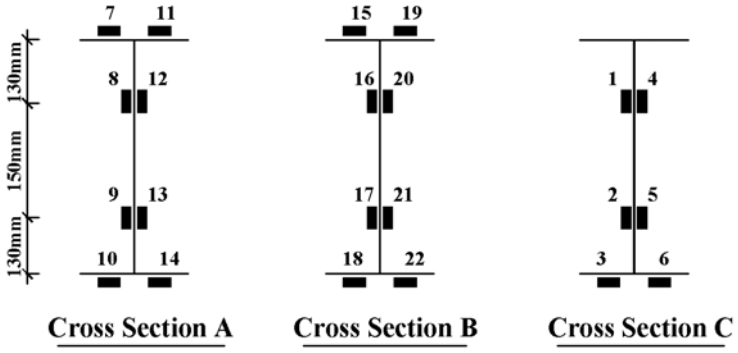

Figure 3.15 Instrumentation of T-beam Girder

3.6. Test Results

The experimental data are organized and plotted. Test results are evaluated and summarized in this section.

3.6.1. Load Distribution Factors

The load distribution factor of is about 0.647, which is for interior girders with 0.6m connection spacing. Similar result is obtained for 1.2m connection spacing and is about

0.644.

As reference, the load distribution factor is calculated by AASHTO code. In AASHTO standard code (AASHTO, 1996), load distribution factor is S/D=0.727 (8ft spacing as for the reference bridge), for which D=5.5 is mainly for concrete deck bridges. While in AASHTO LRFD code (AASHTO, 2004), load distribution factor is 0.655.

Table 3.2 Load Distribution Factor of Test Model

Connection Spacing	0.6m	Diff. (%)
AASHTO Standard	0.727	12.3%
AASHTO LRFD	0.655	1.2%
Phase I Test	0.647	

The test result is about 1.2% more than AASHTO LRFD code and is about 12% more than AASHTO Standard code. Although AASHTO LRFD does not specifically include FRP deck bridges, combine with equivalent properties method to obtain transform bridge section properties (Davalos et al., 2001), it gives out reasonable load distribution factor. Thus, AASHTO LRFD formula can be used as an alternative method to evaluate load distribution factor of FRP deck bridges. More accurate result can be obtained by using a closed-form series solution, which will be proposed in the following chapter.

3.6.2. Local Deck Deflection

As shown in Figure 3.16, the induced deflection profile clearly displays the localized effect at loading position. The loading point, which is at 0.6m of left side of origin, has the largest deflection of about 3.33mm. The local deflection is about 1.65mm to 1.75mm. The deflection is about L/726. In AASHTO LRFD code, there is no deflection limit for

FRP bridge decks. While there is provision for orthotropic bridge deck which is L/300, it is usually for steel orthotropic deck with ribs. Many researchers have suggested L/400 as deflection criteria for FRP decks (Demitz 2003; Zhang and Cai 2007). Therefore, the local deflection for this FRP panel is considered to be acceptable. For bridges with overlays, excessive deformation can cause premature deterioration of the wearing surface. One possible solution to reduce the deformation of FRP deck is to add horizontal steel bracing between stringers and consists of a supporting grid under FRP decks. The FRP deck spacing is subsequently reduced and the deformation is expected to be much smaller than current scheme.

Table 3.3 Deflection Profile of Test Model

0.6m connection spacing		
Deflection Point	Deflection (mm)	Local Deflection (mm)
1	1.905	
2	3.327	1.651
3	1.448	
4	0.203	
5	0.076	
1.2m connection spacing		
Deflection Point	Deflection (mm)	Local Deflection (mm)
1	1.930	
2	3.404	1.753
3	1.397	
4	0.203	
5	0.102	

3.6.3. Degree of Composite Action

As proposed by Park (Park *et al.*, 2006), the degree of composite action is expressed as $\frac{N_p - N_0}{N_{100} - N_0} = DCA$. The only unknown, the neutral axis N_p of T-section, is plotted in Figure 3.17, which is about 213mm to 218mm. Thus, the degree of composite action of

T-section is about 25.3%. As for T-section neutral axis, the impact of connection spacing is only marginal. For both 0.6m and 1.2m connection spacing, they have practically same degree of composite action.

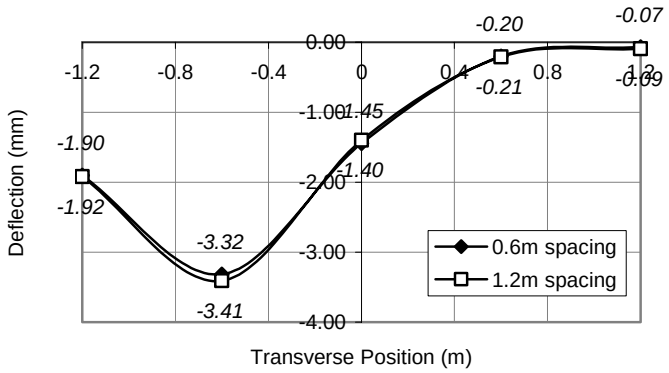

Figure 3.16 Deflection Profile

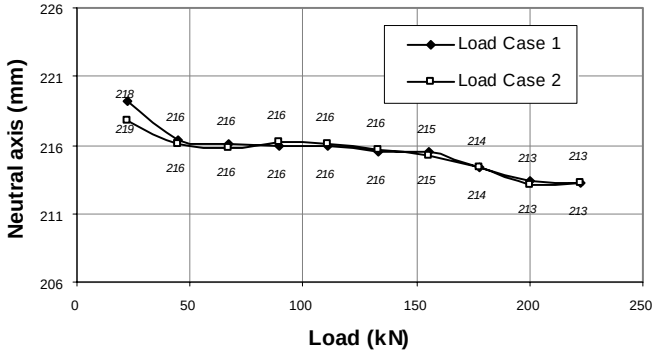

Figure 3.17 Neutral Axis Position for Load Case 1 and 2

3.6.4. Effective Flange Width

Strain profile at mid-span is plotted at both top and bottom of deck surface (Figure 3.18, 3.19). These strain values are connected linearly to form trapezoidal shape stress blocks.

The integral of these stress blocks, or stress resultant, are the summation of area of each stress block (Figure 3.20). Effective flange width is then obtained as the ratio of stress resultants to maximum strain, $b_{eff} = (\int_{-b/2}^{b/2} \sigma_x dx) / \sigma_{\max} = \sum_{i=1}^{n} \sigma_{x,i} h_i / \sigma_{\max}$. The resulted effective flange width is 0.63m, which is about 50% of actual flange width.

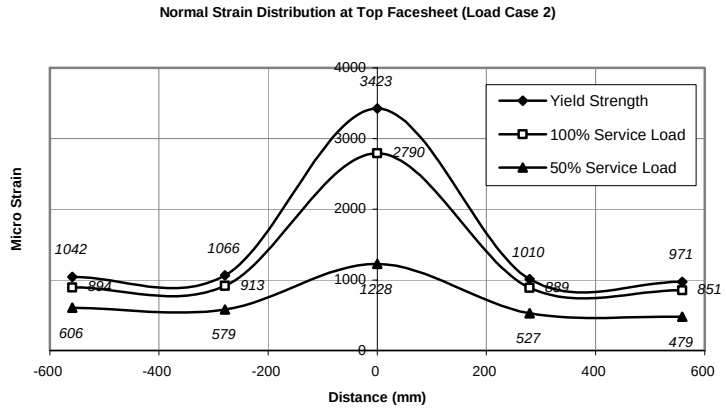

Figure 3.18 Normal Strain Distribution on Top Facesheet of FRP Panel

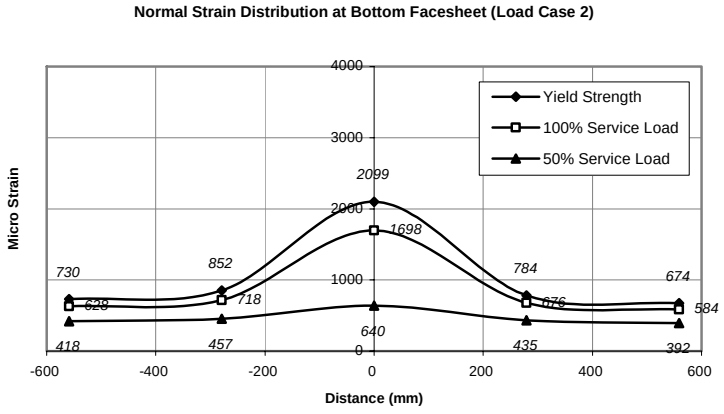

Figure 3.19 Normal Strain Distribution on Bottom Facesheet of FRP Panel

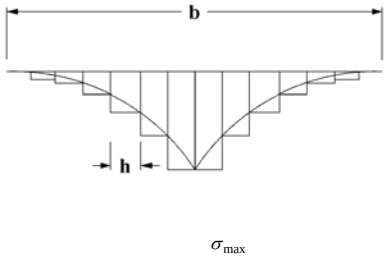

Figure 3.20 Stress Integration of the Flange

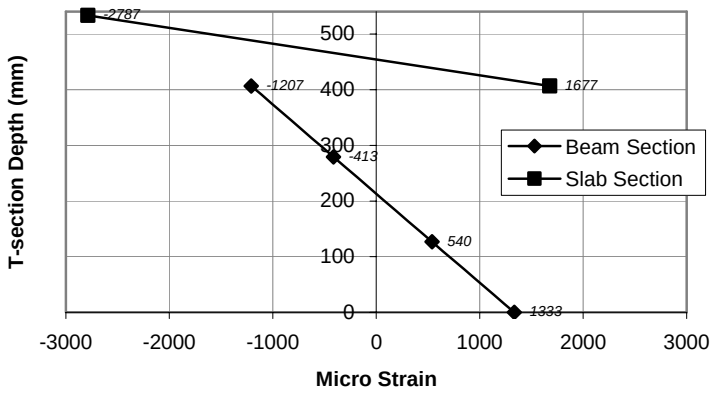

Figure 3.21 Axial Strain Distribution at Mid-span Section (Load Case 1)

3.6.5. Failure Mode at Strength Limit

The T-section displays linear elastic behavior before the load reaches 267kN. Afterwards the load deflection curve is flatter with the maximum load reaches about 356kN. The maximum deflection at ultimate limit stage is about 2.5 times the deflection service limit stage. At ultimate limit stage, the T-section is failed by the flange local buckling of steel stringer. This means FRP bridge deck can not brace the steel girder as effectively as concrete. Further study can be focused on this area.

Figure 3.22 T-section at Failure

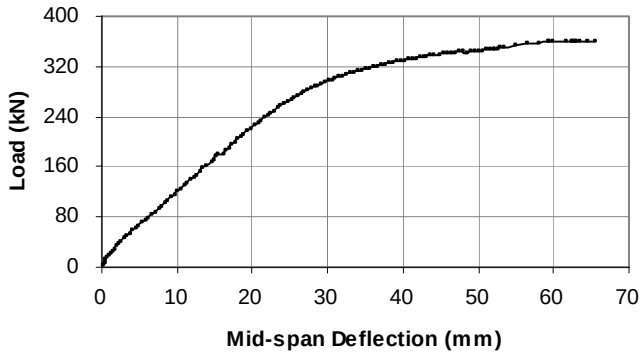

Figure 3.23 Load Deflection Curve for Load Case 2 at Mid-span

3.6.6. Fatigue Resistance

During the fatigue test of bridge model, the loading is stopped at every 2 million cycle interval and the model is statically loaded. The stiffness of the model is measured and shown in Table 3.4, which is the ratio of loading to mid-span deflection. Throughout the

test, the stiffness degradation is only about 4%. Especially after 2 million load cycles, the stiffness remains almost constant. This is mainly because all components, like tongue and groove connection and shear connection, have settled in. Therefore, the bridge model is proved to be able to meet the fatigue resistance requirements by AASHTO code.

Table 3.4 Stiffness Ratio of Bridge Model during Fatigue Test

Load Cycles (mil)	Load (kN)	Deflection (mm)	Stiffness (kN/mm)
0.000	171	17.8	55.044
2.000	169	18.0	53.558
4.000	166	17.9	52.835
6.000	167	17.9	53.432
8.000	167	17.8	53.325
10.500	167	18.0	52.904

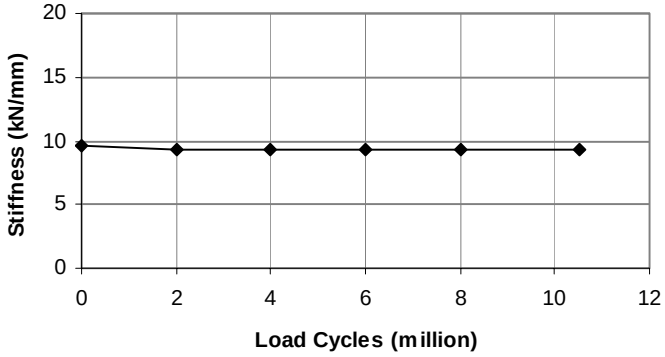

Figure 3.24 Stiffness Ratio Variations during Fatigue Test

3.7. Conclusions and Summaries

The FRP bridge decks model is proved to be structurally viable and effective by the service load test. The model displays linear behavior during the test. Of all the test results, the load distribution factor is close to series solution and FE predictions. The test validates the series solution as a simple analytical method with reasonable accuracy for

FRP bridge decks.

The sleeve type shear connection, the same as these used in push-out test is applied in bridge decks model. It is proved to be able to transfer interface shear force between FRP decks and steel stringers. All three stringers achieve similar degree of composite action. In construction point of view, because it is non-grouted and easy to be installed, the sleeve type shear connection is a cost effective solution for FRP bridge decks application in bridge engineering. Also, the panel local deflections for 2ft and 4ft connection spacing are both within AASHTO LRFD deflection limit. The shear connection concept in FRP decks is proved to be effective in improving the structural performance of FRP bridges.

In fatigue test, the induced shear stress range on shear connections is comparable to the stress range on a reference bridge. The fatigue stress is fairly small and is well within the fatigue stress limit, which is obtained in push-out test in Chapter 2. The overall stiffness of the bridge model has little change throughout the fatigue loading. The shear connection and FRP decks are proved to be able to meet the fatigue resistance requirements by AASHTO code.

Several observations and conclusions are made based on the test results:

(1) About 25% degree of composite action can be achieved with the prototype shear connection. Comparing to non-composite section, T-section with partial composite action gains about 13% increase of service load and 7% increase of ultimate strength. The effective flange width is about 50% of the actual flange width;

(2) The panel local deflection ratio is about L/730. In AASHTO LRFD code, there is no deflection limit for FRP bridge decks. Many researchers have suggested L/400 as deflection criteria for FRP decks. Therefore, the local deflection for this FRP panel is considered to be acceptable;

(3) The failure mode of FRP decks is steel stringer yielding with adequate ductility. The ultimate load mainly depends on the strength capacity of the steel stringers;

(4) Two different connection spacing used in the model, 0.6 m and 1.2 m, does not have significant impact on structural behavior or performance, such as load distribution factor or degree of composite action. Thus, 1.2m connection spacing is an adequate and cost-effective for this FRP deck-connection system;

(5) The FRP panel, shear connection, and tongue and groove connection remained visibly undamaged after the test, even at failure. The shear connection and FRP decks also showed adequate fatigue resistance to satisfy AASHTO fatigue load requirement.

APPENDIX A: DESIGN OF A FRP SLAB-STEEL STRINGER BRIDGE

In order to simulate the interface shear stress state in the test model, a reference bridge is designed follow AASHTO LRFD specification (2004). This two lanes bridge has 5 W40*249 Gr50 rolled steel girders with 8ft center to center girder spacing. This bridge is 36ft wide total and accommodate two design lanes. The span length is 70ft and is simply supported. The reference bridge adopted similar concept of test model as use the FRP panel as bridge deck along with shear connection. 10in thickness FRP honeycomb sandwich panel is connected to the steel girders with shear connection. The FRP panel facesheet lay-up is same as used in the test. The material properties of facesheet and core are referred to chapter 3. Equivalent properties are adopted in this design as well, which means the honeycomb FRP deck is generalized with homogenous panel properties.

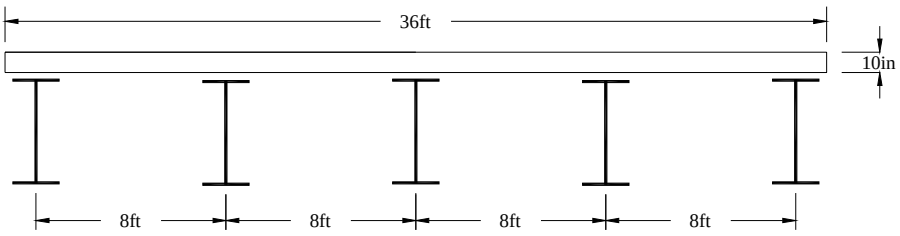

Figure A.1 Cross Section of Reference Bridge

The purpose of design this reference bridge is to simulate the interface shear stress state under fatigue loading. The bridge is designed for interior girder under flexural condition to meet the requirements of strength, service, and fatigue limit state. The bridge is

designed as non-composite section for strength and service limit state for simplicity. For fatigue limit state, partial composite action is considered.

1. Load Combination

Strength I Limit State

$$U = \eta[1.25DC + 1.50DW + 1.75(LL + IM)]$$

Service II Limit State

$$U = 1.0(DC + DW) + 1.0(LL + IM)$$

Fatigue and Fracture Limit State

$$U = 0.75(LL + IM)$$

2. Live Load Effect

For this bridge with 32ft horizontal clearance, the number of lanes is selected as 2 lanes bridges. Multiple presence factor is 1.0.

Strength Limit State

Dynamic allowance is 33%. Distribution factor for moment is obtained from series solution, which is 0.599 for interior girder with two lanes loaded.

Live load moments for truck, tandem, and lane load are

$$M_{tr} = 32(17.5) + (32 + 8)(10.5) = 980 kips - ft$$

$$M_{ta} = 25(17.5 + 15.5) = 825 kips - ft$$

$$M_{\ln} = \frac{0.64(70)^2}{8} = 392 kips - ft$$

Therefore, interior girder moment is

$$M_{LL+IM} = 0.599[980(1.33) + 392] = 1015.5 kips - ft$$

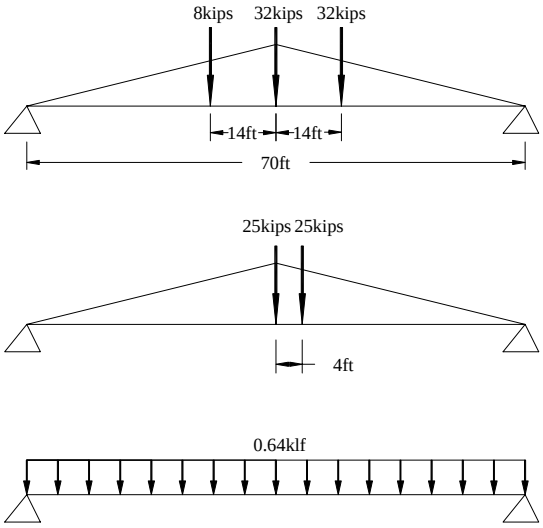

Figure A.2 Truck, Tandem and Lane Load Placement for Maximum Moment

Service Limit State

Distribution factor for live load deflection is DF=m(N_L/N_b)=1*(2/5)=0.4lanes

Fatigue and Fracture Limit State

Dynamic allowance is 15%. Distribution factor for moment is obtained from series solution. 0.401 for interior girder with one lane loaded. The fatigue load is a single design truck with 14ft front axle spacing and 30ft rear axle spacing.

3. Dead Load Effect

The dead load of steel girder is 250lb/ft.The bridge FRP deck is assumed as 15pcf in density.

DC: slab = 0.0125*8=0.1kips/ft

steel girder = 0.25kips/ft

DW: wearing surface = 0.025*8=0.2kips/ft

The induced maximum moment will be

$$M_{DC} = \frac{0.35(70)^2}{8} = 214.4 kips - ft$$

$$M_{DW} = \frac{0.25(70)^2}{8} = 153.1 kips - ft$$

4. Strength Limit State Check for Interior Girder

Factored strength I moment

$$M_u = 0.95[1.25(214.4) + 1.50(153.1) + 1.75(1015.5)] = 2161.0 kips - ft$$

This rolled beam satisfies the compact section requirements. The plastic moment is

$$M_n = ZF_y = 1120 * 50 = 4666.7 kips - ft > M_u$$

5. Service Limit State Check for Interior Girder

Live Load Deflection Control

a. From design truck alone

The front wheel load is P_1=0.4*8*(1+0.33)=4.256kips

Two rear wheel load is P_2=P_3=0.4*32*(1+0.33)=17.024kips

The corresponding deflection can be obtained from AISC manual.

The live load deflection is $\Delta_{tr} = 0.366 + 0.370 = 0.736in < \frac{span}{800} = 1.05in$

b. 25% of design truck and the design lane load

The live load deflection due to 25% truck load is $\Delta_{25\%tr} = 0.184in$

The live load deflection due to lane load is $\Delta_{\ln} = 0.243in$

The total deflection is $\Delta_{total} = \Delta_{25\%tr} + \Delta_{\ln} = 0.184 + 0.243 = 0..427in < \frac{span}{800} = 1.05in$

Permanent Deflection Control

For both flange of non-composite sections

$f_f = 0.80 R_h f_{yf} < 40ksi$

The service II moment is

$M_s = 1.0(214.4 + 153.1) + 1.3(1015.5) = 1687.7kips - ft$

$f_f = \frac{M_s}{S} = \frac{1687.7 \times 12}{993} = 20.39ksi < 40ksi$

6. Fatigue Resistance for Shear Connection

The un-factored maximum shear force range under LL+IM is 62.3kips at support, which is the maximum along the span. The shear range on interior girder could be obtained by multiplying the un-factored shear force range by dynamic load allowance, 1.15, the load distribution factor for 1 lane loaded case, 0.401, and by the load factor for fatigue limit state, 0.75. The resulted shear force range is 21.55kips. This shear range will act on the corresponding T-section with effective width is taken as half of the girder spacing, which

is 4ft.

To calculate the corresponding shear stress range in this partial compositely bridge, a linear elastic analysis procedure is adopted (Newmark *et al.*, 1951). The shear flow at the slab and stringer interface can be obtained. The shear flow reaches the maximum value at bridge support. In order to sustain the fatigue loading, the shear connection should be able to resist this induced shear stress. Detailed analysis procedure can refer to Newmark *et al.* (1951). The induced maximum shear flow at the interface of this bridge is $q = 6.008 \times 10^{-3} kips/in$. Therefore, for 4ft connection spacing case, the shear at this 4ft spacing is obtained by multiply the connection spacing with the shear flow, which is 0.288kips. Therefore, the induced the shear stress at shear connection is 0.479ksi. To simulate the fatigue load condition in test model, the stress range at test model should be the same as in the reference bridge. Therefore, the bridge model is loaded at the mid-span with 0-25.1kips cyclic load.

CHAPTER 4
FE ANALYSIS OF SCALED BRIDGE AND T-SECTION MODEL

4.1. Introduction

Finite element analysis is conducted in this chapter to verify the experimental results. Since this FRP deck-connection system is a partial composite structure, both bridge model and T-section model will be constructed by properly considering the partial composite behavior, which is defined by the connection properties in Chapter 2. The FRP deck as honeycomb structure is cumbersome to be modeled as its actual geometry. Therefore, an equivalent properties method proposed by Davalos (Davalos et. al, 2001) is applied in FE modeling of FRP panel. In this method, the actual honeycomb geometry of FRP panel is represented by a solid panel with same dimension and equivalent homogeneous engineering properties of FRP panel. This equivalent panel then could be modeled as shell element. Steel stringer will be modeled by shell element as well. The FE analysis result will be used to compare with and verify the test result.

4.2. FE Model description

Finite element model of the FRP bridge model and T-section model are constructed by ABAQUS (2002). The model consists of three major components, FRP deck/flange,

shear connection, and steel stringer. The test procedure is simulated in FE analysis. The results are compared with experimental data.

4.2.1 FRP Panel and Equivalent Properties

Due to the uniqueness of FRP composite materials and the honeycomb sinusoidal core structure, to model the actual geometry of FRP honeycomb panel will hugely increase the complexity of FE model. It will also bring up the requirement to model the contact zone of shear connection and panel, which will bring more complexity to the model. In the meantime, more detailed modeling will not guarantee to have better prediction on structural global behavior for the purpose of this study. Therefore, an equivalent properties method will be applied in the modeling of FRP panel to facilitate the modeling process.

Equivalent properties method of FRP panel is proposed by Davalos (Davalos *et al.*, 2001). In this method, the actual honeycomb geometry of FRP panel is represented by a solid panel with same dimension and equivalent homogeneous engineering properties of FRP panel. This equivalent FRP panel has the same global behavior as the panel as actual honeycomb configuration. At the same time, it eliminates the necessity of modeling the sinusoidal core geometry. Therefore, the equivalent properties method will greatly facilitate the modeling process. Subsequently, this equivalent FRP panel is modeled by S4R shell element.

The tested FRP panel is honeycomb sandwich panel with sinusoidal core configuration. It consists of top and bottom facesheet outside and a sinusoidal core inside (Figure 4.1). The laminate lay-up of top and bottom facesheet is balanced. The facesheet has three CDM 3208 laminate with two chop strand mat between them. A $0.256\,(kg/m^2)$ chop strand mat is placed between facesheet and core as a bonding layer. The total thickness of one facesheet is 12.5mm. The total thickness of the FRP panel is 125mm with 100mm height core.

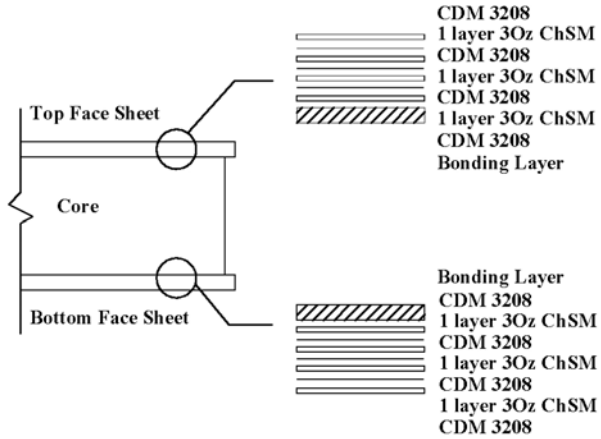

Figure 4.1 Facesheet Lay-up

The properties of facesheet and core material are listed in Table 4.1, 4.2, and 4.3. The equivalent properties of FRP panel, such as bending stiffness and shear stiffness, are listed in Table 4.4. Detailed procedures to obtain the equivalent engineering properties of this FRP panel can be referred to Davalos *et al.* (2001). The equivalent properties are verified by an evaluation test on three discrete panels and adjusted accordingly to reflect the actual panel properties (Appendix B).

Table 4.1 Material Properties of Facesheet

		Nominal Weight (kg/m^2)	Thickness (mm)	V_f
CDM 3208	0°	0.531	0.49	0.424
	90°	0.601	0.55	0.425
	CSM	0.256	0.25	0.396
Bonding Layer	ChSM	0.915	1.91	0.188

Table 4.2 Stiffness Properties of Facesheet Lamina

	$E_1(MPa)$	$E_2(MPa)$	$G_{12}(MPa)$	$G_{23}(MPa)$	ν_{12}	ν_{23}
CDM 3208	35900	11100	2810	3030	0.305	0.509
CDM 3208 CSM	17400	17400	6200	6200	0.406	0.406
Bonding Layer	9820	9820	3510	3510	0.397	0.397

Table 4.3 Stiffness Properties of Facesheet and Core

	$E_x(MPa)$	$E_y(MPa)$	ν_x	$G_{xy}(MPa)$
Facesheet	13600	14100	0.304	3500
Core	530	1.0	0.431	0.7

Table 4.4 Equivalent Properties of FRP Panel

	$E_x(MPa)$	$E_y(MPa)$	ν_x	$G_{xy}(MPa)$
In-Plane	2560	2300	0.303	560
Bending	5640	5640	0.303	1400

4.2.2 Steel Stringer

The steel stringers were also modeled by shell elements. The cross bracing is modeled by two node beam elements. Pin-roller constraint was used to represent the simply-supported boundary conditions of the test.

4.2.3 Shear Connections

Since the FRP panel connection system displays partial composite action as shown in test results, the interface movement of panel and stringer needs to be properly considered in FE model. As illustrated in Chapter 2 and 3, the incomplete interaction in FRP deck is mainly due to relatively low stiffness of shear connection. In order to model the shear connection in FE model, the following assumptions are made. The shear connection is assumed as a connector element with certain length, which is the distance between the centroid of FRP deck and the centroid of steel top flange. It has six degree of freedom. Three rotation degrees of freedom are assumed to be restrained. The distance between FRP panel and steel stringer is assumed to keep unchanged. This assumption restrains the degree of freedom of vertical translation. The interface movement is accommodated by allowing degree of freedom of horizontal translation, which is defined by the stiffness of shear connection (Figure 2.14).

In the FE model, connector elements (CONN32) are used to simulate the actual shear connection properties. Three rotational components are set to be completely restrained as well as the vertical translation. Two horizontal translation components are defined

accordingly to the shear connection stiffness and are taken as 1.46kN/mm for a total interface displacement not to exceed 15 mm.

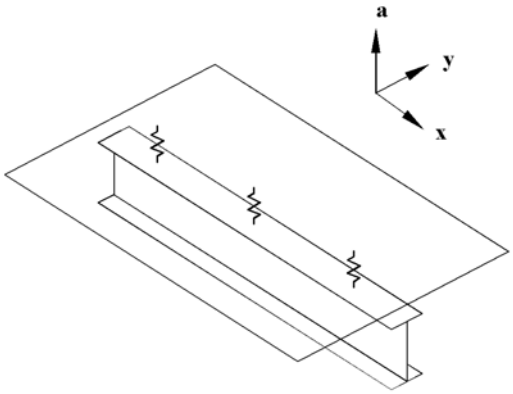

Figure 4.2 Illustration of Connector Element

Figure 4.3 FE Bridge Model

4.3. FE Analysis Results

As the FRP panel is modeled as a homogeneous solid slab in FE model, global behaviors of bridge model and T-section modal are straightforward to be obtained, such as load distribution factor, panel local deflection, effective flange width, and degree of composite action.

4.3.1 Load Distribution Factor

Similar to bridge model test, the load distribution factors are obtained by using the expression $LDF = \frac{\varepsilon_i}{\sum_{i=1}^{3} \varepsilon_i}$. The maximum strain values are obtained from shell element output of steel stringer tension flange at mid-span section. The load distribution factor is obtained accordingly as the ratio of flange maximum strains. Compared with experimental data, the FE model appears to be stiffer and the distribution factor for the center stringer is 0.621. In Chapter 5, an analytical solution is obtained from a first-term approximate series solution. In the series solution, the load distribution factor is expressed as function of stringer interaction forces. The series solution using Eq. (5-33) gives a prediction of about 0.602 and correlates with the FE and test results fairly well. For the edge loading case, applying the load over the edge stringer was not possible, and only predicted values are shown in Table 4.5.

Table 4.5 Load Distribution Factor of Bridge Model

Connection Spacing	0.6m	Diff. (%)
AASHTO LRFD	0.655	1.2
FE model	0.621	-4.0
Series Solution	0.602	-7.0
Phase I Test	0.647	

4.3.2 Local Panel Deflection

The panel local deflection of FE model is about L/1039, which is less than test result, L/726. This result is also within AASHTO LRFD deformation limit for bridge decks, L/800.

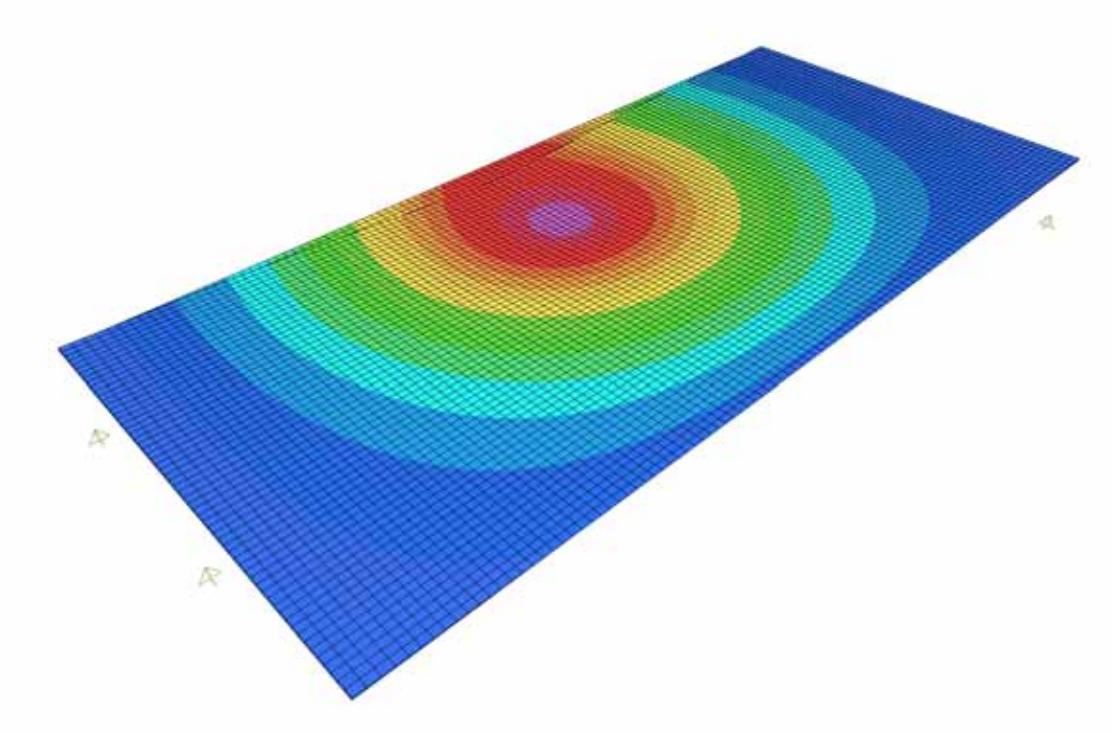

Figure 4.4 Deformed Shape of Panel

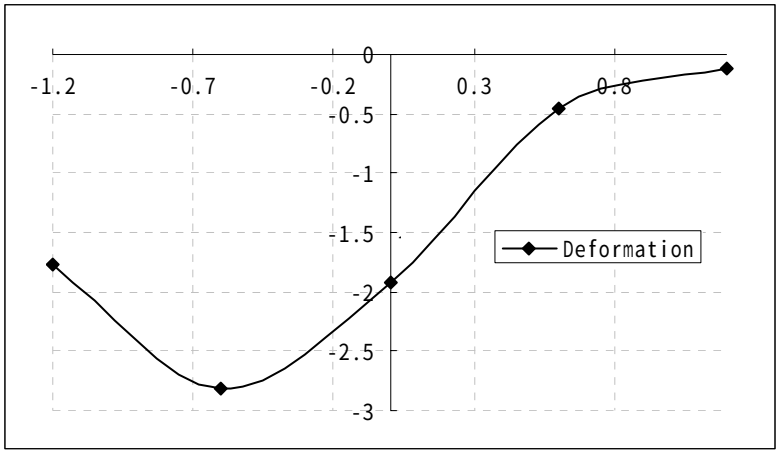

Figure 4.5 Deflection Profile of FRP Panel

Table 4.6 Deflection Profile of Bridge Model

0.6m connection spacing		
Deflection Point	Deflection (mm)	Local Deflection (mm)
1	1.77	
2	2.81	1.12
3	1.54	
4	0.45	
5	0.12	

4.3.3 Effective Flange Width

Similarly as shown in the test, the longitudinal normal stress in FRP deck is non-uniform along its transverse cross section. The normal stress in the deck reaches the maximum at the mid-line junction of the bridge stringer and deck; and decays along the deck transverse section away from the junction line. These strain values are connected linearly to form trapezoidal shape stress blocks. The integral of these stress blocks, or stress resultant, are the summation of area of each stress block (Figure 4.6). Effective flange width is then obtained as the ratio of stress resultants to maximum

strain, $b_{eff} = (\int_{-b/2}^{b/2} \sigma_x dx) / \sigma_{\max} = \sum_{i=1}^{n} \sigma_{x,i} h_i / \sigma_{\max}$. The resulted effective flange width is 0.75m, which is about 63% of actual flange width.

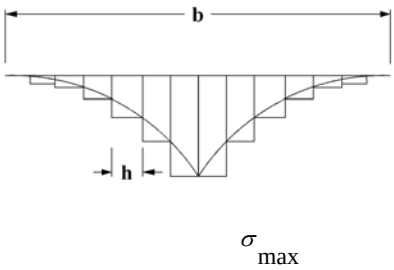

Figure 4.6 Stress Integration of the Flange

In Chapter 6, the approximate solution for full composite FRP decks is presented for FRP bridge decks with full composite action. The analytical solution is validated by FE parametric study. Since the analytical solution only considers full composite action case, a reduction factor R=0.6 is suggested for the FRP bridge decks with partial composite action. Thus, applying the factor R to Eq. (6-18), the effective width can be evaluated as,

$$b_{eff} = R \frac{\int_0^{b/2} \cosh(\xi y) dy}{\cosh(\frac{\xi b}{2})}, \quad \xi = \frac{\pi}{a} (\sqrt{\frac{A_{11}}{A_{66}}}) \tag{4-1}$$

The corresponding effective flange width is about 0.61m.

Test results and FE show that the actual effective flange width of this T-beam is about 50-65% of actual flange width. More tests on effective flange width and degree of composite action are suggested. By further test results, the relation between degree of

composite action and effective flange width could be obtained.

4.4. Summary

Overall, the test results correlated well with FE analysis. The predictions of load distribution factor, effective flange width, and panel local deflection are all within acceptable range. The simplified FE model adopting equivalent panel properties is proved to able to define the global behavior of FRP deck bridges.

APPENDIX B: FRP Panel Properties Evaluation

The equivalent properties method (Davalos *et al.*, 2001) is a perfect tool to study the FRP panel global behavior without involving detailed panel configuration. It avoids the troublesome to model the actual FRP sandwich configurations in FE model and remains reasonable accuracy. However, due to the manufacture imperfection and configuration difference, the actual properties may differ for each FRP panels, which may further influence the accuracy of FE modeling. Therefore, three FRP panels (1.8m*2.7m*0.13m) that will be used for the bridge models and T-section model are evaluated mainly under bending test to obtain the actual properties.

B.1 Test Setup

The FRP panel is simply supported at long span direction, which is 2.7m and is also the longitudinal core direction, where the sinusoidal core is extended along the span direction of the panel. The panel width is 1.8m. The panels are loaded by a 245kN actuator via a 0.6m*0.25m steel plate to the FRP panel (Figure B.1).

Figure B.1 Panel Test Setup

The panels are loaded to 45kN with force control at a loading rate of 9kN/min at 5 different locations, which are numbered from #1 to #5 (Figure B.2). Losition 3 is at the center of panel. Location 1 and 5 are symmetrically placed at longitudinal direction and are both 0.3m away from the center line. Location 2 and 4 are symmetrically placed at transverse direction and are both 0.45m away from the center line. 5 LVDTs and 10 uni-directional strain gauges are attached at these locations to measure the vertical displacement, longitudinal and transverse strain of the panel.

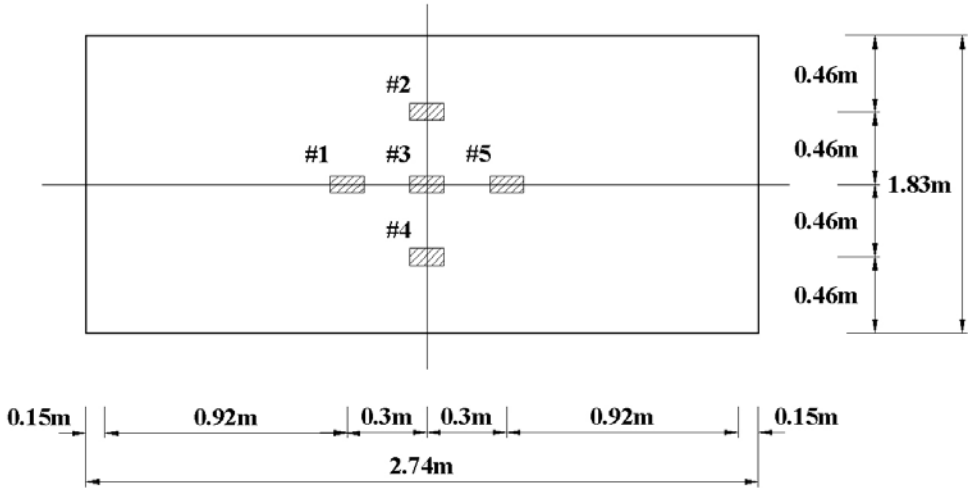

Figure B.2 Loading Positions and Instrumentations

B.2 Test Results

The measured panel deflection is presented as mm/kN to provide uniform comparison data. Similarly, the longitudinal and transverse strains are reduced to microstrain/kN. The results are shown in Table B.1 and B.2. Label 1L, 2L, 3L, 4L, and 5L represent the longitudinal strain at location 1 to 5. Label 1T, 2T, 3T, 4T, and 5T represent the

transverse strain at location 1 to 5. At location 4, the strain gauge at transverse direction is failed and no strain data is available at that position.

Table B.1 Deflection at Location 1 to 5

Test	Deflection (10E-2*mm/kN)				
Load case	1 (LVDT1)	2 (LVDT2)	3 (LVDT3)	4 (LVDT4)	5 (LVDT5)
1.0	-15.3	-15.4	-15.9	-15.7	-12.6
2.0	-14.2	-24.4	-17.5	-12.8	-15.4
3.0	-16.7	-18.2	-19.8	-18.3	-16.9
4.0	-14.1	-12.4	-17.5	-25.0	-15.3
5.0	-12.2	-15.7	-16.1	-16.1	-16.3
Panel 2	-15.0	-18.8	-20.6	-19.4	-17.4
Panel 3	-17.1	-19.6	-21.5	-20.0	-18.4

Table B.2 Longitudinal and Transverse Strain at Location 1 to 5

Test	Longitudinal strain (microsrain/kN)				
Load case	1L	2L	3L	4L	5L
1	19.5	13.8	9.6	13.2	8.4
2	15.7	27.1	16.6	12.5	15.2
3	13.2	19.4	24.1	19.9	12.9
4	12.4	13.1	14.8	25.4	11.3
5	8.9	14.6	9.1	12.8	18.9
	Transverse strain (microsrain/kN)				
Load case	1T	2T	3T	4T	5T
1	13.9	2.0	7.0	N/A	2.5
2	2.4	10.4	3.1	N/A	2.1
3	6.2	2.8	14.8	N/A	6.2
4	1.7	3.8	2.5	N/A	1.7
5	1.4	1.2	6.8	N/A	13.5

B.3 Comparison of FE Model of FRP Panel and Test Results

An FE model of test panel is constructed by shell element. The FE model simulates the testing condition and use equivalent properties method to obtain the panel properties (Table B.3). FE results are compared with test results to obtain the

discrepancy of equivalent properties of panel with actual panel properties. The FRP panel is modeled by 4 nodes (S4R) shell element with 2D orthotropic properties in ABAQUS (2002). Same simply supported boundary condition and load condition as in test is simulated in FE. The deflection and strains data are obtained correspondingly at location 1 to 5 (Table B.4, Table B.5).

Table B.3 Equivalent Properties of Panel

	$E_x(MPa)$	$E_y(MPa)$	ν_x	$G_{xy}(MPa)$
In-Plane	2940	2641	0.303	648
Bending	6488	6488	0.303	1600

Table B.4 Deflection Data from FE Model

FEM	Deflection (10E-2*mm/kN)				
Load case	1	2	3	4	5
1.0	-14.0	-13.6	-13.8	-13.6	-10.2
2.0	-13.6	-23.4	-16.8	-11.9	-13.6
3.0	-13.8	-16.8	-18.2	-16.8	-13.8
4.0	-13.6	-11.9	-16.8	-23.4	-13.6
5.0	-10.2	-13.6	-13.8	-13.6	-14.0
Panel 2	-13.8	-16.8	-18.2	-16.8	-13.8
Panel 3	-13.8	-16.8	-18.2	-16.8	-13.8

In Table B.6 and B.7, the deflection and strain data from tests and FE are compared with each other. Since the load case #1 and #5 are symmetric positioned, it should give out the duplicated results on deflection and strain. The actual difference in test data is due to geometry imperfection of the panel and load position. Therefore, the test data of load case #1 and #5 are averaged. These averaged results are to be compared with FE load case #1. Similarly, results from load case #2 and #4 are symmetric

positioned. The test data of load case #1 and #5 are averaged and compared with FE load case #2. This procedure will eliminate the panel imperfection occurred in the manufacture and possible geometry difference in loading test, such as load position and support conditions.

Table B.5 Longitudinal and Transverse Strain Data from FE Model

FEM	Longitudinal strain (microsrain/kN)				
Load case	1L	2L	3L	4L	5L
1	18.3	11.7	12.1	11.7	7.1
2	11.4	24.8	16.1	10.6	11.4
3	12.1	16.3	20.8	16.3	12.1
4	11.4	10.6	16.1	24.8	11.4
5	7.1	11.7	12.1	11.7	18.3
	Transverse strain (microsrain/kN)				
Load case	1T	2T	3T	4T	5T
1	12.7	2.2	5.0	2.2	1.7
2	1.2	10.1	0.9	-0.7	1.2
3	5.0	2.3	13.0	2.3	5.0
4	1.2	-0.7	0.9	10.1	1.2
5	1.7	2.2	5.0	2.2	12.7

Table B.6 Deflection Correlation between Test and FE results

Location	LC #1		LC #2		LC #3		Panel 2		Panel 3	
	Test	FE	Test	FE	Test	FE	Test	FE	Test	FE
1	-15.9	-14.0	-14.2	-13.6	-16.7	-13.8	-15.0	-13.8	-11.4	-13.8
2	-15.5	-13.6	-24.7	-23.4	-18.2	-16.8	-18.8	-16.8	-19.6	-16.8
3	-16.0	-13.8	-17.5	-16.8	-19.8	-18.2	-20.6	-18.2	-21.5	-18.2
4	-15.9	-13.6	-12.6	-11.9	-18.3	-16.8	-19.4	-16.8	-20.0	-16.8
5	-12.4	-10.2	-15.4	-13.6	-16.9	-13.8	-17.4	-13.8	-18.4	-13.8
Diff (%)	16.7		6.7		13.9		15.0		13.9	

Table B.7 Strain Correlation between Test and FE results

Strain Loc.	LC #1		LC #2		LC #3	
	Test	FE	Test	FE	Test	FE
1L	19.2	18.3	14.0	11.4	13.2	12.1
2L	14.2	11.7	26.3	24.8	19.4	16.3
3L	9.4	12.1	15.7	16.1	24.1	20.8
4L	13.0	11.7	12.8	10.6	19.9	16.3
5L	8.6	7.1	13.2	11.4	12.9	12.1
Diff (%)	7.7		12.6		14.7	
1T	13.7	12.7	2.1	1.2	6.2	5.0
2T	1.6	2.2	10.4	10.1	2.8	2.3
3T	6.9	5.0	5.3	0.9	14.8	13.0
4T	N/A	2.2	-3.8	-0.7	N/A	2.3
5T	1.9	1.7	1.9	1.2	6.2	5.0
Diff (%)	7.2		207.3		20.7	

As can be seen, the difference between test data and FE model are consistent for both deflection and strain. For deflection, the differences between FE and test range from 6.7% to 16.7%. The average difference is that test data are about 13 % larger than FE. For strain, the difference between test and FE analysis is about 7% to 20% in most of case. Except for LC#2, at some locations, the transverse strain gauges give out irregular large strain values, which are due to strain gauge malfunction. The average difference is that test data are about 13% larger than FE.

All three panels show the similar trend is that the tested panel is actual 13% more flexible than the equivalent properties method prediction. Therefore, the equivalent properties of the FRP decks will be divided by a factor of 1.15 ($\frac{100\%}{87\%} = 1.15$) in order to compensate for the differences.

CHAPTER 5

EVALUATION OF LOAD DISTRIBUTION FACTOR BY SERIES SOLUTION

5.1. Introduction

Live load distribution factors (also referred to as girder distribution factors or wheel load distribution factors) are commonly used by bridge engineers in order to simplify the complex, three-dimensional behavior of a bridge system. In slab-on-girder bridge design, the bridge is usually simplified into a T-section and corresponding live load is obtained by using load distribution factor. This procedure is called beam line analysis in which 3D problem is simplified into 1D problem.

These factors have been incorporated in American bridge codes since the publication of the first edition of the AASHTO Standard Specifications in 1931, including the current specifications (AASHTO, 1996). In 1994, AASHTO adopted the LRFD Bridge Design Specifications, which contained new formulations of distribution factors that represented the first major change to these equations since 1931. The relatively recent adoption of the LRFD specifications has resulted in enhanced accuracy for bridges with geometries falls into certain applicable limitations. However, for bridges with span lengths, girder

spacing, and other parameters outside of the applicable ranges, overly conservative results are often obtained. Therefore, there is need to develop distribution factors that can provide more accurate estimations of live load responses while maintaining simplicity of form for applications in practice.

5.2. Objectives and Scope

The motivation for this analytical study is to obtain explicit formulas for load distribution factors for FRP decks over supporting stringers. In this chapter, an approximate series solution for stiffened plate is presented. The load distribution factor is obtained as ratio of interaction forces acting over the steel stringers. Then FE parametric study is conducted on 66 simply-supported slab-on-steel girder bridges. Several parameters, such as span-length, girder spacing, number of lanes, number of girders, and load conditions are considered. The impact of these parameters on load distribution factor is investigated by this parametric study. The FE parametric study is used to validate the accuracy of the analytical series solution. Based on the FE parametric study, the series solution is used to obtain multiple regression functions of load distribution factors in terms of non-dimensional variables. These functions are suitable for design practice.

5.3. Series Solution for Stiffened Plate

An approximate series solution for two-side stiffened orthotropic plate is proposed by Salim *et al.* (1995). The analysis procedure is based on macro flexibility approach. The stiffened plate consists of two major components, slab and stringers, and the slab is

simply supported at two ends and stiffened along the span. The stringers are equally aligned.

First, the governing equations for slab and stringer elements are obtained separately, for both symmetric and anti-symmetric load conditions. The deflection formulations of slab and stringer are contained unknown interaction force at the stringer lines. Then this unknown interaction force between slab and stringers are solved by ensuring the displacement compatibility condition at the stringer lines. Lastly, the load distribution factor of this stiffened plate system is defined as the ratio of single stringer interaction force to the summation of total stringer interaction force.

5.3.1. Series Solution for Stiffened Plate under Symmetric Load

A two-side stiffened orthotropic plate is shown in Figure 5.1. The plate is stiffened at two edges along the span ($y = 0$, $y = b$), as well as equally spaced at middle of plate. It is simply supported at two ends ($x = 0$, $x = a$). Assumptions are made to simplify the formulation

(1) no in-plane force or displacement is considered in the formulation;

(2) no torsional moments or stiffness is considered in the stringers;

(3) stringers are equally spaced and have the same section and material properties;

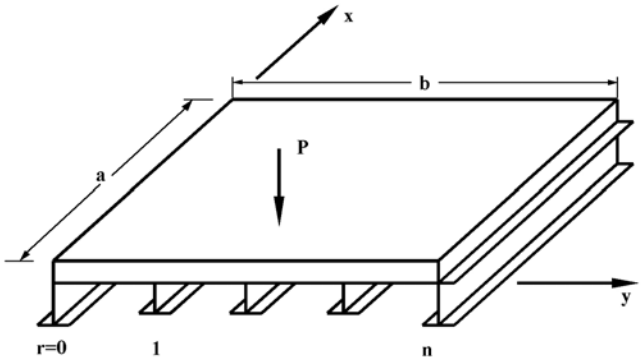

Figure 5.1 Two-side Stiffened Orthotropic Plate with Equally Spaced Stringers

In Macro flexibility approach (Gangarao *et al*., 1975), the stiffened plate is divided into two major components, plate element and stringer element. First, the deflection formulation of plate stiffened with two exterior stringers (Figure 5.2) is obtained from plate governing equation. The deflection formulation contains one unknown term, interaction forces R(x,y) at discrete interior stringer lines. Then the deflection formulation of interior stringers is obtained from stringer governing equations. It contains the same unknown term, interaction force R(x,y) at discrete stringer lines (Figure 5.3). By ensuring the displacement compatibility at these interior stringer lines, the deflection formulation of stiffened plate is solved.

During analysis procedure, the transverse load P is divided into symmetric and antisymmetric load cases. The deflection formulation and interaction force for symmetric and antisymmetric load cases are obtained separately. The deflection formulation and interaction force under asymmetric load P is then obtained by linear superposition.

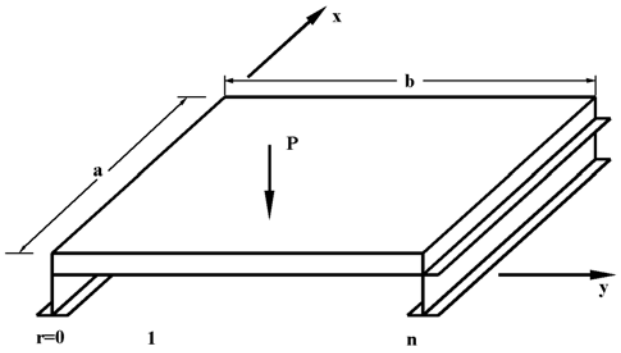

Figure 5.2 Two-side Stiffened Orthotropic Plate with Exterior Stringers Only

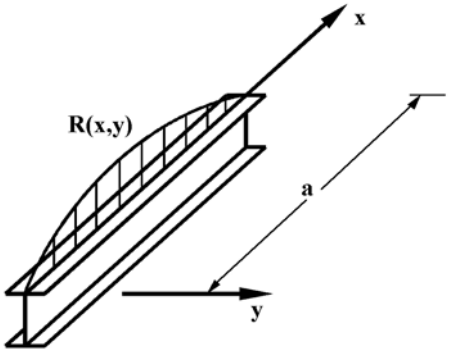

Figure 5.3 Typical Interior Stringer

(a) Orthotropic plate stiffened by exterior stringers only

For the orthotropic plate stiffened by exterior stringers, the governing equation is

$$D_x \frac{\partial^4 w}{\partial x^4} + 2H \frac{\partial^4 w}{\partial x^2 \partial y^2} + D_y \frac{\partial^4 w}{\partial y^4} = q(x, y) \qquad (5\text{-}1)$$

here D_x is flexural rigidity of plate in x-direction and D_y is flexural rigidity of plate in y-direction; ν_x, ν_y is Poisson ratio of plate; H is torsional rigidity of plate and can be expressed as $\nu_x D_y + \nu_y D_x$

The deflection formulation is assumed as

$$w(x,y)=\sum_{i=1,2,3,\ldots}^{\infty}\sum_{j=1,3,5,\ldots}^{\infty}W_{ij}\sin\frac{i\pi x}{a}[\sin\frac{j\pi y}{b}+C_0+C_1(\frac{y}{b})+C_2(\frac{y}{b})^2+C_3(\frac{y}{b})^3] \quad (5\text{-}2)$$

And load function is in the form of

$$q(x,y)=\sum_{i=1,2,3,\ldots}^{\infty}\sum_{j=1,3,5,\ldots}^{\infty}q_{ij}\sin\frac{i\pi x}{a}\sin\frac{j\pi y}{b} \quad (5\text{-}3)$$

In order to simplify the formulation, only first term is taken for the deflection and load formulation, which is expressed as

$$w(x,y)=W_{11}\sin\frac{\pi x}{a}[\sin\frac{\pi y}{b}+C_0+C_1(\frac{y}{b})+C_2(\frac{y}{b})^2+C_3(\frac{y}{b})^3] \quad (5\text{-}4)$$

$$q(x,y)=q_{11}\sin\frac{\pi x}{a}\sin\frac{\pi y}{b} \quad (5\text{-}5)$$

Since the plate is stiffened at two edges ($y=0, y=b$) and is simply supported at two ends ($x=0, x=a$). The boundary conditions are

(1) At $y=0, y=b$, $M_y=0$ with torsinal rigidity and in-plane Poisson's ratio neglected;

$$-D_y[\frac{\partial^2 w}{\partial y^2}]_{y=0,b}=0 \quad (5\text{-}6)$$

(2) At $y=0, y=b$, the interaction force of exterior girder equals to transverse shear force in the plate,

$$B_e[\frac{\partial^4 w}{\partial x^4}]_{y=0,b}=\mp D_y[\frac{\partial^3 w}{\partial y^3}+(\nu_x+\frac{4D_{xy}}{D_y})\frac{\partial^3 w}{\partial x\partial y^2}] \quad (5\text{-}7)$$

Substitute deflection formulation (5-4) into boundary condition (5-6), (5-7). All four unknown coefficients C_1, C_2, C_3, C_4 are able to be obtained with $C_1 = C_2 = C_3 = 0$ and

$$C_0 = \frac{b}{\pi}\frac{D_y}{B_e}\left[\frac{1+(\nu_x + \frac{4D_{xy}}{D_y})\gamma^2}{\gamma^4}\right].$$

Therefore, deflection function can be expressed as

$$w(x, y) = W_{11} \sin\frac{\pi x}{a}(\sin\frac{\pi y}{b} + C_0) \tag{5-8}$$

Substitute deflection formulation (5-8) and load function (5-5) into governing equation (5-1). The unknown coefficient W_{11} is then determined as

$$W_{11} = (\frac{b}{\pi})^4 \frac{q_{11}}{D_s} \tag{5-9}$$

Where

$$D_s = D_x\gamma^4(1 + \frac{4C_0}{\pi}) + 2H\gamma^2 + D_y \tag{5-10}$$

For a concentrated force P at location $x = x_0, y = y_0$, load coefficient q_{11} is

$$q_{11} = \frac{4P}{ab}\sin\frac{\pi x_0}{a}\sin\frac{\pi y_0}{b} \tag{5-11}$$

(b) Interior stringers with unknown interaction force

For an interior girder loaded with line load R(x,y), the governing equation is

($r = 0,1,2,...n$, n is number of stringers)

$$B_e\frac{\partial^4 w^R(x, y)}{\partial x^4} = R(x, r) \tag{5-12}$$

The deflection formulation of interior stringer is in similar form as plate deflection formulation

$$w^R(x,r) = A_{11}\sin\frac{\pi x}{a}(\sin\frac{\pi r}{n} + C_0) \tag{5-13}$$

The applied line load R(x,y) which is the unknown interaction force on the plate is assumed as

$$R(x,r) = R_{11}\sin\frac{\pi x}{a}(\sin\frac{\pi r}{n} + C_0) \tag{5-14}$$

The coefficient A_{11} is solved by substituting $w^R(x,y), R(x,y)$ into governing equation (5-12)

$$A_{11} = \frac{R_{11}}{B_e}(\frac{a}{\pi})^4 \tag{5-15}$$

(c) Orthotropic plate stiffened by both interior and exterior stringers

The unknown interaction force at stringer lines R(x,y) is solved by ensuring the displacement compatibility condition between stringers and plate. The plate deflection equals to the deflection of corresponding stringers. Therefore, the plate deflection consists of two parts, the deflection induced by transverse load P and the deflection induced by stringer reaction force R(x,y). Therefore, the equation of plate deflection with considering this compatibility condition is

$$w^R(x,r) = w(x,r) - \sum_{\alpha=1}^{n-1}\int_0^a R(\xi,\alpha)K^w(x,r,\xi,\alpha)d\xi \tag{5-16}$$

First term $w(x,r)$ is the plate deflection due to transverse load $q(x,y)$.

$$w(x,r) = W_{11} \sin\frac{\pi x}{a}(\sin\frac{\pi r}{n} + C_0) \tag{5-17}$$

Second term $\sum_{\alpha=1}^{n-1}\int_0^a R(\xi,\alpha)K^w(x,r,\xi,\alpha)d\xi$ is the plate deflection due to stringer reaction force R(x,y). $K^w(x,r,\xi,\alpha)$ is kernel function solution. In this case, it is the solution for an arbitrarily located unit load applied at plate where $x=\xi$ and $y=\alpha$. The first term approximation of $K^w(x,r,\xi,\alpha)$ is expressed as

$$K^w(x,r,\xi,\alpha) = K_{11}\sin\frac{\pi x}{\alpha}(\sin\frac{\pi r}{n} + C_0) \tag{5-18}$$

Here $K_{11} = (\frac{b}{\pi})^4 \frac{q_{11}^k}{D_s}$, q_{11}^k is obtained by substituting $P=1$ into equation (5-11).

After performing the integration and applying orthognality conditions to (5-16), the unknown interaction force R(x,y) is solved. The load coefficient R_{11} is expressed as

$$R_{11} = \frac{q_{11}}{\frac{D_s}{\gamma^4 B_e} + \frac{n}{b}(1+\frac{4C_0}{\pi})} \tag{5-19}$$

Therefore, the generalized deflection function of any interior girder under symmetric loading is solved as

$$W^R(x,r) = \frac{R_{11}}{B_e}(\frac{a}{\pi})^4 \sin\frac{\pi x}{a}(\sin\frac{\pi r}{n} + C_0) \tag{5-20}$$

5.3.2. Series Solution for Stiffened Plate under Anti-symmetric Load

Similar procedure is performed for anti-symmetric load case.

(a) Orthotropic plate stiffened by exterior stringers only

For the orthotropic plate stiffened by exterior stringers, the governing equation is

$$D_x \frac{\partial^4 w}{\partial x^4} + 2H \frac{\partial^4 w}{\partial x^2 \partial y^2} + D_y \frac{\partial^4 w}{\partial y^4} = q(x, y) \tag{5-21}$$

The first term approximation of deflection formulation and load function are expressed in similar form as for symmetric load case

$$w(x, y) = W_{12} \sin\frac{\pi x}{a}[\sin\frac{2\pi y}{b} + C_1(1 - 2\frac{y}{b})] \tag{5-22}$$

$$q(x, y) = q_{12} \sin\frac{\pi x}{a} \sin\frac{2\pi y}{b} \tag{5-23}$$

$$C_1 = \frac{1 + (\frac{4D_{xy}}{D_y} + \nu_x)\frac{\gamma^2}{4}}{\frac{B_e}{D_y}(\frac{\gamma^4 \pi}{8b}) + (\frac{4D_{xy}}{D_y} + \nu_x)\frac{\gamma^2}{4\pi}} \tag{5-24}$$

$$W_{12} = (\frac{b}{2\pi})^4 \frac{q_{12}}{D_{as}} \tag{5-25}$$

$$D_{as} = D_x(\frac{\gamma}{2})^4(1 + \frac{2C_1}{\pi}) + 2H(\frac{\gamma}{2})^2 + D_y \tag{5-26}$$

$$q_{12} = \frac{4P}{ab} \sin\frac{\pi x_0}{a} \sin\frac{2\pi y_0}{b} \tag{5-27}$$

(b) Interior stringers with unknown interaction force

The deflection formulation and interaction force for stringer r is

$$w^R(x,r) = A_{12}\sin\frac{\pi x}{a}[\sin\frac{2\pi r}{n} + C_1(1-\frac{2r}{n})] \tag{5-28}$$

$$R(x,r) = R_{12}\sin\frac{\pi x}{a}[\sin\frac{2\pi r}{n} + C_1(1-\frac{2r}{n})] \tag{5-29}$$

$$A_{12} = \frac{R_{12}}{B_e}(\frac{a}{\pi})^4 \tag{5-30}$$

(c) Orthotropic plate stiffened by interior and exterior stringers

By ensuring the displacement compatibility condition at stringer line, the only unknown load coefficient R_{12} is solved in similar fashion as in symmetric load case

$$R_{12} = \frac{q_{12}}{\frac{16D_{as}}{\gamma^4 B_e} + \frac{n}{b}(1+\frac{2C_1}{\pi})} \tag{5-31}$$

Therefore, the generalized deflection function of any interior girder under anti-symmetric loading is expressed as

$$W^R(x,r) = \frac{R_{12}}{B_e}(\frac{a}{\pi})^4\sin\frac{\pi x}{a}[\sin\frac{2\pi r}{n} + C_1(1-\frac{2r}{n})] \tag{5-32}$$

5.3.3. Series Solution for Stiffened Plate under Asymmetric Load

Since this series solution is for elastic analysis, the deflection formulation of asymmetric load is obtained by simply superimposing the deflection formulation of symmetric and anti-symmetric load case.

5.3.4. Load Distribution Factors by Series Solution

After obtain the deflection and stringer force formulation, the load distribution factor is expressed as $LDF = \frac{R^r}{\sum_{r=1}^{n+1} R^r}$. It is the ratio of interaction force on single stringer to the sum of total interaction force for all stringers.

More specifically, for symmetric load case, the load distribution factor is

$$LDF_{symm} = \frac{R_0(x,r)}{\sum_{r=0}^{n} R_0(x,r)} = \frac{R_{11}\sin\frac{\pi x}{a}(\sin\frac{\pi r}{n} + C_0)}{\sum_{\alpha=0}^{n} R_{11}\sin\frac{\pi x}{a}(\sin\frac{\pi \alpha}{n} + C_0)} \tag{5-33}$$

For anti-symmetric load case, the load distribution factor is

$$LDF_{antisym} = \frac{R_1(x,r)}{\sum_{r=0}^{n} R_1(x,r)} = \frac{R_{12}\sin\frac{\pi x}{a}[\sin\frac{2\pi r}{n} + C_1(1-\frac{2r}{n})]}{\sum_{\alpha=0}^{n} R_{12}\sin\frac{\pi x}{a}[\sin\frac{2\pi \alpha}{n} + C_1(1-\frac{2r}{n})]} \tag{5-34}$$

For asymmetric load case, the load distribution factor is

$$LDF_{asym} = \frac{R_0(x,r) + R_1(x,r)}{\sum_{r=0}^{n} R_0(x,r) + \sum_{r=0}^{n} R_1(x,r)} = \frac{R_{11}[\sin\frac{\pi r}{n} + C_0] + R_{12}[\sin\frac{2\pi r}{n} + C_1(1-\frac{2r}{n})]}{\sum_{\alpha=0}^{n}\{R_{11}[\sin\frac{\pi r}{n} + C_0] + R_{12}[\sin\frac{2\pi r}{n} + C_1(1-\frac{2r}{n})]\}} \tag{5-35}$$

5.4. Parametric Study on Load Distribution Factors

5.4.1. FE Model Descriptions

Parametric study on typical simply supported slab-on-girder bridge is conducted by using finite element analysis in order to validate the series solution. A total of 66 concrete slab-

on-steel girder bridges, designed in accordance with the provisions of AASHTO and West Virginia state guidelines, were modeled and analyzed in ABAQUS (2002). The following assumptions in finite element modeling are made in order to simplify the analysis effort while retaining adequate accuracy:

1. The bridge deck is idealized as a horizontal slab of uniform thickness. The material in the slab is homogeneous, elastic and isotropic;
2. The slab is supported by various numbers of girders. These girders are equally spaced and are parallel I-shaped steel girders;
3. The edge of the slab and the girder ends are simply supported at the abutments;
4. Full composite action is assumed between the supporting girders and slab. This means that there is no interface slip at the girder slab interface;
5. No truck wheel load is closer than 0.61m from the roadway edge.

These bridge models consist of two-lane and three-lane bridges. The bridge widths are 9.3m for two-lane bridges and 13.0m for three-lane bridges. For two-lane bridges, the number of underlying girders is three, four and five, respectively. For three-lane bridges, the number of underlying girders is four, five and six. These six cross section configurations are numbered from CS1 to CS6. The corresponding cross section configurations are shown in Figure 5.4 and Table 5.1. All the bridges are straight bridges with no skew angle. The major geometrical variables are span-length and girder-spacing. The selected girder spacing covers the practical range for slab-on-girder bridges. They are 2m, 2.6m, and 3.5m for two-lane bridges, 2.3m, 2.74m, and 3.5m for thee-lane bridges. The selected span lengths also cover practical ranges for simply-supported slab-

on-girder bridges. A total of eleven different span lengths were selected. They are varied from 15.2m to 91.4m, with a 7.6m increment.

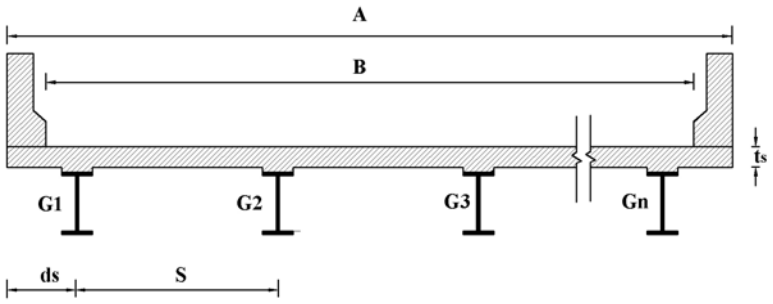

Figure 5.4 Typical Cross Section of Bridge Model

Table 5.1 Parameter for Each Cross Section

Parameters	Two-lane Bridge			Three-lane Bridge		
	CS1	CS2	CS3	CS4	CS5	CS6
A	9.3m	9.3m	9.3m	13.0m	13.0m	13.0m
B	8.53m	8.53m	8.53m	12.2m	12.2m	12.2m
S	3.51m	2.60m	1.98m	3.51m	2.74m	2.29m
ds	1.15m	0.77m	0.69m	1.23m	1.00m	0.77m
ts	0.24m	0.20m	0.20m	0.24m	0.22m	0.20m
N	3	4	5	4	5	6

Simplified three-dimensional finite element bridge model is adopted. Linear four-node quadrilateral shell element (S4R) is used to model the concrete slab and steel girders. Two-node beam element (B31) is used to model diaphragms and cross bracings. Multiple-point constraint (MPC) rigid element is used to model the shear connection in the composite bridges (Figure 5.5). This rigid element constrains both rotation and displacement degree of freedom. It is able to simulate the full composite action in the bridges. Pin-roller constraint is used to simulate the simply supported boundary condition. The concrete slab is assumed to be un-cracked and the stiffness does not change during

the loading. No reinforcing steel is considered in the FE model. Therefore, the analysis limited to static and linear elastic response.

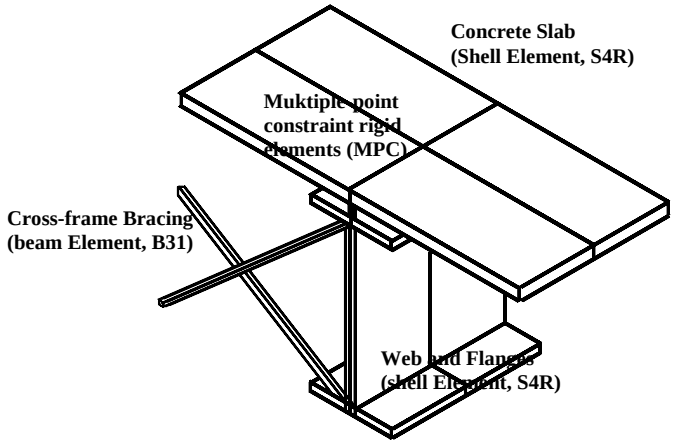

Figure 5.5 Configuration of Finite Elements

5.4.2. Live Load Position

Point load is used to simulate the AASHTO HS20 truck wheel load. For two-lane bridges, they are loaded with one or two lane HS20 truck load. For three-lane bridges, they are loaded with one, two, or three lane HS20 truck load (Figure 5.6). The critical longitudinal and transverse position of truck load need to be decided in order to determine the truck load position where the maximum moment on critical girders is induced. First, the longitudinal position of the truck load is defined by using influence lines. This critical longitudinal position is where the maximum bending moment occurred in the mid-span section. For simply supported bridge, the location is where the middle axle right on mid-span line (Figure 5.7).

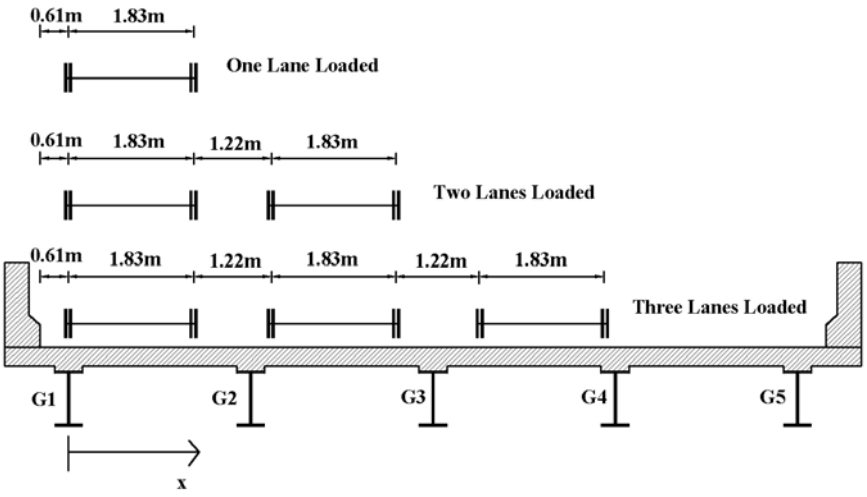

Figure 5.6 AASHTO HS20 Truck Load for 1-, 2-, and 3- lane Loaded Case

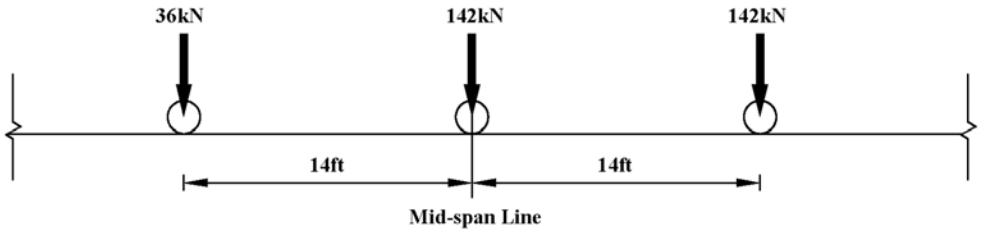

Figure 5.7 AASHTO HS20 Truck Load Longitudinal Position

The critical transverse location of truck load is then evaluated by a preliminary study. This purpose is to obtain the relation between transverse load location and distribution factor in critical girder. By this study, the transverse position of the truck load is found out at where the maximum distribution factor occurred.

As shown in Figure 5.6, the transverse position of the truck is defined by coordinate x, with origin at a distance which is 0.61m away from the left roadway edge. Then starting from origin, the truck load is moved to the right at 0.61m interval. The distribution

factors for each girder are obtained at these transverse truck locations. As an example, Figure 5.8 shows the relation of load distribution factor and wheel load position for a three-lane bridge with four girder, 30.5m span length, and one-lane truck load. With the truck load moving to the right, the distribution factor of the left girders decrease and the distribution factor of the right girders increase (Figure 5.8). In this case, for exterior girders, the critical transverse wheel load location is x=0 and for interior girders is x = 2.44m. For bridges with other cross section configurations and load conditions, the critical transverse load positions can be obtained in similar fashion. As discovered by the preliminary study, exterior girders always have larger distribution factors than interior girders. For interior girders, the first interior girder next to exterior girder always has the largest distribution factor.

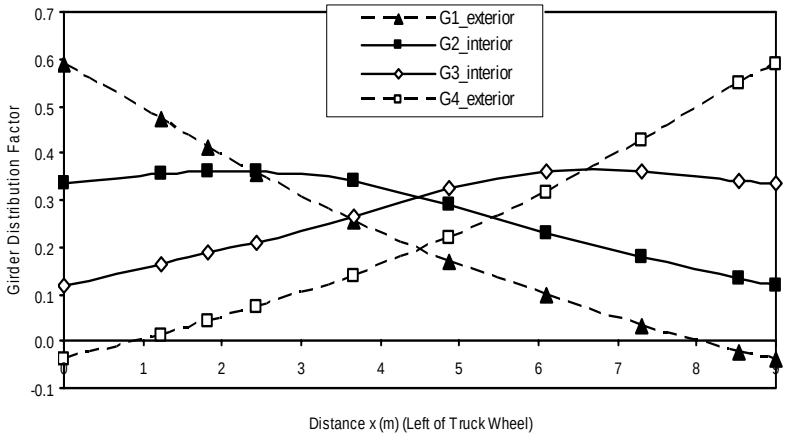

Figure 5.8 Critical Transverse Position for Three-lane Bridge CS4 with 30.5m Span length (One Lane Loaded)

5.4.3. Load Distribution Factor and FE Results

As suggested by Eom and Nowak (2001), expression $LDF = \frac{\varepsilon_i w_i}{\sum_{i=1}^{3} \varepsilon_i w_j}$ is adopted to obtain the load distribution factor from FE model. If the stringers have same section modulus, which is the case in this study, this expression can be simplified into $LDF = \frac{\varepsilon_i}{\sum_{i=1}^{3} \varepsilon_i} N$. Here ε_i is the maximum strain at the bottom of the stringer i, N is the number of lane loaded. Therefore, in FE analysis, the load distribution factor can be obtained as the ratio of maximum strain of one stringer over the summation of strain values for all stringers.

5.4.4. Assessment and Discussion of FE Results and Series Solution

Several variables including girder spacing, span length, number of lanes loaded, and cross section stiffness, are assessed to evaluate their impact on load distribution factor. The importance of these parameters on load distribution factor is identified.

5.4.4.1. Girder Spacing

In Figure 5.9 and 5.10, it shows the relation between distribution factors and girder spacing. Figure 5.9 and 5.10 show the distribution factors of the live load moment versus girder spacing. From FE results, as the girder spacing increases, the load distribution factor increases. This is mainly due to the increase of tributary area of the deck slab to girders, i.e. more live load is carried by each girder. By varying the girder spacing from 2.29 to 3.51 m, the live load distribution factor is increased by an average of 14.2% for

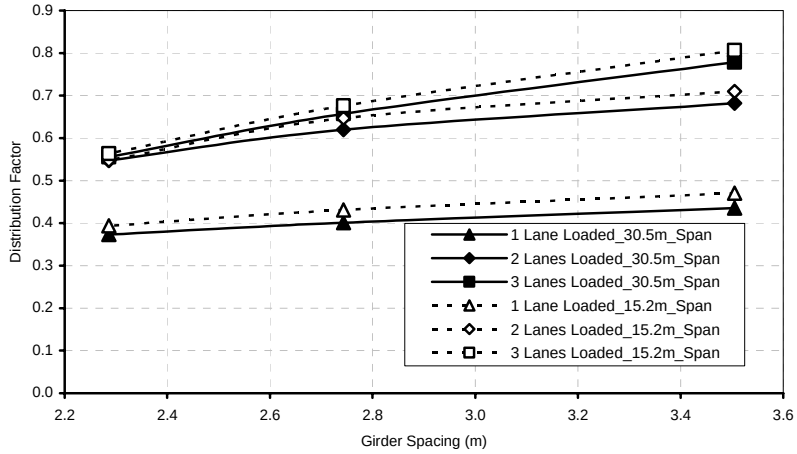

Figure 5.9 Influence of Girder Spacing for interior girder with three lanes bridges (bridge spans 15.2m and 30.5m)

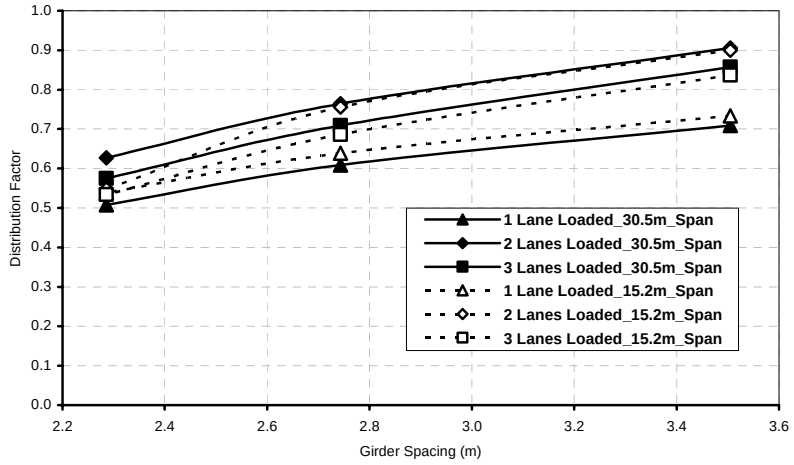

Figure 5.10 Influence of Girder Spacing for exterior girder with three lanes bridges (bridge spans 15.2m and 30.5m)

the interior girder and 39.4% for the exterior girder, for the case of one-lane load. Larger increases resulted for two- and three-lane loaded cases. For example, for three lanes loaded average increases of 39.6% for the interior and 50.6% for the exterior girders are obtained. The girder spacing is one of the most important parameters affecting the load distribution characteristic.

5.4.4.2. Span Length

As illustrated in Figure 5.11 and 5.12, for interior girder, distribution factors decrease as the span length increases. For exterior girder, distribution factors increase with the span length increases, but all are within small range. Similar results and trend were found by other researchers (Bishara *et al*., 1993; Tabsh and Tabatabai, 2001). Although some researchers found that span length has significant influence on distribution factor, this confliction may be due to the reason that in their study the girder cross section remains constant while span length increasing (Mabsout *et al*., 1999), which is not realistic in design practice. It can be concluded that span length has only small effect on load distribution factor.

5.4.4.3. Number of Lane Loaded

In Table 5.2 and 5.3, the distribution factors for load conditions, one-lane, two-lane, and three-lane loaded are listed for three-lane bridges, which consist of cross section configurations of CS4, CS5, and CS6. As expected, with more traffic lanes loaded, the distribution factor becomes larger. However, multiplied with multi-presence factor, three-lane loaded cases gives out the maximum load distribution factor for interior girder and

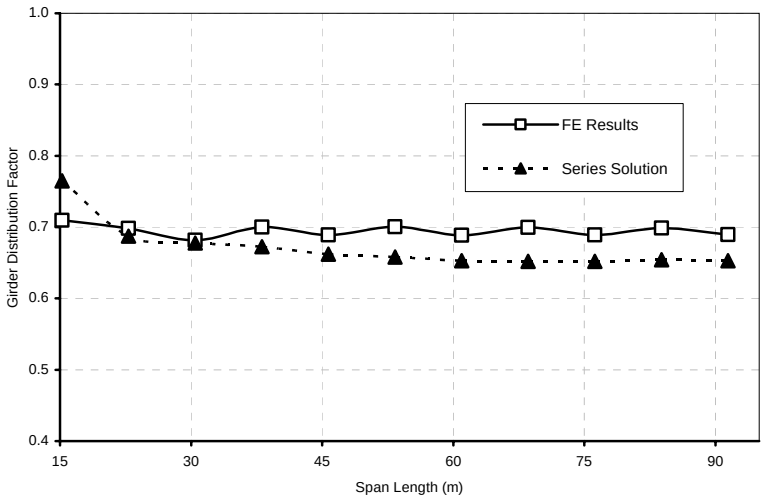

Figure 5.11 Influence of Span Length on Distribution Factor for Interior Girder with Two-lane Loaded (Cross Section CS4)

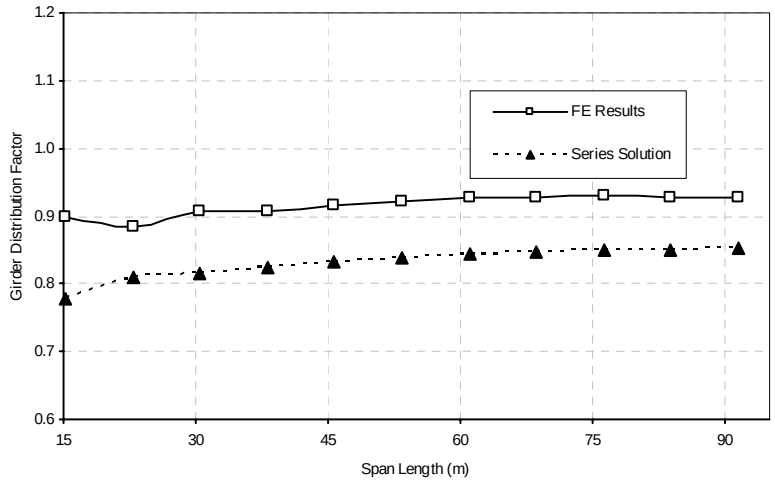

Figure 5.12 Influence of Span Length on Distribution Factor for Exterior Girder with Two-lane Loaded (Cross Section CS4)

two-lane loaded case gives out the maximum load distribution factor for exterior girder (Figure 5.13, 5.14). This phenomenon also applies to bridges with other cross section configurations. The number of lanes loaded is determined as the other major parameters that affects load distribution factors.

Table 5.2 Distribution Factors for Three-lane Bridge (Interior Girder)

Cross Section	Span(ft)	Number of Lanes Loaded		
		One-lane	Two-lane	Three-lane
CS4	15.2	0.470	0.709	0.806
	38.1	0.448	0.700	0.788
	68.6	0.441	0.700	0.782
	91.4	0.433	0.689	0.774
CS5	15.2	0.431	0.647	0.676
	38.1	0.420	0.639	0.666
	68.6	0.418	0.641	0.665
	91.4	0.411	0.632	0.660
CS6	15.2	0.394	0.548	0.563
	38.1	0.396	0.562	0.563
	68.6	0.401	0.565	0.565
	91.4	0.386	0.558	0.561

Table 5.3 Distribution Factors for Three-lane Bridge (Exterior Girder)

Cross Section	Span(ft)	Number of Lanes Loaded		
		One-lane	Two-lane	Three-lane
CS4	15.2	0.733	0.900	0.837
	38.1	0.725	0.907	0.852
	68.6	0.734	0.927	0.872
	91.4	0.718	0.927	0.878
CS5	15.2	0.639	0.755	0.686
	38.1	0.625	0.763	0.704
	68.6	0.631	0.778	0.722
	91.4	0.611	0.777	0.724
CS6	15.2	0.538	0.548	0.534
	38.1	0.521	0.626	0.571
	68.6	0.525	0.637	0.583
	91.4	0.511	0.637	0.586

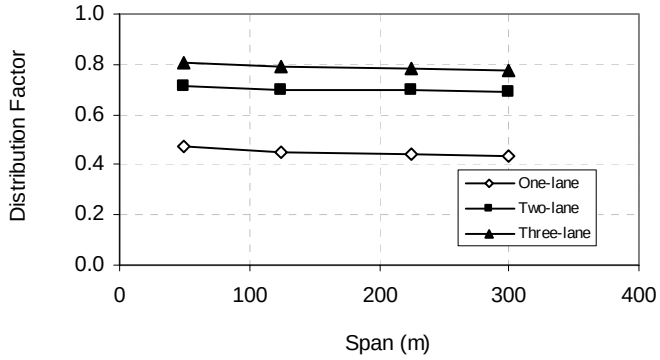

Figure 5.13 Influence of Number of Lanes Loaded on Distribution Factor for Interior Girder (Cross Section CS4)

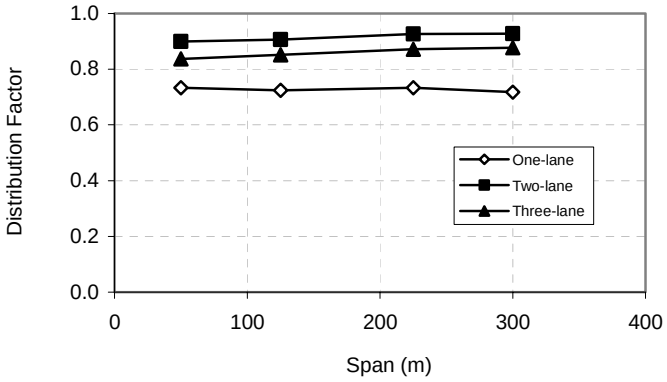

Figure 5.14 Influence of Number of Lanes Loaded on Distribution Factor for Exterior Girder (Cross Section CS4)

5.4.4.4. Cross Section Stiffness

Figure 5.15 shows the relation between stiffness of composite bridge section with distribution factors for all 66 bridge models. For example, for cross section configuration

CS1, cross section stiffness has only minor effect on distribution factor. With cross section stiffness increasing, the distribution factor remains almost constant. This also applies to other cross section configurations. It can be concluded that the cross section stiffness has only marginal impact on load distribution factor.

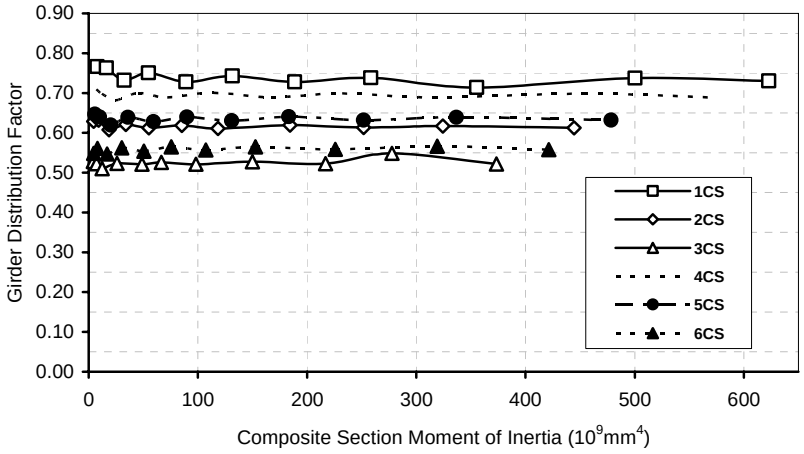

Figure 5.15 Influence of Composite Section Moment of Inertia on Distribution Factors

5.4.5. Comparison of Distribution Factor from Series Solution Formulation and FE Analysis

Certain assumptions are made in series solution to obtain the load distribution factor. (1) The HS20 truck is idealized as six asymmetric point loads to represents six wheel loads. Each point load is further decomposed into symmetric and anti-symmetric load as required by series solution; (2) The same load position as in FE models are applied in series solution; (3) No deck overhang and lateral bracing are considered in series solution. Maple computer program is used to obtain the load distribution factor.

Table 5.4 Comparison of Distribution Factor for Series Solution and FE

Section	L(m)	Interior Girder			Exterior Girder		
		Series	FE	% Diff.	Series	FE	% Diff.
1CS	15.2	0.985	0.984	0.18	0.596	0.597	-0.15
	38.1	0.744	0.742	0.23	0.716	0.717	-0.11
	68.6	0.703	0.702	0.10	0.737	0.373	-0.04
	91.4	0.694	0.694	0.04	0.742	0.742	-0.02
2CS	15.2	0.729	0.731	-0.20	0.441	0.440	0.31
	38.1	0.592	0.592	-0.02	0.569	0.569	0.02
	68.6	0.569	0.569	0.00	0.593	0.593	0.00
	91.4	0.562	0.562	0.00	0.599	0.599	0.00
3CS	15.2	0.560	0.561	-0.13	0.361	0.360	0.20
	38.1	0.477	0.478	-0.01	0.479	0.479	0.01
	68.6	0.470	0.470	0.00	0.496	0.496	0.00
	91.4	0.468	0.468	0.00	0.501	0.501	0.00
4CS	15.2	0.987	0.986	0.15	0.579	0.581	-0.22
	38.1	0.735	0.733	0.32	0.780	0.781	-0.24
	68.6	0.685	0.683	0.19	0.826	0.827	-0.12
	91.4	0.672	0.672	0.08	0.838	0.839	-0.05
5CS	15.2	0.810	0.811	-0.19	0.453	0.451	0.40
	38.1	0.644	0.645	-0.02	0.655	0.655	0.03
	68.6	0.615	0.615	0.00	0.702	0.702	0.01
	91.4	0.610	0.610	0.00	0.712	0.712	0.00
6CS	15.2	0.645	0.646	-0.15	0.377	0.376	0.31
	38.1	0.557	0.557	-0.01	0.552	0.552	0.02
	68.6	0.543	0.543	0.00	0.597	0.597	0.00
	91.4	0.541	0.541	0.00	0.604	0.604	0.00

Table 5.5 Difference between Series Solution and FE

Number of lanes loaded	Diff. (%) of series solutions to FE results					
	Interior Girder			Exterior Girder		
	average	max.	min.	average	max.	min.
One-lane loaded	4.91	22.0	-1.50	-5.7	1.22	-31.7
Two-lane loaded	-1.01	17.5	-7.48	-21.2	-13.6	-54.8
Three-lane loaded	-3.40	20.2	-11.4	-46.8	-29.0	-132

Distribution factor from series solution are compared with FE results in Table 5.4. For interior girders, the overall prediction by series solution is very close to FE analysis. The series solution underestimates the distribution factors as 5% at average, except for 15.2m span length, where the series solution overestimates the distribution factors as much as

28%. For exterior girders, the differences are larger. For 15.2m span length, the differences between series solution and FE range from 45% to 67%. For other span length cases, the differences range from 5% to 28%. Overall, the series solution underestimates the distribution factor. In Table 5.5, the average, minimum, and maximum differences are reported for both interior and exterior girders under each load cases.

For the larger differences of exterior girder cases, several factors may contribute to this. First, the series solution does not take into account the strengthen effect of deck overhangs brought to the exterior girders. In actual bridge, this strengthen effect will attract more loads to exterior girder. Secondly, the diaphragm and other secondary stiffening member have not been taken into account in series solution, which will also affect the bridge behavior. Overall, the series solutions are reasonably accurate and efficient for prediction of distribution factors for interior girders.

5.4.6. Application of Series Solution to FRP Deck

The series solution given above was used to obtain load distribution factor for the scaled bridge model described in Chapter 4. The test specimen consisted of an FRP deck attached to three steel stringers. Table 5.6 shows close correlation of results. The favorable results obtained indicate that this solution can be applied to actual bridges in practice, irrespective of degree of composite action between FRP deck and supporting stringers.

Table 5.6 Comparison of Distribution Factor for FRP Deck Bridge Model

Connection Spacing	0.6m	Diff. (%)
AASHTO LRFD	0.655	1.2
FE model	0.621	-4.0
Series Solution	0.602	-7.0
Phase I Test	0.647	

5.4.7. Regression Function for Distribution Factor

Based on the parametric study, girder spacing has the most significant impact on load distribution factor. Moment of inertia of composite section, number of lanes loaded, and span length are the secondary factors. Therefore, a multiple regression function is presented. Four non-dimensionalized parameters, the aspect ratio $\frac{b}{a}$, thickness ratio $\frac{t}{a}$, flexural rigidity ratio $\frac{E_b I_b}{D \cdot a}$, and number of girders N , were selected as independent variables in multiple regression analysis. An exponential model was defined to conduct the multiple regression analysis by statistical software. The regression data is based on the distribution factor from series solution.

As shown from the comparison of series solution and FE, series solution underestimates the distribution factor in most of load cases, especially for exterior girder with two-lane and three-lane loaded. Therefore, a modification factors will be applied in the regression function to gain better results. For exterior girder with one-lane loaded and interior girder with two- and three-lane loaded, the distribution factors are multiplied by 1.05. For exterior girder with two-lane loaded and three-lane loaded, the distribution factors are multiplied by 1.25 and 1.45, respectively.

Therefore the exponential model is

$$\ln(DF) = \ln(m_0) + m_1 \ln(\frac{b}{a}) + m_2 \ln(\frac{t}{a}) + m_3 \ln(\frac{E_b I_b}{D \cdot a}) + m_4 \ln(N) \qquad (5\text{-}36)$$

the regression function thus can be expressed as

$$DF = e^{m_0} \cdot (\frac{b}{a})^{m_1} \cdot (\frac{t}{a})^{m_2} \cdot (\frac{E_b I_b}{D \cdot a})^{m_3} \cdot (N)^{m_4} \qquad (5\text{-}37)$$

m_0, m_1, m_2, m_3, m_4 are constants, and $D = \frac{E_s t^3}{12(1-\nu^2)}$, E_s, E_b are young's modulus of slab and beam respectively, ν is slab's Poisson's ratio, t is slab thickness, a is span length, b is slab width, N is girder number. The regression functions of distribution factors are listed in Table 5.7.

Table 5.7 Regression Function of Distribution Factors

One-lane Loaded	Interior Girder	$DF = 1.36 \times (\frac{b}{a})^{0.27} \times (\frac{t}{a})^{0.11} \times (\frac{EI}{Da})^{0.12} \times (N)^{-0.20}$
	Exterior Girder	$DF = 0.16 \times (\frac{b}{a})^{0.33} \times (\frac{t}{a})^{-0.69} \times (\frac{EI}{Da})^{-0.11} \times (N)^{-1.12}$
Two-lane Loaded	Interior Girder	$DF = 0.89 \times (\frac{b}{a})^{0.95} \times (\frac{t}{a})^{-0.49} \times (\frac{EI}{Da})^{0.16} \times (N)^{-1.16}$
	Exterior Girder	$DF = 0.005 \times (\frac{b}{a})^{1.39} \times (\frac{t}{a})^{-1.84} \times (\frac{EI}{Da})^{-0.14} \times (N)^{-1.78}$
Three-lane Loaded	Interior Girder	$DF = 4.64 \times (\frac{b}{a})^{0.51} \times (\frac{t}{a})^{-0.05} \times (\frac{EI}{Da})^{0.13} \times (N)^{-1.08}$
	Exterior Girder	$DF = 0.15 \times (\frac{b}{a})^{-0.55} \times (\frac{t}{a})^{-0.43} \times (\frac{EI}{Da})^{-0.32} \times (N)^{-0.88}$

5.5. Summary and Conclusion

A first-term approximate series solution for stiffened plate system is presented. Closed-form solution is obtained for deck deflection. Distribution factor is then obtained from this approximate series solution. Then FE parametric study on 66 simply supported slab-on-girder bridges is conducted. Several major parameters, such as girder spacing, span length, number of lanes, number of girders, and load conditions are varied in FE model to study their impact on load distribution factor. The results show that girder spacing is the predominant variable, while moment of inertia of composite section, number of lanes loaded, and span length also affect the distribution factor to some extent. By comparing the distribution factors from FE and series solution, it is found that the series solutions predict the distribution factor fairly well for interior girder, for which the average differences are within 5%. For exterior girder, the differences are larger. This is mainly because the series solution neglects the deck overhang and other secondary strengthening effect. Using limited experimental data, the series solution provides close values with FE results for a scaled bridge model, consisting of an FRP deck and steel stringers (see Chapter 4). The distribution factors from series solution are established as database for a multiple regression analysis. A set of regression function is presented for bridge design.

As an alternative to FE analysis, the approximate series solutions can be used to conduct parametric study on large number of bridges. By conducting a preliminary study by FE analysis, this series solution can be calibrated and then used as a more efficient approach than FE analysis. Subsequently, regression function can be obtained by the parametric study and can be used in design practice.

CHAPTER 6

EFFECTIVE FLANGE WIDTH OF FRP BRIDGE DECKS

6.1. Introduction

In bridge design practice, a deck-and-stringer system acting compositely (i.e., no interface slippage) is usually simplified as an isolated T-beam section and analyzed by elementary beam theory, which is usually called beam-line analysis. However, due to in-plane shear flexibility of the deck or panel section, the longitudinal normal stress in a bridge deck is non-uniform along its transverse cross section, which is known as shear lag phenomenon. The normal stress in the deck, along the longitudinal stringer or bridge-span direction, reaches maximum at the mid-line junction of the bridge stringer and deck; and the stress decays along the deck transverse section away from the junction line. Analytical solution for this stress distribution is very cumbersome and not practical for design. Therefore, effective flange width is defined as an alternative solution to address shear lag phenomenon in design practice.

Currently, the AASHTO LRFD bridge design specification (2004) includes guidelines for effective-width of primarily concrete decks to account for shear lag phenomenon. The

effective-width is defined as a reduced width of deck, in relation to center-to-center spacing of stringers, over which the normal or longitudinal stresses are assumed to be uniformly distributed as in beam theory for a relatively compact T-beam section.

The studies on FRP bridge decks are mostly based on field- or lab-scale testing results. Keelor *et al*. (2004) conducted a field study on a short-span bridge located in Pennsylvania. This bridge has a pultruded FRP deck over five steel girders equally spaced at 1.75 m; the span-length is 12.65 m, and the deck thickness is 19.5 cm. The FRP deck was assumed to achieve full composite-action through grouted stud connections welded to the stringers. Their results showed that under service load condition, this design resulted in effective-widths corresponding to about 90% for interior and 75% for exterior, respectively, of stringer-spacing and half stringer-spacing.

Keller and Gurtler (2005) conducted lab tests on two large scale T-sections to study composite action and effective-width. Each test model was 7.5 m long with a pultruded FRP deck section of 1.5 m wide adhesively bonded to the top flange of a steel supporting beam. The normal strain distribution across the width of the FRP section was recorded at both upper and lower FRP facesheet components. The results showed that under service limit state, the normal stress was almost uniform across the panel section. While under failure limit state, the normal stress decreased towards the panel edges, indicating a more pronounced effect of shear lag under ultimate load.

6.2. Objectives and Scope

Besides experimental studies as those mentioned above, there is currently no analytical solution to define effective-deck-width for FRP bridge panels. In this chapter, based on harmonic analysis developed for FRP thin-walled sections, an approximate effective-width expression is developed for FRP panels compositely connected to steel supporting stringers. A finite element analysis of 44 selected FRP deck-and-stringer practical bridges is conducted to validate the analytical solution for effective-width.

6.3. Shear Lag Model

For full composite-action of FRP-deck over steel-stringer bridges, without considering the torsional moment in the stringer and the twisting moment in the panel, a section of an FRP panel stiffened by two steel edge-beams can be isolated as a typical element (Figure 6.1), with edge-stiffeners corresponding to bridge stringer spacing. The panel loaded by edge shear tractions and axial stress resultants is shown in Figure 6.2.

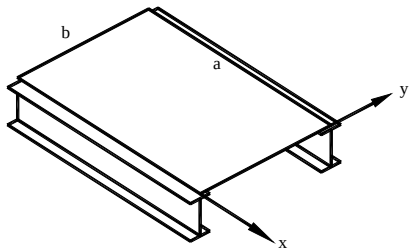

Figure 6.1 Typical Panel Element with Two Sides Stiffened

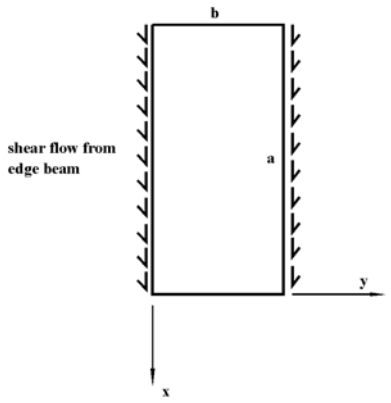

Figure 6.2 Shear flow in Flange Element

Based on equilibrium and boundary conditions at the edges, the panel governing equation can be solved. Several assumptions are made: (1) the axial force N_y and moment M_y are assumed to be zero; (2) the twisting moment in the plate, $M_{xy} = 0$. By using equivalent properties, the FRP panel can be represented as an orthotropic plate at macroscopic scale, with constitute and compliance matrices given as

$$\begin{Bmatrix} N_x \\ N_{xy} \\ M_x \end{Bmatrix} = \begin{bmatrix} A_{11} & 0 & 0 \\ 0 & A_{66} & 0 \\ 0 & 0 & D_{11} \end{bmatrix} \begin{Bmatrix} \varepsilon_x \\ \gamma_{xy} \\ \kappa_x \end{Bmatrix} \tag{6.1}$$

$$\begin{Bmatrix} \varepsilon_x \\ \gamma_{xy} \\ \kappa_x \end{Bmatrix} = \begin{bmatrix} \frac{1}{A_{11}} & 0 & 0 \\ 0 & \frac{1}{A_{66}} & 0 \\ 0 & 0 & \frac{1}{D_{11}} \end{bmatrix} \begin{Bmatrix} N_x \\ N_{xy} \\ M_x \end{Bmatrix} \tag{6.2}$$

For an isolated element in the panel (Figure 6.3), the equilibrium equations is

$$\frac{\partial N_x}{\partial x} + \frac{\partial N_{xy}}{\partial y} = 0 \tag{6.3}$$

The compatibility equation is given as

$$\frac{\partial^2 \varepsilon_x}{\partial y^2} + \frac{\partial^2 \varepsilon_y}{\partial x^2} = \frac{\partial^2 \gamma_{xy}}{\partial x \partial y} \tag{6.4}$$

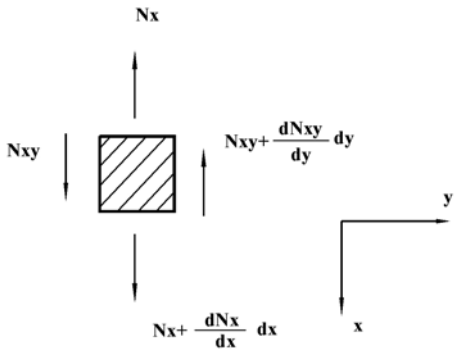

Figure 6.3 Isolated Panel Elements

Neglecting the transverse normal strain ε_y and assuming that M_x remains constant along the y-direction, the panel is not deformable at y-direction and the flexural moment at panel cross section are constant. Equation (6.3) and (6.4) are substituted into the compliance matrix (6.2), to obtain the panel governing equation as

$$\frac{1}{A_{11}} \frac{\partial^2 N_x}{\partial y^2} + \frac{1}{A_{66}} \frac{\partial^2 N_x}{\partial x^2} = 0 \tag{6.5}$$

This partial differential equation can be reduced to an ordinary differential equation by using harmonic analysis proposed by Salim and Davalos (2005), which was used to

analyze shear lag in thin-walled open and closed composite beams. The panel in Figure 6.1 is simply supported, or hinged at $x = 0, a$; thus, the axial panel force can be defined as

$$N_x(x,y) = \sum_{j=1}^{\infty} N_j(y)\sin(\frac{j\pi x}{a}) \tag{6.6}$$

where, $N_j(y)$ is an amplitude function. Substituting (6.6) into (6.5) leads to:

$$\frac{\partial^2 N_j}{\partial y^2} = \xi_j{}^2 N_j \quad , \qquad (\xi_j = \frac{j\pi}{a}\sqrt{\frac{A_{11}}{A_{66}}}) \tag{6.7}$$

The general solution for equation (6.7) is given as

$$N_j(y) = C_{1j}\cosh(\xi_j y) + C_{2j}\sinh(\xi_j y) \tag{6.8}$$

Where, C_{1j} and C_{2j} are determined by compatibility of boundary condition and loading condition at the stiffened edges of the panel. Therefore, the variation of shear flow can be expressed as

$$\frac{\partial N_{xy}}{\partial y} = -\sum_{j=1}^{\infty}\frac{j\pi}{a}[C_{1j}\cosh(\xi_j y) + C_{2j}\sinh(\xi_j y)]\cos(\frac{j\pi x}{a}) \tag{6.9}$$

From the Mechanics of Laminated Beam model presented by Barbero *et al.* (1993), the in-plane shear variation can be defined as

$$\frac{\partial N_{xy}}{\partial y} = -\frac{V(x)}{D}[\overline{A}e(y) + \overline{B}\cos\phi] \tag{6.10}$$

Where, $\overline{A}$ is the extensional stiffness of the cross section; $\overline{B}$ is the bending-extension coupling stiffness, but since an FRP panel is usually designed as symmetric and balanced, is neglected and set to zero; the term $e(y)$ is the distance between the neutral axis of the cross section and the middle surface of the flange; $V(x)$ is the resultant shear force acting

on the cross section; D is the cross section bending stiffness; and ϕ is the orientation of non-horizontal flange. The in-plane variation of shear $\frac{\partial N_{xy}}{\partial y}$ can be written in the form of Fourier series, as

$$\frac{\partial N_{xy}}{\partial y} = \sum_{j=1}^{\infty} Q_j \cos(\frac{j\pi x}{a}) \tag{6.11}$$

And the coefficient in Equation (6.11) can be defined as

$$Q_j = \frac{2}{a}\int_0^a \frac{\partial N_{xy}}{\partial y}\cos(\frac{j\pi x}{a})dx \tag{6.12}$$

Substituting equation (6.10) into (6.12), (I_j depends on loading condition):

$$Q_j = -\frac{2\bar{A}e(y)}{aD} I_j \tag{6.13}$$

If the origin of the y-axis is located at the center of the cross section, then due to symmetry, $C_{2j} = 0$, and equation (6.8) is reduced to

$$N_j(y) = C_{1j}\cosh(\xi_j y) \tag{6.14}$$

By ensuring compatibility of shear flow at the junction of flange and web ($y = -b/2, b/2$), C_{1j} can be obtained by equating (6.9) and (6.11). Therefore, the normal force resultant and normal stress along the panel are

$$N_x(x,y) = -\sum_{j=1}^{\infty} \frac{a}{j\pi} Q_j [\frac{\cosh(\xi_j y)}{\cosh(\frac{\xi_j b}{2})}]\sin(\frac{j\pi x}{a}) \tag{6.15}$$

$$\sigma_x(x,y) = \frac{N_x(x,y)}{\bar{A}} \tag{6.16}$$

Based on definition of effective-panel-width, the longitudinal normal stress is assumed to

be uniformly distributed along the panel section, resulting in an equivalent static response as that caused by the variable stress that in fact exists (Figure 6.4). The effective-width can be expressed as the integral of normal stress distribution divided by the maximum stress value at the panel-stiffener intersection:

$$b_{eff} = \frac{\int_{-b/2}^{b/2} \sigma_x dx}{\sigma_{\max}} = \frac{2\int_{0}^{b/2} \sigma_x dx}{\sigma_{\max}} \tag{6.17}$$

$\sigma_{\max}$ = maximum stress at junction of deck and stringer. Here, $\sigma_{x,\max}(x,y) = \frac{N_x(x,y)}{\overline{A}}$.

Substituting (6.15) and (6.16) into (6.17), and taking a first-term approximation for simplicity, the expression for effective-panel-width is given as

$$b_{eff} = \frac{\int_{0}^{b/2} \cosh(\xi_1 y) dy}{\cosh(\frac{\xi_1 b}{2})} \tag{6.18}$$

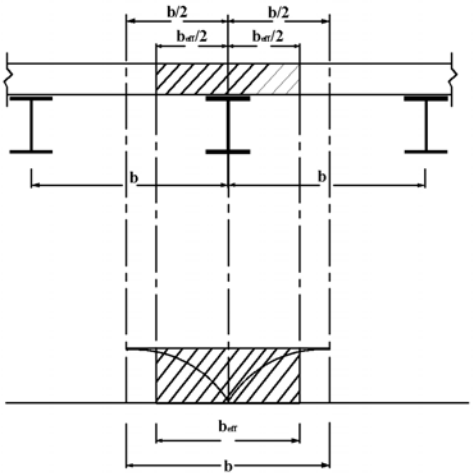

Figure 6.4 Effective Flange Width

6.4. Parametric Study on Effective Flange Width

6.4.1. FE Model Descriptions

A total of 44 simple-span FRP-deck and steel-stringer bridges were selected to conduct a finite element analysis on effective-width. Full composite-action was assumed in all the bridge models. Bridge cross sections 1CS, 2CS, 3CS, and 4CS were selected and the bridge deck was an FRP honeycomb panel produced by KSCI. By adopting the equivalent property method (Davalos *et al.*, 2001), the FRP sandwich panel is idealized as a structurally orthotropic panel with homogeneous equivalent engineering properties. This idealized orthotropic panel is then modeled by 4 nodes (S4R) shell element with 2D orthotropic properties in ABAQUS (2002). The bridge configurations and equivalent properties for the FRP panel are shown in Table 6.1 and 6.2. Detailed procedure to obtain the equivalent engineering properties of panel can refer to Davalos *et al.* (2001).

The number of lanes considered was 2 and 3 with widths of 9.31m for two-lane bridges and 12.97m for three-lane bridges. The main geometric parameters varied in the study were span-length and stringer-spacing. The stringer-spacing selected was: 1.98m, 2.59m and 3.51m for two-lane bridges, and 3.51m for three-lane bridges. A total of 11 span-lengths were selected from 15.24m to 91.44m, with increments of 7.62m. The bridges were modeled and analyzed with ABAQUS (2002). The FRP panel and steel I-beam components were all modeled using shell elements, and beam elements were used to model the cross frame bracings. Multiple-point constraint (MPC) rigid elements were used to simulate the interaction between the panel and stringers.

Table 6.1 Parameter for Each Cross Section

Parameter	CS1	CS2	CS3	CS4
A	9.3m	9.3m	9.3m	13.0m
B	8.53m	8.53m	8.53m	12.2m
S	3.51m	2.60m	1.98m	3.51m
ds	1.15m	0.77m	0.69m	1.23m
ts	0.24m	0.20m	0.20m	0.24m
N	3	4	5	4

Table 6.2 Equivalent Properties of FRP Panel

	$E_x(MPa)$	$E_y(MPa)$	ν_x	$G_{xy}(MPa)$
In-Plane	2560	2300	0.303	560
Bending	5640	5640	0.303	1400

The following assumptions in finite element modeling are made in order to simplify the analysis effort while retaining adequate accuracy:

1. The bridge deck is idealized as a horizontal slab of uniform thickness. The material in the slab is homogeneous, elastic and orthotropic;
2. The slab is supported by variable number of girders. These girders are equally spaced and are parallel I-shaped steel girders;
3. The edge of the slab and the girder ends are simply supported at the abutments;
4. Full composite action is assumed between the supporting girders and slab. This means that there is no interface slip at the girder slab interface;
5. No truck wheel load is closer than 0.61m from the roadway edge.

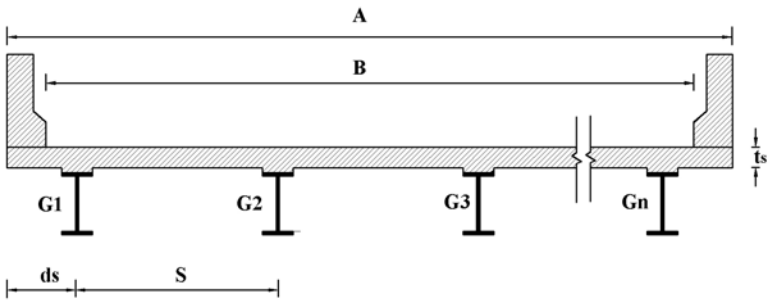

Figure 6.5 Typical Cross Section of Bridge Model

6.4.2. Live Load Position

The AASHTO LRFD service II load combination was applied. From previous research, the number of lanes loaded had small influence on effective-width, and therefore only one-lane loaded case was included in the analysis. The live load was positioned longitudinally at a selected location to induce maximum moment in the bridge models. For cross section CS1, CS2, and CS3, one- and two-lane loaded cases were selected. For cross section CS4, one-, two-, and three-lane loaded cases are selected (Figure 6.6).

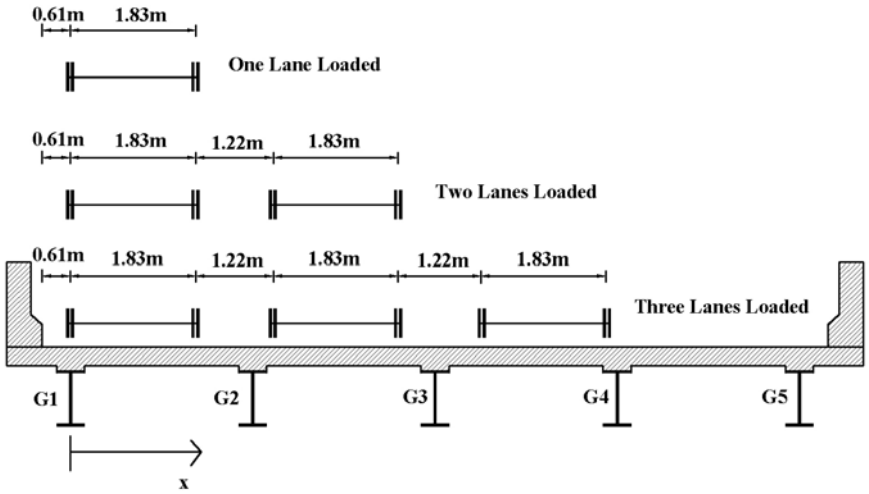

Figure 6.6 AASHTO HS20 Truck Live Load

6.4. 3. Effective Flange Width Data Reduction from FE Results

$b_{eff} = \frac{\int_{-b/2}^{b/2} \sigma_x dx}{\sigma_{\max}} = \frac{2\int_{0}^{b/2} \sigma_x dx}{\sigma_{\max}}$ is defined as a general expression for effective flange width.

To obtain the corresponding effective-width from FE analysis, the integral on the

numerator was obtained by approximation from the FE output. In FE element stress output, the average normal stress for each shell element $\sigma_{x,i}$ is uniform along its discrete length, as shown in Figure 6.7. The height of each rectangle corresponds to the element longitudinal stress value, and the width is equal to the element mesh size, which is 152mm in this case. Therefore, the integral of the normal stresses, or normal stress resultant, corresponds to the summation of the discrete values over the panel section. It is expressed as $\int_{-b/2}^{b/2} \sigma_x dx = \sum_{i=1}^{n} \sigma_{x,i} h_i = 6 \sum_{i=1}^{n} \sigma_{x,i}$, where $\sigma_{x,i}$ is the normal stress of discrete shell element. Denominator $\sigma_{\max}$ is the stress value at the panel-stringer center line. The effective width therefore can be obtained.

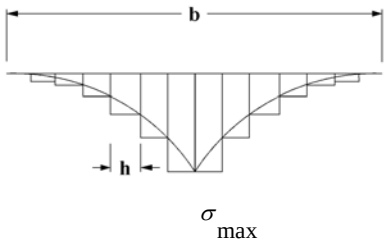

Figure 6.7 Stress Integration along the Flange Width

6.4.4. Assessment and Discussion of FE Results and Analytical Solution

Several major variables, number of lanes loaded, flange thickness, deck aspect ratio, and in-plane extensional modulus/shear modulus ratio, are assessed to evaluate their impact on load distribution factor. The importance of these parameters on load distribution factor is identified.

6.4.4.1. Number of Lanes Loaded

In order to determine the live load pattern, for 2 lanes bridges CS1, CS2, and CS3, one- and two-lane loaded cases are selected. For three lanes bridge CS4, one-, two-, and three-lane loaded cases are selected. For each of these cross section configurations, the effective width ratio is used as a non-dimensional parameter to facilitate the comparison instead of using effective width. As can be seen in Table 6.3, the effective flange widths are very close for bridges with different lanes loaded cases. For CS1 and CS3, which has symmetrical cross section configuration, the average difference between one-lane loaded and two-lane loaded cases is within 0.2%. For CS2 and CS4, which has asymmetrical cross section configuration, the average difference between one-lane loaded and two-lane loaded cases is within 2%. It is fair to conclude that the number of lanes loaded has only minor impact on effective flange width. Therefore, all the bridge models in this parametric study are loaded with only one traffic lane.

Table 6.3 Comparison of Effective Width with Different Number of Lanes Loaded

Cross Section	Span(m)	B/L	Be/B	Be/B	Diff. (%)
			One-lane Loaded	Two-lane Loaded	
CS1	15.2	0.230	0.872	0.870	0.290
	38.1	0.092	0.953	0.954	-0.098
	68.6	0.051	0.974	0.976	-0.174
	91.4	0.038	0.968	0.974	-0.616
CS2	15.2	0.170	0.886	0.915	-3.186
	38.1	0.068	0.956	0.969	-1.379
	68.6	0.038	0.974	0.985	-1.120
	91.4	0.028	0.958	0.973	-1.546
CS3	15.2	0.130	0.918	0.918	-0.070
	38.1	0.052	0.976	0.975	0.112
	68.6	0.029	0.986	0.985	0.042
	91.4	0.022	0.961	0.958	0.316
CS4	15.2	0.230	0.812	0.778	4.330
	38.1	0.092	0.951	0.935	1.659
	68.6	0.051	0.975	0.963	1.202
	91.4	0.038	0.964	0.956	0.875

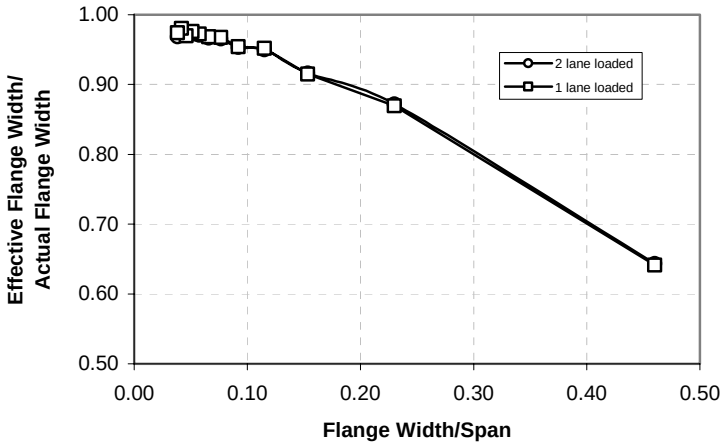

Figure 6.8 Comparison of Number of Lane Loaded for Bridge Section CS1

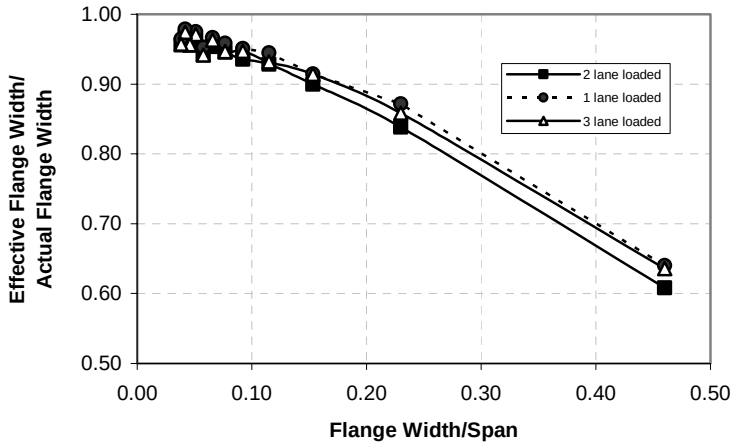

Figure 6.9 Comparison of Number of Lane Loaded for Bridge Section CS4

6.4.4.2. Flange Thickness

Based on previous research, flange thickness is generally not a prominent parameter affecting the effective width. In this FE analysis, cross section CS1 and CS4 have the

same slab thickness of 240mm, while CS2 and CS3 have the same slab thickness of 205mm. However, they do not share the same aspect ratio step. In order to compare these cross sections directly, by using curve fitting, these models are interpolated and extrapolated to certain aspect ratio B/L. From comparison, the differences of models with different slab thickness are small. For example, the difference between CS1 and CS2 is only 2.1%. For CS3 and CS4, the difference is also small. Therefore, it can be concluded that within the practical range, the slab thickness is not a major factor on effective width.

6.4.4.3. Aspect Ratio

For span length L and girder spacing B, they are considered as predominant factors that affect the effective width. They are usually combined into a non-dimensional parameter, aspect ratio, which is defined as the ratio of girder spacing to span length, B/L. With the span length increasing, the system shows more beam action. Therefore, effective flange width increases while B/L decreases (Figure 6.10). The effective width approaches to full girder spacing when the aspect ratio approach zero. For $B/L < 0.1$, the effective width is larger than 95% of the actual width and effective width ratio $B_e/B > 0.95$, for which the effective width is essentially full girder spacing.

6.4.4.4. In-plane Extensional Modulus/Shear Modulus Ratio

As the FRP panel idealized as a homogenous panel with equivalent properties, the in-plane extensional modulus/shear modulus ratio is $E/G = 3.84$ for this FRP panel. While for isotropic material like reinforced concrete, it is usually rated as $E/G = 2(1+\nu) = 2.4$. In other words, the FRP panel is more deformable than concrete slab when it is under in-

plane shear. Therefore, shear lag phenomenon is expected to be more pronouncing in FRP panel, which will lead to smaller effective flange width.

Table 6.4 Aspect Ratio versus Effective Width

	CS1		CS2		CS3		CS4	
Span(m)	B/L	Be/B	B/L	Be/B	B/L	Be/B	B/L	Be/B
7.62	0.46	0.643	0.34	0.695	0.26	0.812	0.46	0.636
15.2	0.23	0.872	0.17	0.886	0.13	0.918	0.23	0.856
22.9	0.15	0.916	0.11	0.931	0.09	0.960	0.15	0.914
30.5	0.12	0.950	0.09	0.948	0.07	0.955	0.12	0.932
38.1	0.09	0.953	0.07	0.956	0.05	0.976	0.09	0.947
45.7	0.08	0.965	0.06	0.949	0.04	0.951	0.08	0.947
53.3	0.07	0.967	0.05	0.967	0.04	0.982	0.07	0.963
61.0	0.06	0.971	0.04	0.959	0.03	0.958	0.06	0.942
68.6	0.05	0.974	0.04	0.974	0.03	0.986	0.05	0.971
76.2	0.05	0.970	0.03	0.958	0.03	0.960	0.05	0.956
83.8	0.04	0.973	0.03	0.975	0.02	0.986	0.04	0.974
91.4	0.04	0.968	0.03	0.958	0.02	0.961	0.04	0.957

Table 6.5 Effective Width of FRP Panel and Concrete Panel

Cross Section	Span(m)	B/L	Be/B	Be/B	Diff. (%)
			Concrete	FRP	
CS1	7.62	0.46	0.643	0.551	16.86
	38.1	0.09	0.953	0.912	4.51
	68.6	0.05	0.974	0.941	3.56
	91.4	0.04	0.968	0.930	4.09
CS2	7.62	0.34	0.695	0.642	8.13
	38.1	0.07	0.956	0.925	3.36
	68.6	0.04	0.974	0.962	1.22
	91.4	0.03	0.958	0.923	3.80
CS3	7.62	0.26	0.812	0.762	6.54
	38.1	0.05	0.976	0.966	1.03
	68.6	0.03	0.986	0.975	1.08
	91.4	0.02	0.961	0.911	5.53
CS4	7.62	0.46	0.636	0.537	18.41
	38.1	0.09	0.947	0.892	6.21
	68.6	0.05	0.971	0.955	1.74
	91.4	0.04	0.957	0.935	2.36

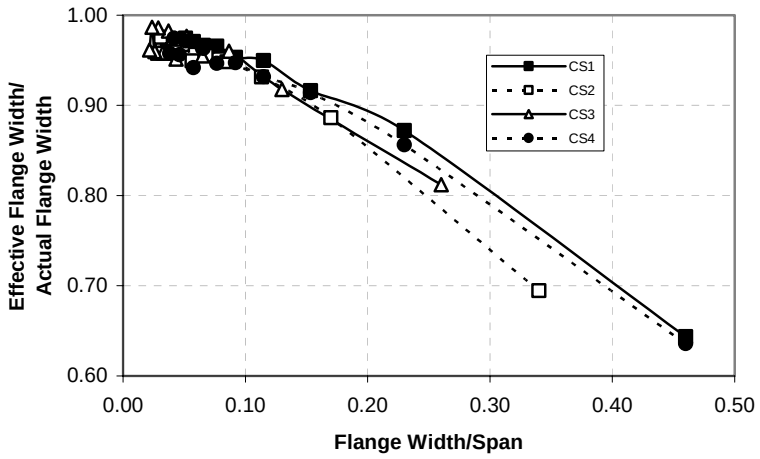

Figure 6.10 Aspect Ratio vs. Effective Width

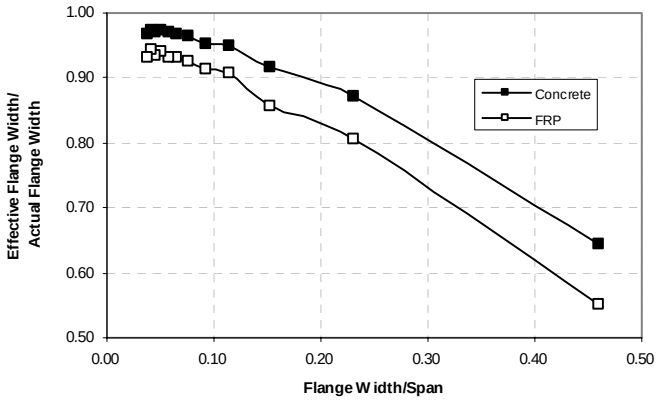

Figure 6.11 Effective Width of FRP Panel vs. Concrete Panel for Bridge Section CS1

In order to study the effect of modulus ratio on effective width, FE analysis is conducted on both FRP panel and concrete panel, with the bridge model configurations remain unchanged. The effective width for both FRP panel and concrete panel are shown in Table 6.5 and Figure 6.11. The average difference in effective width for FRP and

concrete panel is 5%. The difference becomes larger when the aspect ratio is high. For 7.62m span length and aspect ratio at 0.46, the difference of effective width for FRP and concrete deck could be as large as 19%. It can be concluded that other than aspect ratio B/L, the modulus ratio E/G is another factor that affect the effective width.

6.4.5. Comparison between Shear Lag Model and FE Analysis

Effective flange widths from shear lag model are compared with the FE results in Table 6.6. The results show that shear lag model overestimates the effective flange width by an average error about 6.4%. Overall, shear lag model and FE show similar trend in effective width prediction. The effective width expression of shear lag model consists of two major parameters, aspect ratio b/L and modulus ratio E/G, which is represented as A_{11}/A_{66} in shear lag model. In parametric study, these two parameters are determined to be predominant parameters to affect the effective width. With the aspect ratio decreases, the effective width increases. When the aspect ratio is less than 0.1, the effective width is close to 96% of flange width. The largest error is found in model with 7.62m span length, which is about 8%-14%. For other span length, the effective width from shear lag model is close to FE analysis.

6.4.6. Comparison between Shear Lag Model and Empirical Function

Tenchev (1996) conducted FE parametric study on effective width for orthotropic flanges. Boundary conditions, load conditions, and cross section dimensions are the main variables in his parametric study. Pin-roller and fixed support conditions are considered. Concentrate and uniformly distributed load conditions are both applied in the FE

Table 6.6 Comparison of Shear Lag Model and FE

Cross Section	Span(m)	B/L	Be/B	Be/B	Diff. (%)
			Shear Lag	FE	
CS1	7.62	0.460	0.626	0.551	11.997
	38.1	0.092	0.974	0.912	6.354
	68.6	0.051	0.992	0.941	5.127
	91.4	0.038	0.995	0.930	6.541
CS2	7.62	0.340	0.744	0.642	13.667
	38.1	0.068	0.986	0.925	6.179
	68.6	0.038	0.995	0.962	3.315
	91.4	0.028	0.997	0.923	7.502
CS3	7.62	0.260	0.829	0.762	8.004
	38.1	0.052	0.991	0.966	2.525
	68.6	0.029	0.997	0.975	2.209
	91.4	0.022	0.999	0.911	8.774
CS4	7.62	0.460	0.626	0.537	14.172
	38.1	0.092	0.974	0.892	8.436
	68.6	0.051	0.992	0.955	3.749
	91.4	0.038	0.995	0.935	6.023

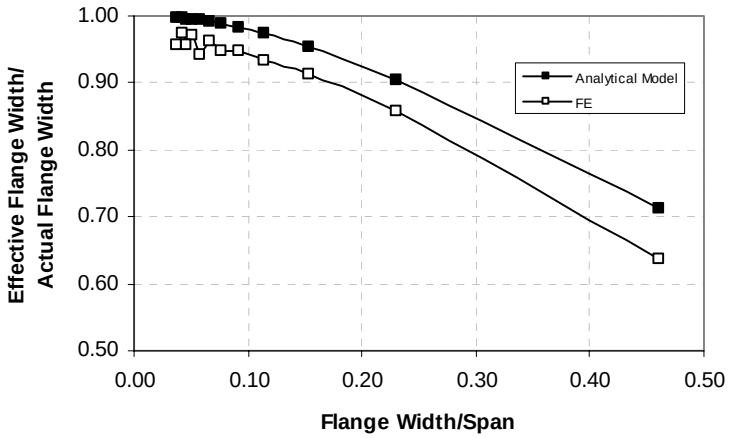

Figure 6.12 Comparison of Shear Lag Model and FE for Bridge Section CS4

modeling. The main geometric and material parameters are: (1) aspect ratio, $0.03 < b/L < 1.0$; (2) modulus ratio, $1.0 < E/G < 30$; (3) web/flange thickness ratio,

$0.05 < T_f / T_w < 3.0$ while T_w is varied on two steps; $0.05H$ and $0.02H$. Beam depth $H = 0.5b$ and span length $L = 16.7\,ft$ are fixed. 640 FE models are analyzed and effective widths are obtained. Based on these effective width values, empirical functions are proposed by curve fitting the FE data. The effective width is represented as effective width ratio $\frac{b_e}{b}$. The empirical function is

$$\lambda_{emp} = \frac{b_e}{b} = \frac{0.57}{C_1 C_2}(\frac{b}{L})^{-0.85}(\frac{E}{G})^{-0.416} \tag{6.19}$$

$$C_1 = 1 + 5e^X, \quad X = -6.4\frac{b}{L}\sqrt{\frac{E}{G}} \tag{6.20}$$

$$C_2 = 1 + 0.31e^{-0.9Y}, \quad Y = (\frac{E}{G})(\frac{b}{L})^{-1} \tag{6.21}$$

b = actual beam flange width;

L = span length;

E = beam flange Young's modulus in longitudinal direction;

G = beam flange in-plane shear modulus;

In order to verify the shear lag model, a numerical T-beam model is established with two major parameters E/G and b/L varying. Three modulus ratios E/G are selected as 1, 10, and 30. Accordingly, aspect ratio b/L is varied from (1) 0.1 to 1 at $E/G = 1$; (2) 0.08 to 0.88 at $E/G = 10$; and (3) 0.03 to 0.60 at $E/G = 30$. The boundary condition of this numerical model is set as simply supported and the load condition is set as uniform distributed load.

The results from shear lag model and empirical function are compared in Table 6.7, 6.8, and 6.9. At $E/G=1$, the shear lag model consistently overestimates the effective width than empirical function. Overall, the average error is 6.6% between empirical function and shear lag model. After $b/L<0.5$, the predicted effective width from shear lag model is closer with empirical function (Figure 6.13). At $E/G=10$ and $E/G=30$, the shear lag model has better predictions and the average errors are 1.5% and 3.8%, respectively. This comparison shows that overall the correlation between shear lag model and empirical function is good, especially for aspect ratio $b/L<0.5$. The shear lag model displays its advantage that it can be applied to the bridges with wider range of parameters, while maintaining adequate accuracy. Therefore, it is suitable for future design and parametric study for composite slab-on-girder bridges.

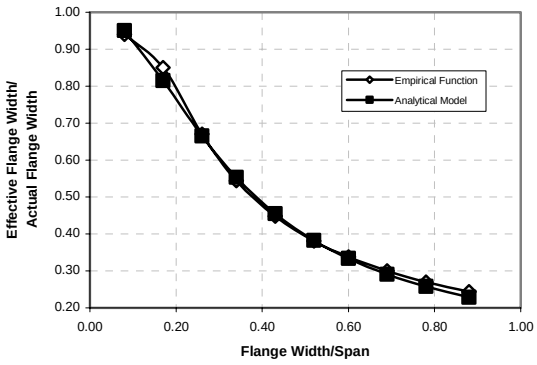

Figure 6.13 Comparison between Shear Lag Model and Empirical Function for E/G=10

Table 6.7 Comparison between Shear Lag Model and Empirical function at E/G=1

B/L	Be/B		Diff. (%)
	Empirical	Shear lag	
1.00	0.502	0.584	16.29
0.90	0.551	0.628	14.06
0.80	0.608	0.676	11.29
0.70	0.673	0.728	8.19
0.60	0.743	0.781	5.13
0.50	0.812	0.835	2.85
0.40	0.867	0.886	2.18
0.30	0.901	0.932	3.42
0.20	0.933	0.968	3.75
0.10	1.000	0.992	-0.81
Average			6.63

Table 6.8 Comparison between Shear Lag Model and Empirical function at E/G=10

B/L	Be/B		Diff. (%)
	Empirical	Shear lag	
0.88	0.244	0.229	-6.20
0.78	0.270	0.258	-4.58
0.69	0.300	0.291	-2.91
0.60	0.338	0.334	-1.15
0.52	0.381	0.383	0.38
0.43	0.448	0.455	1.67
0.34	0.544	0.553	1.58
0.26	0.670	0.665	-0.67
0.17	0.850	0.815	-4.13
0.08	0.940	0.950	1.08
Average			-1.49

Table 6.9 Comparison between Shear Lag Model and Empirical function at E/G=30

B/L	Be/B		Diff. (%)
	Empirical	Shear lag	
0.60	0.214	0.193	-9.53
0.54	0.234	0.215	-8.09
0.48	0.258	0.242	-6.48
0.41	0.295	0.282	-4.51
0.35	0.338	0.330	-2.37
0.29	0.397	0.395	-0.42
0.22	0.500	0.504	0.77
0.16	0.646	0.639	-1.06
0.10	0.852	0.809	-5.08
0.03	0.993	0.978	-1.49
Average			-3.83

6.4.7. Application of Shear Lag Model to FRP Deck

The analytical solution was used to obtain effective for the scaled bridge model described in Chapter 4. The corresponding effective width is about 1.01m. Since the analytical solution only considers full composite action case, a reduction factor R=0.6 is suggested for the FRP bridge decks with partial composite action. Thus, applying the factor R to Eq. (6-18), the effective width can be evaluated as,

$$b_{eff} = R\frac{\int_0^{b/2}\cosh(\xi y)dy}{\cosh(\frac{\xi b}{2})},\ \xi = \frac{\pi}{a}(\sqrt{\frac{A_{11}}{A_{66}}}) \qquad (6\text{-}22)$$

The corresponding effective flange width is about 0.61m. Also, evaluation by FE analysis shows the resulted effective flange width of bridge model is 0.75m, which is about 63% of actual flange width. Test results and FE show that the actual effective flange width of this T-beam is about 50-65% of actual flange width. More tests on effective flange width and degree of composite action are suggested. By further test results, the relation between degree of composite action and effective flange width could be obtained.

6.5. Conclusions

In this chapter, an approximate effective-deck-width expression is developed for FRP deck and-stringer bridges with full composite-action. By adopting a modification factor R, the formulation obtained can be modified to accommodate for partial composite action as shown in section 4.3, Eq. (4.1). A finite element analysis of 44 selected FRP-deck and steel-stringer bridges is conducted, and the analytical solution for effective-width is validated by FE results. From the FE parametric study, it can be concluded that effective

width is independent of the number of lanes loaded. Girder spacing and span length are two major parameters that affect the effective width. These two parameters can be represented as aspect ratio b/L. The modulus ratio E/G is another major variable which will affect the effective width. Comparing with FE, the approximate expression overestimates the effective width for about 6%. Combined with equivalent orthotropic properties for FRP cellular and sandwich decks, the proposed analytical expression provides sufficient accuracy and is relatively simple to be used in design practice. Since the analytical solution only considers full composite action case, a reduction factor is suggested for FRP bridge decks with partial composite action.

CHAPTER 7

CONCLUSIONS AND DESIGN RECOMMENDATIONS

7.1. Conclusions

The major outcomes of the engineered FRP deck-steel stringer bridge system are summarized in the following sections.

7.1.1. Overview

As the most critical structural component of FRP deck-steel stringer system, a new type of shear connection is thoroughly studied by push-out test and bridge model test. It is proved to meet the code requirements for strength and fatigue resistance. Its stiffness, strength, and fatigue resistance are well defined and used as design basis for FRP bridge decks. The prototype shear connection also has the ability to transfer shear force at deck-stringer interface and is expected to achieve a certain degree of composite action.

At the second stage of study, a reduced scale FRP deck bridge model is tested. The bridge model consists of FRP deck panels, steel supporting stringers, and the proto type shear connection. The test program consists of three phases. Phase I is a scaled FRP deck

bridge model test with the objectives to study: (1) field deck attachment procedure; (2) transverse load distribution factors; and (3) local deck deflections and strains. Phase II test is a bridge model fatigue test with the objectives to evaluate FRP deck-connection system fatigue behavior. Phase III test is a T-section of 1.2 m wide, which is cut out from the bridge model, tested to failure. Phase III test focuses on: (1) effective deck-width; (2) degree of composite action and spacing of connectors; and (3) service-limit and ultimate-limit states under flexure loads.

The test program is then verified by FE analysis and analytical solutions. A simplified FE model is constructed which considers partial composite action of the deck. An approximate series solution on load distribution factor is presented. Then, a harmonic analysis that was developed for FRP thin-walled sections is formulated to predict the effective-width of FRP decks.

Based on this study, the engineered FRP deck-steel stringer system is proved to be able to achieve partial degree of composite action. The structural behaviors, such as degree of composite action, effective width, load distribution factor, local deflection of panels, are well defined. Its favorable service limit and ultimate limit performance make the FRP deck-steel stringer bridge an excellent option for both rehabilitation projects and new constructions.

7.1.2. Effective Prototype Shear Connection

Through push-out test on both static and fatigue resistance, the load displacement curve

was established as a segmentally linear model. The connection shows good ductility after yield. The S-N curve was established for this shear connection by fatigue test. The shear connection was able to sustain cyclic fatigue loading equivalent to 75 years bridge service life-span. The shear connection was then further tested in a scaled FRP bridge deck model to evaluate its performance in a bridge system, showing nearly no stiffness degradation.

During the study, the shear connection shows: (1) the proposed shear connection provides adequate connectivity for FRP sandwich panels; (2) The shear connection can effectively transfer shear force between deck and girder while allows certain amount of interface slip. This property will develop partial composite action in FRP decks; (3) this shear connection is capable of sustaining cyclic fatigue loading of about 75 years bridge service-life span under AASHTO live load; (4) the installation process is also straightforward and easy. The study on prototype shear connection shows that this connection is structurally efficient and can be used in practice.

7.1.3. Load Distribution Factor

Following shear connection test, a reduced scale FRP bridge model is tested to investigate the load distribution and local deflection of the FRP panels. The load distribution factor of interior girders is obtained under concentrate loading condition. The test results correlate well with FE model analysis. In addition, an analytical solution is obtained from a first-term approximate series solution. In series solution, the load distribution factor is expressed as a ratio of stringer interaction force. The series solution

predicts the load distribution factor fairly well with the reference bridge in parametric study. For interior girders, the prediction is within 5% difference. For exterior girders, the differences are larger, which is due to neglecting the deck overhang and other secondary strengthening effect in series solution. The solution is suggested as a simplified method for load distribution factor.

7.1.4. Panel Local Deflection

In panel local deflection test, the deflection ratio is about L/730. In AASHTO LRFD code, there is no deflection limit for FRP bridge decks. Many researchers have suggested L/400 as deflection criteria for FRP decks. Therefore, the local deflection for this FRP panel is considered to be acceptable. One possible solution to reduce the deformation of the FRP deck is to add horizontal steel bracing between stringers consisting of a supporting grid under FRP decks. Thus, FRP deck spacing is reduced and the deformation is expected to be much smaller than the current scheme.

7.1.5. Degree of Composite Action and Effective Flange Width

Degree of composite action and effective flange width are two properties that are interrelated. For T-beam section, the degree of composite action is about 25% and the corresponding effective FRP flange width is about 50% of actual width. The distribution of normal stress proves the existence of shear lag phenomenon in FRP flange. Top facesheet displays much more pronounced shear lag phenomenon than bottom facesheet, which is mainly due to low shear transferring capability of the core. Since the core

material does not have much out-of-plane stiffness, the top and bottom facesheet are mostly act separately under bending action.

An approximate effective flange width expression is developed for FRP bridge decks with full composite action. The analytical solution is validated by FE parametric study. Since the analytical solution only considers full composite action case, a reduction factor is suggested for FRP bridge decks with partial composite action. Test and FE results show that the actual effective flange width of this T-beam is about 50-65% of actual flange width. More tests on effective flange width and degree of composite action are suggested. By further test outcomes, the relation between degree of composite action and effective flange width would be able to obtain.

7.1.6. Shear Connection Spacing

In reduced scale bridge model test and T-beam test, two different connection spacing, 0.6m and 1.2m, are tested. In terms of structural performance, the difference between these two connection spacings is only marginal. The difference between these two connection spacings on service load level, ultimate strength, and degree of composite action are all within 2%. It is suggested that 1.2m connection spacing may be a good compromise in cost and performance in FRP bridge decks design.

7.1.7. Service Load and Failure Mode

The failure mode of T-beam is a ductile failure with steel stringer yielding. The ultimate strength thus mainly depends on the capacity of stringer. At the failure stage, the FRP

panel shows large compression deformation at the loading position where the panel shows obvious sagging shape. However, there is no visible damage to the FRP panel, neither at the tongue and groove connection locations. The whole FRP panel remains intact, as well as the shear connection and steel sleeve. The integrity of whole FRP decks is provided by both shear connection and tongue and groove connection.

7.2. Summaries

Overall, the test results correlated quite well with FE and analytical solutions. Several observations and conclusions are made: (1) Using closely-spaced connection spacing (0.6 m instead of 1.2 m) does not significantly improve structural bridge behavior or performance; thus, a 1.2m connection spacing is adequate and cost-effective in design. (2) The FRP panel remained visibly undamaged during all tests conducted, including the T-beam section tested to failure, and also there was no damage observed to the stud-sleeve connector and the tongue-and-groove connection; thus, the deck-to-stringer and panel-to-panel connection systems were shown to be structurally efficient concepts for FRP bridge decks. (3) About 25% degree of composite action was achieved with the prototype shear connection, which represented an increases of 13% service-load and 7% yield-strength capacities for the T-beam section compared to non-composite section. (4) For this degree of composite action, the effective flange width of the T-beam was about 50% of the actual flange width. (5) The FRP panel local deflections from tests were, respectively, 1.65 mm and 1.75 mm for 0.6 m and 1.2 m connection spacing; the deflection ratio is about L/730. In AASHTO LRFD code, there is no deflection limit for FRP bridge decks. Many researchers have suggested L/400 as deflection criteria for FRP decks. Therefore,

the local deflection for this FRP panel is considered to be acceptable. (6) The failure mode of FRP decks with steel stringers was established in this study as steel stringer yielding with adequate ductility; the ultimate load mainly depends on the capacity of the steel stringers. (7) The approximate series solution provided adequate accuracy and simplicity to be used in design practice. (8) The shear connection and FRP decks showed more than adequate fatigue resistance to satisfy AASHTO fatigue live load requirement.

7.3. FRP Deck Bridge Design Recommendations and Flow Chart

The basic steps for FRP deck bridge design is outlined here. For FRP deck slab-on-girder bridges, the general design procedure should follow AASHTO LRFD specification with corresponding section. The most relevant section is the section for steel bridge structure design. Certain modifications are highlighted here to address the distinct properties of FRP deck bridges.

1. For the stud-sleeve type shear connection used, due to its low stiffness, only partial composite action can be achieved. For FRP bridges with normal span range (~30m), the shear stiffness of the connection is taken as 1.46 kN/mm. The fatigue stress range on a single shear connection should be limited to no more than the fatigue stress threshold, which was established at 53 MPa;
2. For load distribution factors, the approximate series solution can be used as a simplified analytical method to obtain design factors for interior and exterior girders;
3. For panel local deflection, as for 2.4m girder spacing and 250mm panel thickness, the local deflection is about L/730. The deformation is considered to be acceptable;

4. The effective flange width is suggested to be taken as about 50% of the actual flange width of panels (center-to-center spacing of stringers). Consequently, the service load can be obtained by transform section method;
5. Since the FRP deck is not able to provide full lateral support to the steel compression flange, the steel stringer should be designed accordingly to ensure its compactness or prevent flange compression buckling;

7.4. Future Works

Further study on tongue-and-groove connection properties, such as bending strength and fatigue resistance, is needed to better understand its behavior. Also the in-plane shear stiffness of the honeycomb sandwich FRP panel needs to be investigated. Because of the low in-plane shear stiffness of the core, the shear force is distributed unevenly between the top facesheet and bottom facesheet. The shear transferring mechanism between top and bottom facesheets is identified as a critical factor for defining effective width as characterized by shear lag of FRP deck components.

REFERENCES

AASHTO (1996), *AASHTO Standard Specifications for Highway Bridges, 16th Edition*, American Association of State Highway and Transportation Officials, Washington D.C.

AASHTO (2004), *AASHTO LRFD Bridges Design Specifications, 3rd Edition*, American Association of State Highway and Transportation Officials, Washington D.C.

ABAQUS (2002), *User's Manual, V 6.3*, HKS, Inc., RI, USA.

Adekola, A.O. (1968), "Effective Widths of Composite Beams of Steel and Concrete", *The Structural Engineer*, Vol. 46, No. 9, pp. 285-289.

Adekola, A.O. (1974), "The Dependence of Shear Lag on Partial Interaction in Composite Beams", *International Journal of Solids Structures*, Vol. 10, pp. 389-400.

Ahn, II-Sang, M. Chiewanichakorn, S.S. Chen, and A.J. Aref (2004), "Effective Flange Width Provisions for Composite Steel Bridges", *Engineering Structures*, Vol. 26, pp. 1843-1851.

Amadio, C., C. Fedrigo, M. Fragiacomo, and L. Macorini (2004), "Experimental Evaluation of Effective Width in Steel-Concrete Composite Beams", *Journal of Constructional Steel Research*, Vol. 60, pp. 199-220.

Barker, R. M., J. A. Puckett (1997), *Design of Highway Bridges*, John Wiley & Sons, Inc.

Bakht, B., F. Moses (1988), "Lateral Distribution Factors for Highway Bridges", *Journal of Structural Engineering*, Vol. 114, No. 8, pp. 1785-1803.

Bakht, B., L.G. Jaeger (1990), "Bridge Evaluation for Multipresence of Vehicle", *Journal of Structural Engineering*, Vol. 116, No. 3, pp. 603-618.

Bakis, C.E., L.C. Bank, V.L. Brown, E. Cosenza, J.F. Davalos, J.J. Lesko, A. Machida, S.H. Rizkalla, and T.C. Triantafillou (2002), "Fiber-reinforced Polymer Composites for Construction – State-of-the-art Review", *Journal of Composites for Construction*, Vol. 6, No. 2, pp. 73-87.

Bishara, A.G., M. C. Liu, and D. El-Ali Nasser (1993), "Wheel Load Distribution on Simply Supported Skew I-Beam Composite Bridges", *Journal of Structural Engineering*, Vol. 119, No. 2, pp. 399-419.

Cheung, M.S., M.Y.T. Chan (1978), "Finite Strip Evaluation of Effective Flange Width of Bridge Girders", *Canadian Journal of Civil Engineering*, Vol. 5, No. 2, pp. 174-185.

CSA (1988), *Canadian Highway Bridge Design Code (CAN/CSA-S6-88)*, CSA International.

CSA (2000), *Canadian Highway Bridge Design Code (CAN/CSA-S6-00)*, CSA International.

Davalos, J.F., H.A. Salim (1993), "Effective Flange Width for Stress-Laminated T-System Timber Bridges", *Journal of Structural Engineering*, Vol. 119, No. 3, pp. 938-953.

Davalos, J.F., P.Z. Qiao, X.F. Xu, J. Robinson, and K.E. Barth (2001), "Modeling and Characterization of Fiber-reinforced Plastic Honeycomb Sandwich Panels for Highway Bridge Applications", *Composite Structures*, Vol. 52, pp. 441-452.

Dean, D.L., C. Omid'varan (1969), "Analysis of Ribbed Plates", *Journal of the Structural Division, Proceeding of the American Society of Civil Engineers*, Vol. 95, No. ST3, pp. 411-440.

Demitz, J. R., Mertz, D. R., and Gillespie, J. W. (2003), "Deflection requirements for bridges constructed with advanced composite materials" *Journal of Bridge Engineering*, Vol. 8, No. 2, pp. 73-83.

Eom, J., A.S. Nowak (2001), "Live Load Distribution for Steel Girder Bridges", *Journal of Bridge Engineering*, Vol. 6, No. 6, pp. 489-497.

Finch, T.R., J.A. Puckett (1992), *Enhancement of Existing Engineering Software, Vol.5-Transverse Load Distribution in Slab-Girder Bridges*, Mountain-Plains Consortium Publications 92-9.5, North Dakota State University, ND.

Fu, C.C., M. Elhelbawey, M. A. Sahin, and D. R. Schelling (1996), "Lateral Distribution Factor from Bridge Field Testing", *Journal of Structural Engineering*, Vol. 122, No. 9, pp. 1106-1109.

Gangarao, H.V.S., A.A. Elmeged, and V.K. Chaudhary (1975), "Macroapproach for Ribbed and Grid Plate Systems", *Journal of the Engineering Mechanics Division, Proceeding of the American Society of Civil Engineers*, Vol. 101, No. EM1, pp. 25-43.

Gangarao, H.V.S., H.J. Farran (1986), "Macro-Element Analysis of Skewed and Triangular Orthotropic Thin Plates with Beam Boundaries", *Computers and Structures*, Vol. 22, No. 3, pp. 399-404.

Gangarao, H.V.S., V.K. Chaudhary (1988), "Analysis of Skew and Triangular Plates in Bending", *Computers and Structures*, Vol. 28, No. 2, pp. 223-235.

Hays, C.O., L. M. Sessions, and A. J. Berry (1986), "Further Studies on Lateral Load Distribution Using a Finite Element Method", *Transportation Research Record*, Vol. 1072, pp. 6-14.

Keelor, D.C., Y. Luo, C.J. Earls, and W. Yulismana (2004), "Service Load Effective Compression Flange Width in Fiber Reinforced Polymer Deck Systems Acting Compositely with Steel Stringers", *Journal of Composites for Construction*, Vol. 8, No. 4, pp. 289-297.

Keller, T., H. Gurtler (2005), "Composite Action and Adhesive Bond between Fiber-Reinforced Polymer Bridge Decks and Main Girders", *Journal of Composites for Construction*, Vol. 9, No. 4, pp. 360-368.

Keller, T., T. Tirelli (2004), "Fatigue Behavior of Adhesively Connected Pultruded GFRP Profiles", *Composites Structures*, Vol. 65, pp. 55-64.

Keller, T., H. Gurtler (2005), "Quasi-static and Fatigue Performance of a Cellular FRP Bridge Deck Adhesively Bonded to Steel Girders", *Composites Structures*, Vol. 70, pp. 484-496.

Kim, S., A. S. Nowak (1997), "Load Distribution and Impact Factors for I-girder Bridges", *Journal of Bridge Engineering*, Vol. 2, No. 3, pp. 97-104.

Kukreti, A.R., Y. Rajapaksa (1987), "Analysis Procedure for Ribbed and Grid Plate Systems Used for Bridge Decks", *Journal of Structural Engineering*, Vol. 116, No. 2, pp. 372-391.

Kukreti, A.R., E. Cheraghi (1993), "Analysis Procedure for Stiffened Plate Systems Using An Energy Approach", *Computers and Structures*, Vol. 46, No. 4, pp. 649-657.

Lopez-Anido, R., H.V.S. Gangarao (1995), "Macroapproach Closed-Form Series Solution for Orthotropic Plates", *Journal of Structural Engineering*, Vol. 121, No. 3, pp. 420-432.

Mabsout, M.E., K. M. Tarhini, G. R. Frederick, and A. Kesserwan (1999), "Effect of Multilanes on Wheel Load Distribution in Steel Girder Bridges", *Journal of Bridge Engineering*, Vol. 4, No. 2, pp. 99-106.

Mainstone, R.J., J.B. Menzies (1967), "Shear Connectors in Steel-Concrete Composite Beams for Bridges, Part 1: Static and Fatigue Tests on Push-Out Specimens", *Concrete*, Vol. 1, No. 9, pp. 291-302.

Mainstone, R.J., J.B. Menzies (1967), "Shear Connectors in Steel-Concrete Composite Beams for Bridges, Part 2: Static and Fatigue Tests on beams", *Concrete*, Vol. 1, No. 9, pp. 291-302.

Moffat, K.R., P.J. Dowling (1975), "Shear Lag in Steel Box Girder Bridges", *The Structural Engineer*, Vol. 53, No. 10, pp. 439-448.

Moffat, K.R., P.J. Dowling (1978), "British Shear Lag Rules for Composite Girders", *Journal of the Structural Division*, Vol. 104, No. st7, pp. 1123-1130.

Moon, F.L., D.A. Eckel, and J.W. Gillespie (2002), "Shear Stud Connections for the Development of Composite Action between Steel Girders and Fiber-Reinforced Polymer Decks", *Journal of Structural Engineering*, Vol. 128, No. 6, pp. 762-770.

Moon, F.L., J.W. Gillespie (2005), "Experimental Validation of a Shear Stud Connection between Steel Girders and a Fiber-Reinforced Polymer Deck in the Transverse Direction", *Journal of Composites for Construction*, Vol. 9, No. 3, pp. 284-287.

Newmark, N.M., C.P. Siess, and I.M. Viest (1951), "Test and Analysis of Composite Beams with Incomplete Interaction", *Experimental Stress Analysis*, Vol. 9, No. 1, pp. 75-92.

Nie, J., C.S. Cai (2003), "Steel-Concrete Composite Beams Considering Shear Slip Effects", *Journal of Structural Engineering*, Vol. 129, No. 4, pp. 495-505.

Oehlers, D.J., M.A. Bradford (1995), *Composite Steel and Concrete Structural Members*, Elsevier Science Inc.

OHBDC (1983), *Ontario Highway Bridge Design Code (2nd edition)*, Ministry of Transportation of Ontario, Canada.

OHBDC (1991), *Ontario Highway Bridge Design Code (3rd edition)*, Ministry of Transportation of Ontario, Canada.

Park, K.T., S.H. Kim, Y.H. Lee, and Y.K. Hwang (2005), "Degree of Composite Action Verification of Bolted GFRP Bridge Deck-to-Girder Connection System", *Composite Structures*, Vol. 72, pp. 393-400.

Righman J. (2002), *Development of an Innovative connection for FRP Bridge Decks to Steel Girders*, Master Thesis, West Virginia University.

Righman, J., K.E. Barth, and J.F. Davalos (2004), "Development of an Efficient Connector System for Fiber Reinforced Polymer Bridge Decks to Steel Girders", *Journal of Composites for Construction*, Vol. 8, No. 4, pp. 279-288.

Salim, H.A., J.F. Davalos, H.V.S. Gangarao, and P.R. Raju (1995), "An Approximate Series Solution for Design of Deck-and-Stringer Bridges", *International Journal for Engineering Analysis and Design*, Vol. 2, pp. 15-31.

Salim, H.A., J.F. Davalos, Pizhong Qiao, and S.A. Kiger (1997), "Analysis and Design of Fiber Reinforced Plastic Composite Deck-and-Stringer Bridges", *Composite Structures*, Vol. 38, No. 1-4, pp. 295-307.

Shahawy, M., D. Huang (2001), "Analytical and Field investigation of Lateral Load Distribution in Concrete Slab-on-Girder Bridges", *ACI Structural Journal*, Vol. 98, No. 4, pp. 590-599.

Slutter, R.G., J.W. Fisher (1966), "Fatigue Strength of Shear Connectors", *Highway Research Record*, Highway Research Board, Wshington, D.C., No. 147, pp. 65-88.

Song, Qi-gen, A.C. Scordelis (1990), "Shear-Lag Analysis of T-, I-, and Box Beams", *Journal of Structural Engineering*, Vol. 116, No. 5, pp. 1290-1305.

Song, Qi-gen, A.C. Scordelis (1990), "Formulas for Shear-Lag Effect of T-, I-, and Box beams", *Journal of Structural Engineering*, Vol. 116, No. 5, pp. 1306-1319.

Tabsh, S.W., M. Tabatabai (2001), "Live Load Distribution in Girder Bridges Subject to Oversized Trucks", *Journal of Bridge Engineering*, Vol. 6, No. 1, pp. 9-16.

Tarhini, K.M., G. R. Frederick (1992), "Wheel Load Distribution in I-Girder Highway Bridges", *Journal of Structural Engineering*, Vol. 118, No. 5, pp. 1285-1294.

Tenchev, R.T. (1996), "Shear Lag in Orthotropic Beam Flanges and Plates with Stiffeners", *International Journal of Solids Structures*, Vol. 33, No. 9, pp. 1317-1334.

Zhang, Y., and Cai, C. S. (2007), "Load distribution and dynamic response of multigirder bridges with FRP decks", *Engineering Structures*, Vol. 29, No. 8, pp. 1676-1689.

Zokaie, T. (2000), "AASHTO-LRFD Live Load Distribution Specifications", *Journal of Bridge Engineering*, Vol. 5, No. 2, pp. 131-138.